Polymer Electrolytes for Rechargeable Lithium/Sulfur Batteries

by

Kazem Jeddi

A thesis

presented to the University of Waterloo

in fulfillment of the

thesis requirement for the degree of

Doctor of Philosophy

in

Chemical Engineering (Nanotechnology)

Waterloo, Ontario, Canada, 2015

Author's Declaration

I hereby declare that I am the sole author of this thesis. This is a true copy of the thesis, including any required final revisions, as accepted by my examiners.

I understand that my thesis may be made electronically available to the public.

Abstract

The lithium/sulfur (Li/S) battery is one of the most promising candidates for energy storage systems due to sulfur's high theoretical specific capacity at 1672 mAh g^{-1}. This capacity is an order of magnitude higher than that of conventional electrodes and gives packaged Li/S cells an energy density of 400–600 W h kg^{-1}, which is two or three times higher than that of current lithium-ion batteries. In addition, low cost, abundance and environmental friendliness of sulfur offer the opportunity to produce cheap, safe and commercializable high-energy density batteries. Despite these advantages, the practical application of Li/S batteries is still prevented by modest practical capacity, short cycle life and low Coulombic efficiency. These problems are mainly due to:(i) low electronic conductivity of sulfur, which leads to low sulfur utilization; (ii) generation of various forms of soluble intermediate lithium polysulfides during the electrochemical reactions, which dissolve in the electrolyte and induce the so-called shuttle effect causing irreversible loss of sulfur active material over repeat cycles; (iii) volume change of sulfur upon cycling, which leads to its mechanical rupture and, consequently, rapid degradation of the electrochemical performance.

Since the early development of Li/S batteries by Abraham and Peled in the 1980s, a large number of studies have been done to understand the electrochemical mechanism of the Li/S cell and overcome its drawbacks. Studies have focused on increasing the electronic conductivity of sulfur by encapsulating sulfur with conducting materials such as porous carbon or conductive polymers, and suppressing polysulfide dissolution into the liquid electrolyte by coating with conductive polymers and oxides. It should be pointed out that most of the research efforts to improve the performance of Li/S batteries have focused on the cathode electrode.

From the electrolyte perspective, the use of conventional liquid electrolytes deteriorates battery performance due to polysulfide dissolution and their shuttle between cathode and anode that leads to fast capacity degradation and low Coulombic efficiency. Moreover, the use of these liquid electrolytes raises safety concerns since they are prone to leakage and safety hazard. The motivation for this PhD work is to search for better electrolyte systems for Li/S batteries. We aim to study the effect of these electrolytes on the performance of Li/S batteries in conjunction with designed cathode materials using sulfur/conductive polymer and sulfur/carbon composites.

In the first part of the thesis, we introduce gel polymer electrolytes (GPEs) into Li/S batteries with sulfur–polyacrylonitrile (S/PAN) composite cathodes. GPEs, consisting of solid matrices and embedded liquid electrolytes, may generally be defined as a polymer membrane that possesses ionic transport properties comparable to that of liquid electrolytes. In particular, for Li/S batteries, it is expected that the polymer membrane can act as a physical barrier, which can help control the dissolution of the polysulfide anions from the cathode and also prevent their migration to the anode. Specifically, the GPE was formed by trapping solutions of lithium hexafluorophosphate ($LiPF_6$) in ethylene carbonate electrolyte in a poly(vinylidene fluoride-co-hexafluoropropylene) (PVdF-HFP)-based polymer matrix. However, these Li/GPE/S cells suffer from performance fade after a few cycles due to the inability to retain liquid electrolyte in the GPE. A wide variety of methods were studied in order to improve the stability of the GPE and the performance of Li/S cells, including incorporation of layered nanoparticles, synthesis and addition of functionalized polymers and synthesis and addition of mesoporous nanoparticles. It was observed that incorporation of organically modified nanoparticles (OMMT) or functional polymer bearing inorganic domains reduces the pore size and improves the uniformity of pore size in the PVdF-HFP membrane, which prevents the release of electrolyte solution during cycling and suppresses the dissolution of polysulfides. The Li/S cell with the PVdF-HFP/OMMT nanocomposite electrolyte delivered an initial capacity of 1622 mAh g^{-1} and maintained a capacity of 500 mAh g^{-1} after 300 cycles. When the PVdF-HFP/functionalized PMMA electrolyte was used, the Li/S battery had an initial discharge capacity of 1600 mAh g^{-1} and a stable capacity of 1050 mAh g^{-1} after more than 100 cycles. Furthermore, utilization of the PVdF-HFP/functionalized PMMA/mesoporous silica composite electrolyte resulted in an initial discharge capacity of 1648 mAh g^{-1} and a stable discharge capacity of 1143 mAh g^{-1} after more than 100 cycles. The preparation procedures employed have the advantage of being reproducible, simple and inexpensive.

In the second part of the thesis, gel polymer electrolyte systems were prepared and tested in Li/S batteries with sulfur/carbon (S/C) composite cathodes. Sulfur/carbon (S/C) composite cathodes are of great interest since they potentially offer higher loading of sulfur (>60 wt%). However, severe capacity fading and low cycling efficiency due to lithium polyslfide dissolution and diffusion result in poor cyclability. Therefore, it is difficult to find a suitable electrolyte for this category of sulfur-based composite cathodes. The high-energy and low-cost S/C composite

cathode was synthesized through a facile one-step solution processing method, in which activated hardwood charcoal (AHC) powder was used as a scaffold to embed the sulfur active material and improve its electronic conductivity and its utilization in the battery cell. Results showed that normal gel polymer electrolytes could not effectively prevent polysulfide dissolution and performance fading. However, when a fluorinated liquid electrolyte containing1,1,2,2-tetrafluoroethyl-2,2,3,3-tetrafluoropropyl ether was employed, a significant improvement in the electrochemical performance of the Li/S cell was achieved. It was observed that such a low-cost Li/S cell can be operated for more than 300 cycles while still maintaining high specific capacity (600 mAh g^{-1}) and 97% Coulombic efficiency. Further analyses confirmed that such an enhanced performance was due to the confinement of lithium polysulfides inside the cathode electrode that prevented their shuttling between cathode and anode. This minimized the severe active mass loss that leads to fast capacity degradation and low Coulombic efficiency. The electrochemical performance of this new Li/S battery configuration represents a significant improvement in comparison to that of conventional electrolytes under the same testing conditions.

Acknowledgements

First and foremost, I would like to give my sincere thanks to my supervisor, Dr. Pu Chen, for his strong dedication towards my development of knowledge and skills in research. During my PhD study, I received great help from the following colleagues: Mahmoodreza Ghaznavi, Kaveh Sarikhani, Dr. The Nam Long DOAN, Dr. Denise Gosselink, Dr. Zhumabay Bakenov and Morteza Torabi. I give everlasting gratitude to them all.

I would also appreciate the nice collaboration with Dr. Yongguang Zhang and Aishuak Konarov. Many thanks to all of the members of Biomedical Engineering and Energy Storage Group especially Ran Pan, Parisa Sadatmousavi, Sameh Saad, Mohammad Mohammadi, Mousa Jafari, Majid Soltani, Mohammadali Sheikholeslam. All of them were always ready to help in any part of the project.

Special thanks go to my family for endless support and love. Without them, none of my achievements would be possible. The thesis is dedicated to all of them.

Table of contents

List of figures

List of Abbreviations

NMP: 1-methyl-2-pyrrolidinone

THF: Tetrahydrofuran

LiTFSI: Lithium bistrifluoromethanesulfonamide

$LiPF_6$: Lithium hexafluorophosphate

EC: Ethylene carbonate

DMC: Dimethylcarbonate

DEC: diethyl carbonate

DOL: 1,3-dioxolane

DME: 1,2-dimethoxyethane

TTE: 1,1,2,2-tetrafluoroethyl-2,2,3,3-tetrafluoropropyl ether

PAN: Polyacrylonitrile

PVdF: Polyvinylidene fluoride

PVDF-HFP: Poly(vinylidenefluoride-co-hexafluoropropylene)

PMMA: Poly(methylmethacrylate)

TEGDME: Tetraethylene glycol dimethyl ether

FTIR: Fourier Transform Infrared Spectroscopy

XRD: X-ray diffraction

BET: Brunauer-Emmet-Teller

CV: Cyclic voltammetry

EDX: Energy Dispersive Spectroscopy

SEM: Scanning electron microscopy

TEM: Transmission electron microscopy

KB: KetjenBlack

MMT: Montmorillonite nanoclay

Chapter 1

Introduction and Motivation

1.1 Overview

Demand for energy and environmental concerns associated with fossil fuel resources have triggered a search for alternative, clean and renewable energy sources [1-2]. Due to their high energy density, rechargeable lithium-ion batteries are among the most promising candidates for energy storage systems. In recent years, the interest has been steadily increasing to develop lithium-ion rechargeable batteries with high specific energy and extend their application to the fields of emerging technologies, such as electric vehicles (EV) and long-lasting portable electronic devices [3]. Limited by the relatively low capacity of cathode materials, the present lithium-ion batteries have practical energy densities below 300 W h kg^{-1}, which is insufficient for most of the aforementioned applications [3-5]. In this regard, alternative electrode materials with much higher charge capacities are of great interest.

Elemental sulfur possesses a theoretical specific capacity of 1672 mAh g^{-1} and specific energy of 2600 Wh kg^{-1}, which are the highest values among known cathode materials [4-9]. Comparison of theoretical specific energy and energy density of the lithium/sulfur cell with those of current lithium-ion cells is presented in Figure 1.1 [10]. In addition, the abundance and low price of sulfur offer the opportunity of producing cheap, safe and high-energy density cathodes. In contrast to conventional lithium-ion batteries, lithium-sulfur (Li/S) batteries operate on "integration chemistry", which enables the battery cell to tolerate excess charges or discharges, minimizing overcharge dangers characteristics of lithium-ion batteries [7-8].

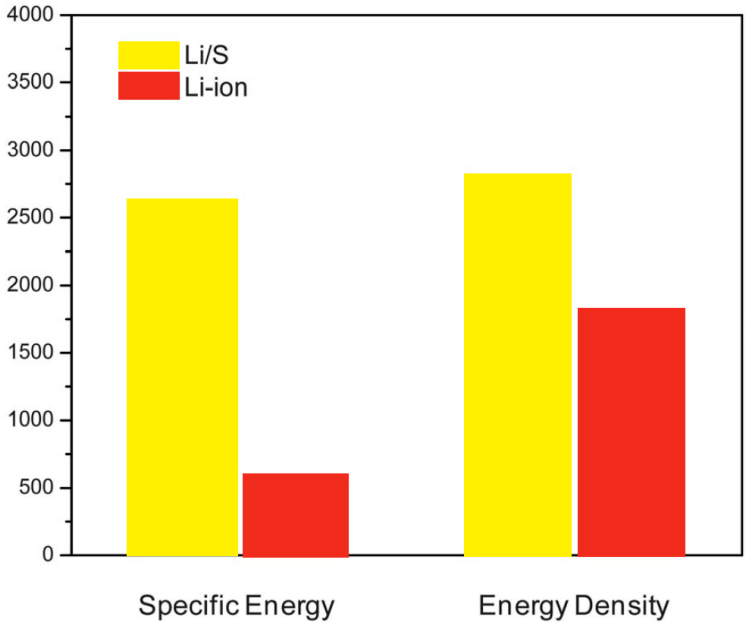

Figure 1.1 Comparison of the theoretical specific energy and energy density of Li/S batteries with those of state-of-the-art Li-ion batteries. Reprinted from Ref. [10] with permission of the Royal Society of Chemistry.

In a typical Li/S cell, elemental sulfur, as the cathode material, goes through a series of reduction reactions to convert high-order polysulfides Li_2S_n ($8 \leq n \leq 2$) to Li_2S during discharge process. This reaction is highly reversible and provides a high specific capacity of 1675 mAh g^{-1} and a theoretical gravimetric energy densities of ~ 2600 Wh kg^{-1} sulfur, with an average cell voltage value of about 2.15V [9]. This energy density is 3–5 times higher than any commercial Li-ion cell, as shown in Figure 1.1.

1.1 Fundamental chemistry of Li/S batteries

1.1.1 Discharge process

In a Li/S battery, discharge proceeds through two stages (Figure 1.2), associated with reduction reactions [10]. In the first step, within the potential range of 2.5–2.0 V (vs Li^+/Li), elemental sulfur is dissolved into the electrolyte solution and forms lithium octsulfide, as described below in a simplified form [11-15].

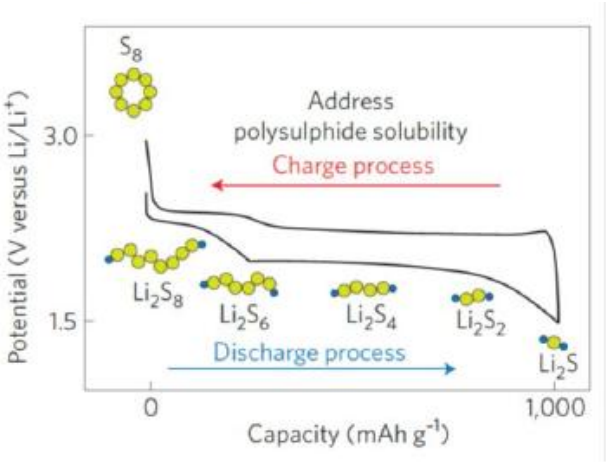

Figure 1.2 Typical charge/discharge curves of Li/S batteries. Reprinted from ref. [10] with permission from Nature Publishing Group.

$$S_8 + 2e^- + 2Li^+ \longrightarrow Li_2S_8,$$

$$Li_2S_8 \longrightarrow Li_2S_n + (8-n)S.$$

In the second step, the high-order polysulfides are further reduced and eventually produce insoluble Li_2S through a series of complex reactions. Below is one of the schemes suggested by Kolosnitsyn [11]:

$$Li_2S_n + 2e^- + 2Li^+ \longrightarrow Li_2S\downarrow + Li_2S_{(n-1)},$$

$$Li_2S_{n-1} + 2e^- + 2Li^+ \longrightarrow Li_2S\downarrow + Li_2S_{(n-2)},$$

$$Li_2S_2 + 2e^- + 2Li^+ \longrightarrow 2Li_2S\downarrow;$$

Barchasz [16] concluded that the discharge process of Li/S batteries depends on the electrolyte used in these cells. He then proposed a mechanism with 3 stages coupled with disproportion and electrochemical reactions, and observed the formation of a passivation layer on the positive electrode at the end of the discharge due to the precipitation of insoluble Li_2S_2 and Li_2S, which limited the accessibility and utilization of sulfur active material and the overall discharge capacity of the cell.

1.1.2 Charge Process

The charge process of Li/S cells also has two steps. In the first step, the high-order lithium polysulfides (Li_2S_n) are transformed to medium-order polysulfides (Li_2S_k) by reacting with insoluble Li_2S [11].

$$Li_2S + Li_2S_n \longrightarrow Li_2S_k + Li_2S_{n-k+1},$$
$$Li_2S_2 + Li_2S_n \longrightarrow Li_2S_k + Li_2S_{n-k+2}.$$

The second step of the reaction starts when the insoluble lithium polysulfide Li_2S is fully consumed. Here, the high-order lithium polysulfides are transformed to elementary sulfur by oxidation. The potential of this reaction is about 2.4-2.6 V (*vs* Li+/Li) [11].

$$mLi_2S_n - 2e^- - 2Li^+ \longrightarrow (m-1)Li_2S_{n-k} + S$$

Despite all of the advantages, the practical development of Li/S batteries is still prevented by the fast decay of capacity during cycling and the relatively low practical specific capacity (low utilization of sulfur active material), due to the poor electronic conductivity of sulfur, dissolution of lithium polysulfides, their high reactivity with the anode, and the significant volume change upon lithiation [7,9]. Since the early developments of Li/S batteries by Abraham [18] and Peled [19] in 1980s, a huge number of studies have been done to understand the electrochemical mechanism of this cell and overcome the drawbacks. Many studies have focused on increasing the electronic conductivity of sulfur and suppressing polysulfide dissolution into the liquid electrolyte [20-23]. Encapsulation of sulfur with conducting materials, such as porous carbon or conductive polymers, enables them to become electrically wired and therefore electrochemically active. Conductive polymers such as polyacrilonitrile (PAN) [24] and polypyrrole (PPY) [25,26] are usually used to prepare sulfur/polymer composites. Although sulfur/polymer composites generally improve the cycling performance of Li/S cells, a large amount of the conductive polymer should be mixed into the cathode, resulting in low sulfur content of the electrode. As a result, the purpose of this strategy seems to be more academic than practical [27]. On the other hand, a sulfur/carbon (S/C) composite potentially offers higher loading of sulfur. Various carbon materials, such as macro-, meso-, micro-porous carbon, carbon nanofibers, carbon nanotubes, carbon spheres have been used to prepare S/C composites.

However, poor cyclability and low cycling efficiency still persist [20,23,28-29]. A few recent studies have reported the use of activated carbon with high porosity and surface area in sulfur composite cathodes [30-31]. Activated carbon is a cheap and abundant material, which can be easily obtained from the carbonization of different materials such as wood, coal, and lignite [31].

In addition to deterioration of battery performance due to polysulfide dissolution, the use of liquid electrolytes raises some safety concerns since they are flammable and prone to leakage. Replacement of liquid electrolytes with gel polymer electrolyte provides advantages in simplified and flexible design and fabrication of Li/S batteries [32]. Gel polymer electrolytes consist of solid matrices and embed liquid electrolytes, that can provide mechanical strength and effectively reduce leakage of liquid electrolytes, while maintaining high lithium ion conduction.

It should be pointed out that most of the research efforts to improve the performance of Li/S batteries have focused on the cathode and neglected the role of the electrolyte. In this research, the electrolyte component in the Li/S battery cell is studied. In the first part of the thesis, we focus on the fabrication and utilization of a gel polymer electrolyte into Li/S batteries as an alternative to common liquid electrolytes in order to improve the electrochemical performance of these batteries by preventing polysulfide dissolution and migration. A wide variety of synthesis methods was evaluated to control the morphology and consequently the properties of GPEs. The preparation techniques employed have the advantage of being reproducible, simple and inexpensive, compared with most procedures reported in the literature.

In the second part of the thesis, we focus on the introduction of a fluorinated liquid electrolyte into the Li/S battery cell to suppress the dissolution of lithium polysulfide and improve its cycle life. In order to prevent the severe shuttle effect (polysulfide dissolution and migration) in conventional liquid electrolytes, we studied the incorporation of a fluorinated solvent, 1,1,2,2-tetrafluoroethyl-2,2,3,3-tetrafluoropropyl ether (TTE), in the electrolyte formulation and compared the performance of the conventional liquid electrolyte and the new fluorinated electrolyte in a Li/S cell under the same testing conditions.

Chapter 2

Background and Literature

2.1 General introduction to electrolytes for lithium/sulfur batteries

An electrolyte is any substance that contains free ions. Usually, an electrolyte consists of salt or salts that are dissolved in a medium. The role of the electrolyte in a battery cell is to provide a medium for transporting ions from one electrode to another, while simultaneously functioning as an electronic insulator so that electrons travel through the outer circuit of the device [33-36].

Based on the type of electrolyte material used, a Li/S battery cell can be divided into two categories: liquid Li/S and solid Li/S. The electrolyte in liquid Li/S battery usually consists of a lithium salt dissolved in an organic solvent or a mixture of solvents [37-39]. However, in the case of solid Li/S batteries, the electrolyte is composed of a polymer matrix containing dry lithium salt (so-called, solid polymer electrolyte) or salt dissolved in organic solvent contained within a polymer membrane (so-called, gel polymer electrolyte) [40-41]. The difference between gel polymer electrolytes and liquid electrolytes is the lack of mobile electrolyte solution which is stationary in the polymer structure.

2.1.1 Liquid electrolyte systems

These electrolytes consist of a lithium salt dissolved in an appropriate solvent or a mixture of solvents and an electronically isolated membrane (so-called, separator) to prevent a short circuit between the electrodes. They possess attractive properties such as high ionic conductivity, thermal stability within the ambient conditions, relatively large electrochemical stability window, ease of obtaining and handling [33-39]. The solvent choice is limited to those capable of solvating and conducting ions and that have low melting point, high boiling point and relatively low vapor pressure to provide a wide working temperature range. Ethylene carbonate (EC), propylene carbonate (PC) and diethylene carbonate (DEC) are the most common organic solvents used in liquid electrolyte systems. Since all of these criteria cannot be addressed by a single solvent, a mixture of solvents with varying chemical and physical properties are often

used together. Therefore, liquid electrolyte systems are commonly composed of a lithium salt dissolved in a mixture of two or more solvents [42-43].

Lithium salt also plays an important role in the liquid electrolyte of a lithium-ion battery. This salt provides lithium ions within the cell that move between positive and negative electrode during charge and discharge cycles of the battery. Different lithium salts are used in these liquid electrolytes and directly affect the battery performance in terms of capacity and cycle life. Most popular lithium salts are $LiClO_4$, $LiPF_6$, $LiBF_4$, and LiTFSI. Although $LiClO_4$ provides high ionic conductivity due to ease of its dissociation in organic solvents, its usage in lithium ion batteries is limited because of its very strong oxidizing nature which raises some safety issues [39]. $LiPF_6$ is another commonly used lithium salt which provides high ionic conductivity. Furthermore, this salt is very cheap, inherently flame-retardant and has excellent oxidation and reduction stability [44].

Cui et al. [45] synthesized a graphene-sulfur composite cathode material. PEG-containing surfactant-coated sulfur particles were synthesized and wrapped by carbon black decorated graphene oxide sheets. 1.0 M LiTFSI dissolved in 1,3-dioxolane (DOL)and 1,2-dimethoxyethane (DME) (volume ratio 1:1) was used as the electrolyte. A relatively stable specific capacity of ~600 mAh g^{-1} and less than 15% decay over 100 cycles were obtained (Figure 2.1).

Liang et al. [46] used $LiNO_3$ as an additive to modify liquid electrolytes in Li/S battery cells. The basic liquid electrolyte was composed of 0.5 M $LiCF_3SO_3$ dissolved in DOL/TEGDME (tetraethylene glycol dimethyl ether) (volume ratio 1:1). As shown in Figure 2.2, the new Li/S battery cell showed improved columbic efficiency and discharge capacity compared to the cell using the basic liquid electrolyte. This improvement was ascribed to the formation of a protective film on the lithium anode in the modified electrolyte which prevented the direct contact between lithium polysulfides and lithium metal anode.

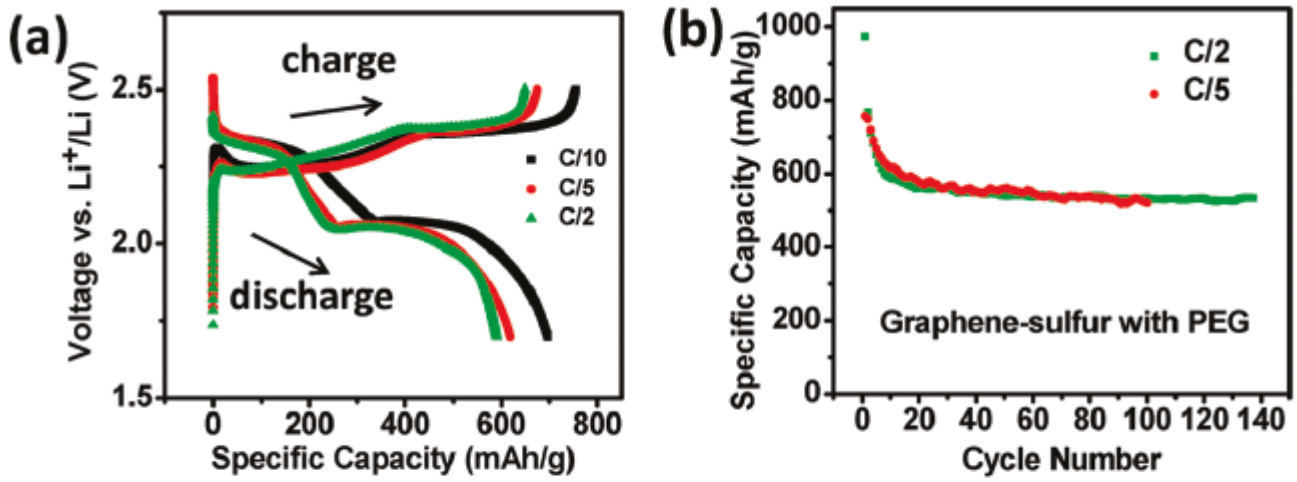

Figure 2.1. Electrochemical characterization of the Li/S cell (a) 10th cycle charge and discharge voltage profiles of the grapheme-sulfur composite with PEG coating at various rates. (b) Cyclability of the cell at rates of 0.2C and 0.5C. Reprinted from Ref. [45] with permission from American Chemical Society.

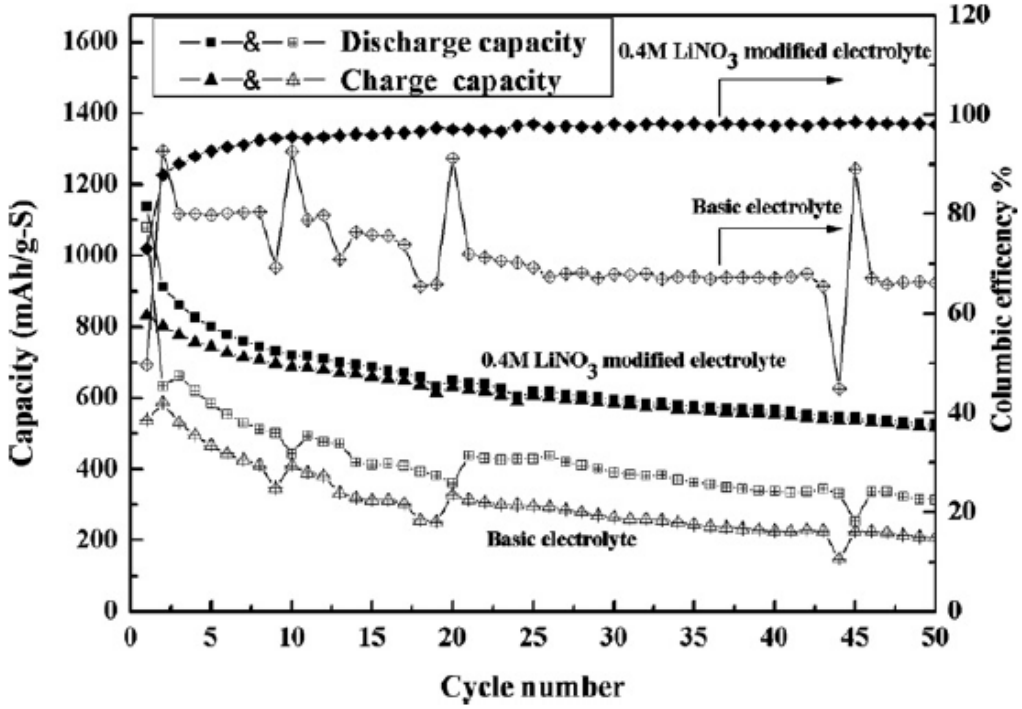

Figure 2.2. Cycling performances of the lithium sulfur batteries cycled with the 0.4 M LiNO3 modified electrolyte and the basic electrolyte. Reprinted from Ref. [46] with permission from Elsevier.

2.1.2 Solid polymer electrolyte systems

Solid electrolyte systems are interesting alternatives to the conventional liquid electrolytes in Li/S batteries due to their wider operating temperature range, long shelf life, flexibility of cell design and fabrication [47], improved cycle life by avoiding polysulfide dissolution which is a major issue in Li/S cells using liquid electrolytes. This category of electrolyte system provides achieving a solid-state Li/S battery configuration in which the polymer electrolyte plays a critical role in conducting lithium ions while blocking electronic flow.

In one classification, solid polymer electrolytes can be divided into two different categories [48];

1) Solvent-free or salt-polymer complexed systems in which lithium ion conduction is coupled to segmental and structural motions of polymer chains at temperatures higher than the glass transition of the polymer. 2) Gel or hybrid systems in which the ion conduction occurs through the liquid solvent upheld within the polymer structure.

Research efforts into developing polymer electrolytes for practical applications in Li/S batteries are centered on achieving high ionic conductivity at room temperature (about 10^{-3} S/cm), good electrochemical and mechanical stability. Therefore, the choice of polymer electrolyte plays an important role in the future of Li/S batteries [49].

2.1.2.1 Solvent-free electrolytes

In 1973, Wright et al. discovered that polyethylene oxide (PEO) complexes with alkali metals showed ionic conductivity. Since then, many research groups have focused on solvent-free solid state electrolytes and their possible application in lithium-ion batteries. PEO has been considered as the most promising candidate for this purpose because of its solvation power, complexing ability and ability to transport ions directly connected with the alkaline salt (Li^+) [40]. When lithium salt is added to the polymer matrix, it dissociates due to the polar effect of the ether oxygen in the polymer backbone. Then, the lithium ions can hop among the negative charge sites and move along the polymer chains. This type of ion conduction is facilitated by

movements of flexible polymer chains and can only occur in amorphous polymer chains in which segmental dynamics and rearrangements can occur [50-52]. PEO is a semi-crystalline polymer with crystallinity of about 72% at room temperature [47].

The major drawback of using solvent-free polymer electrolytes in lithium-ion batteries is their low ionic conductivity at ambient temperature. Thus, a large number of studies have been performed to inhibit PEO crystallization [53-57]. Jeon et al. [58], fabricated a solid polymer electrolyte composed of PEO and tetra(ethylene glycol dimethyl ether) and used it in a Li/S battery cell. This cell exhibited poor capacity retention. Changes in the morphology of sulfur-based composite cathode was studied by scanning electron microscopy (SEM), and a model for the changes in morphology of the cathode electrode was proposed (Figure 2.3). The authors suggested a mechanism for the capacity fading of the battery cell which was ascribed mainly to the heterogeneous and non-uniform distribution of sulfur in the cathode.

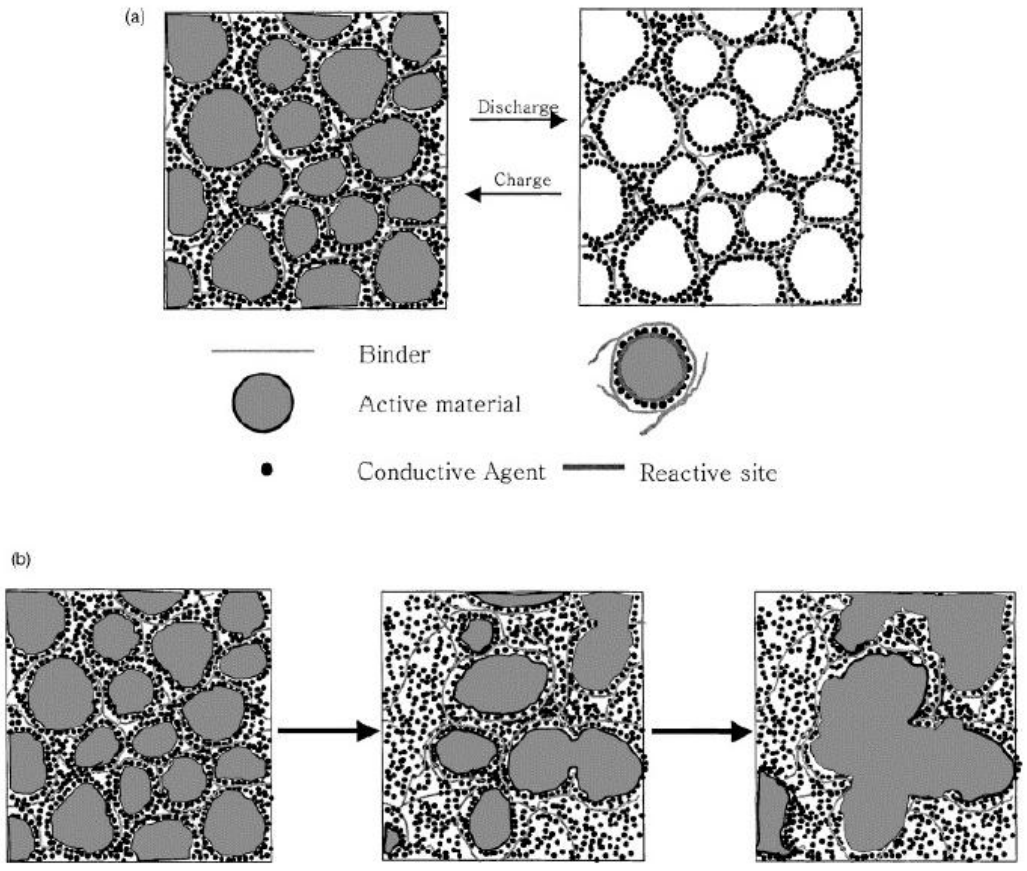

Figure 2.3. A Model proposed for the changes in the morphology of cathode electrode during cycling: (a) ideal case; (b) real case. Reprinted from Ref. [58] with permission from Elsevier.

Shin et al. [59] fabricated $(PEO)_{10}LiCF_3SO_3$ solid polymer electrolytes consisting titanium oxide particles (Ti_2O_3, TiO and Ti_2O). They investigated the ionic conductivity as well as the interfacial stability of this dry polymer electrolyte and the performance of Li/S cells with this $(PEO)_{10}LiCF_3SO_3$ polymer electrolyte. They found that titanium oxide is a good candidate as ceramic filler in $(PEO)_{10}LiCF_3SO_3$ dry polymer electrolyte. The size of Titanium Oxide particles was in the range of sub-micron to several microns prepared by high speed ball milling for a long time (100 h). Incorporation of titanium oxide (Ti_2O_3, TiO and Ti_2O) into the polymer electrolyte improved the ionic conductivity mainly due to the changes in -C-O-C- vibration and ionic structure of polymer electrolyte by the decrease in crystallinity of PEO polymer matrix. Moreover, the interfacial resistance between polymer electrolyte and lithium electrode was considerably decreased by reducing the contact area between lithium and electrolyte.

Scrosati et al. [49] developed another PEO-based solid state electrolyte for Li/S battery applications. The ionic conductivity of the polymer electrolyte and therefore the performance of this Li/S cell was found to be very dependent on the operating temperature. The polymer electrolyte showed ionic conductivity values of practical interest, i.e. on the order of 10^{-4} –10^{-3} S /cm at 70 °C and above (Figure 2.4). A relatively low specific capacity was obtained at 70 ^{o}C, while the capacity at 90 °C was close to the theoretical capacity of Li/S cell (Figure 2.5).

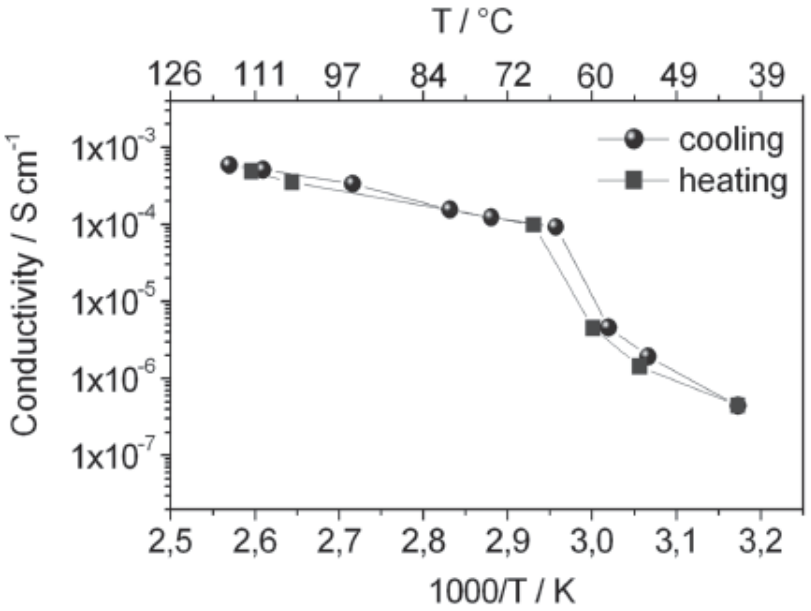

Figure 2.4. Arrhenius conductivity plot for the polymer electrolyte on heating and cooling scans. Reprinted from Ref. [49] with permission from Wiley.

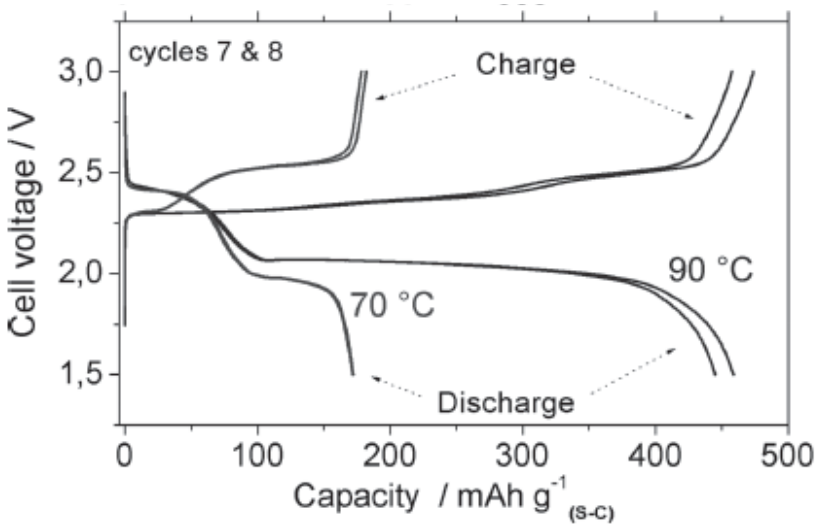

Figure 2.5. Discharge-charge cycles of a solid-state Li/S battery at 70 °C and 90 °C at C/20 rate over the 1.5–3 V voltage range. The specific capacity is reported in terms of total composite mass. Reprinted from Ref. [49] with permission from Wiley.

Jeong et al. [60] studied $(PEO)_6LiBF_4$ solid polymer electrolyte. They prepared these electrolytes with three different mixing procedures: ball-milling, ball-milling the polymer electrolyte with 10 wt% Al_2O_3, and stirring. They observed that the Li/S cell with ball-milled $(PEO)_6LiBF_4$-Al_2O_3 composite electrolyte showed a higher initial discharge capacity than other cells (1670 mAh g^{-1}). Furthermore, the Li/S cell with ball-milled $(PEO)_6LiBF_4$-Al_2O_3 showed a significantly improved cycling performance as compared to the other cells. The cycle life of this Li/S polymer battery was further improved by modifying the procedure of preparing sulfur-based composite cathode. Sulfur was mixed with PEO through thermal melting at 180 °C in a sealed container. The SEM was used to investigate the mechanism of capacity fading in this cell. They concluded that capacity fading was mostly due to aggregation of sulfur active material or lithium polysulfides during cycling.

Wen et al. [61] proposed an $Al_2O_3(PEO)_{20}Li(CF_3SO_2)_2N$-$\gamma LiAlO_2$ electrolyte to improve the performance of the solid-state Li/S batteries. This all-solid-state Li/S cell was tested at 75 °C and exhibited an average capacity of 290 mAh g^{-1} after 50 cycles. Another study combined $(PEO)_{18}Li(CF_3SO_2)_2N$-$SiO_2$ polymer electrolyte and sulfur/mesoporous-carbon composite cathode in a Li/S cell [51]. The ionic conductivity of this polymer electrolyte reached 5×10^{-4} S cm^{-1} at 70 °C. The battery cell showed a good cycling performance with a reversible discharge capacity of about 800 mAh g^{-1} at 70 °C after 25 cycles.

In a recent study, Yu et al. [62] fabricated an all-solid-state Li/S battery with utilization of siloxane cross-linked network solid electrolyte at ambient temperatures. This polymer electrolyte (SPE) was synthesized by crosslinking reaction between a homogeneous precursor solution of siloxane cross-linker, tetra (ethylene oxide) dimethyl ether, lithium salt ($LiCF_3SO_3$) and benzoyl peroxide (BPO) as an initiator. The obtained polymer electrolyte showed a relatively high ionic conductivity (3×10^{-4} S cm^{-1} at ambient temperature) and a wide electrochemical stability window (0 - 3.85 V vs Li). The all-solid-state Li/S battery was assembled by sandwiching the polymer electrolyte between lithium metal and sulfur-based cathode electrode as shown in Figure 2.6. This battery delivered an initial discharge capacity of 1044 mAh g^{-1} at room temperature. However, the discharge capacity rapidly decreased to 512 mAh g^{-1} after 10 cycles.

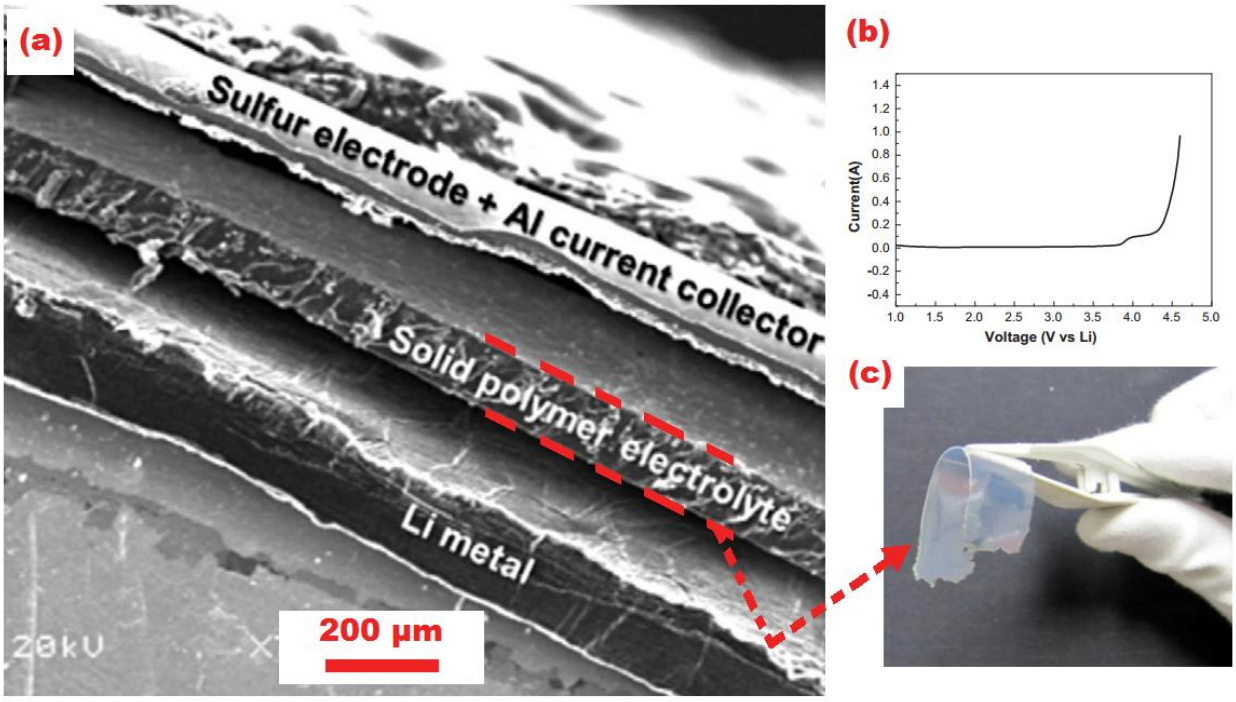

Figure 2.6. (a) A cross-sectional SEM image of the all-solid-state Li/S battery, (b) Linear voltammetry graph of polymer electrolyte at ambient temperature, (c) The photograph the solid polymer electrolyte. Reprinted from Ref. [62] with permission from Elsevier.

2.1.2.2 Gel polymer electrolytes

Despite the large number of studies on solvent-free polymer electrolytes, their low ionic conductivity at ambient temperatures has made them an unrealistic choice for practical lithium-ion and lithium/sulfur battery applications. However, gel polymer electrolytes (GPEs) seem to be a promising alternative in these batteries. GPEs consist of three constituents; polymer, organic solvent and lithium salt. The lithium salt is dissolved in the solvent to form the electrolyte and is responsible for the electrochemical properties. The polymer matrix provides mechanical strength and holds the electrolyte solution.

GPEs can provide ionic conductivities as high as 10^{-3} S/cm at room temperature [63]. The electrolyte solution can act as a plasticizer and lower the T_g of the polymer matrix and facilitate segmental motions of the polymer chains and improve lithium ion conduction in the system. Therefore, lithium ion conduction in a GPE occurs through segmental motions of polymer chains combined with the solution [59, 63-64]. So, the higher the amount of electrolyte solution present, the higher is the ionic conductivity. Unfortunately, an increase in the amount of electrolyte solution causes the mechanical properties of the polymer electrolyte to degrade. Thus, control of the amount of the electrolyte present is key to achieving gel polymer electrolytes with optimum properties [63].

Beside ionic conductivity, the electrochemical stability, thermal stability and mechanical strength are other key parameters in evaluating the quality of a GPE. Electrochemical stability determines the operating voltage range of the GPE. This parameter can be obtained by recording the response of current versus voltage through cyclic voltammetry measurements. The GPE is electrochemically stable up to the voltage in which current begins to increase. An electrochemically unstable GPE can affect the ongoing charge and discharge reactions between the electrodes and lead to reduced capacity and energy density. Thermal stability of the GPE is another important parameter to ensure the safety of the Li/S battery cell. Charge and discharge reactions produce heat which can affect and partly decompose or melt the polymer electrolyte, which may cause short circuits in the cell. Also, this heat can cause self-discharging of the cell and shortening of the shelf life. Mechanical stability of the GPE is another key parameter in fabricating, processing and finally inserting the GPE in the battery cell.

Similar to the liquid electrolyte systems, the choice of lithium salt and organic solvent plays a key role in overall performance of the GPE. More importantly, the affinity of the polymer and electrolyte solution is a key factor in GPE development. The polymers generally studied for these systems are poly(ethylene oxide) (PEO) [66-67], polyvinylidene fluoride (PVdF) [61,65], poly(methylmetacrylate) (PMMA) [68-69], poly(acrylonitrile) (PAN) [70], poly(vinylchloride) (PVC) [71-72] and polyvinylidene fluoride-*co*-hexafluoropropylene (PVdF-HFP) [73-80]. PMMA and PAN have the advantages of easy synthesis procedures and relatively low interfacial resistance with lithium metal. However, poor mechanical stability due to their ductility is a limiting factor for practical applications. PVdF provides high thermal and electrochemical stability and has a relatively high dielectric constant ($\varepsilon = 8.4$) for a polymer, which can facilitate ionization of lithium salts and provide a high concentration of charges [81-82]. PVdF-based GPEs are expected to have stability against oxidation due to the strong electron-withdrawing functional group (–C–F). However, poor electrolyte solution uptake and low plasticity due to its crystalline nature are the remaining problems.

In a recent work, Scrosati et al. [83] built a lithium metal-free battery as shown in Figure 2.7. They replaced the common liquid organic solutions with a GPE that was formed by trapping ethylene carbonate/dimethylcarbonate lithium hexafluorophosphate (EC: DMC/LiPF6) solution saturated with lithium sulfide in a PEO/$LiCF_3SO_3$ polymer matrix [84]. Incorporation of Zirconium dioxide (ZrO_2) ceramic filler improved the mechanical properties of the GPE and also improved liquid retention within the bulk of GPE [85]. AC Impedance studies revealed the low and stable resistance of the GPE with time, and a high ionic conductivity, around 10^{-2} S▪ cm^{-1} (Figure 2.8). The battery cell assembled with Sn/C anode, Li2S/C cathode and PEO based GPE delivered a high initial discharge of ~ 1200 mAh g^{-1} (based on Li2S mass only) at 38 $mAcm^{-2}g^{-1}$.

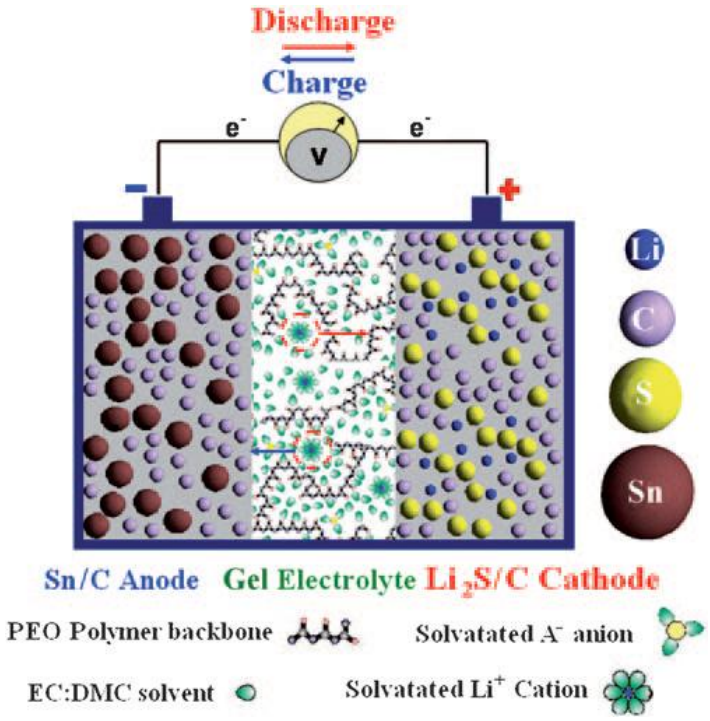

Figure 2.7. Scheme of the Sn-C/CGPE/Li2S-C polymer battery. Reprinted by permission from Wiley-VCH Verlag GmbH & Co. KGaA. from Ref. 83.

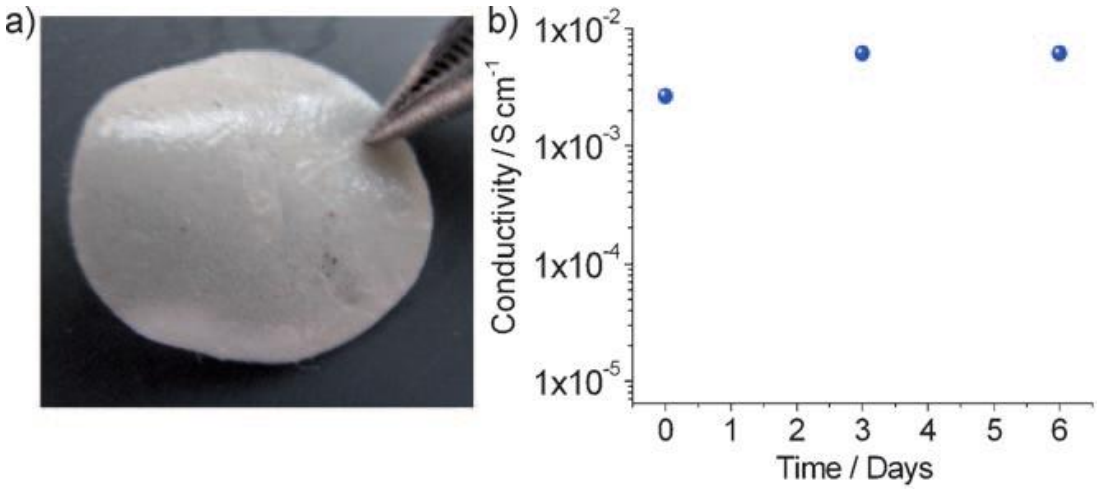

Figure 2.8. Characteristics of the PEO based GPE. Reprinted by permission from Wiley-VCH Verlag GmbH & Co. KGaA. from Ref. 83.

This research group further investigated this new polymer battery [86]. In situ XRD analysis on this cell revealed that during charge process lithium polysulfides can be converted into elemental sulfur. During the following process, elemental sulfur can be re-converted back

into polysulfides. This new GPE efficiently allowed the electrochemical processes within the battery cell. This means that this safe and highly conductive GPE is a perfect replacement for the unstable organic electrolyte solution. Moreover, the Li2S-C composite cathode can be considered as a promising alternative for the novel rechargeable lithium-ion sulfur batteries in which the reactive and unsafe lithium metal anode is replaced by a reliable, high capacity Sn-C composite anode.

A detailed discussion regarding the discharge process of Li/PVDF/S was presented by Ryu *et al.* [87] prepared a GPE based on PVDF as matrix, $LiCF_3SO_3$ as lithium-ion resource, tetraglyme as plasticizer. A freestanding GPE was obtained and tested in a Li/S cell. This delivered an initial discharge capacity of 1268 mAh g^{-1} with two distinct plateaus-like potential regions. The capacity dropped to 1028 mAh g^{-1} after second discharge and the upper plateau region disappeared. A model was proposed based on the results obtained from XRD and DSC of the sulfur electrode (shown in Figure 2.9**)** which suggested that elemental sulfur converted into Li2Sn ($n > 4$) at the upper plateau region and Li_2S was formed at the low plateau region.

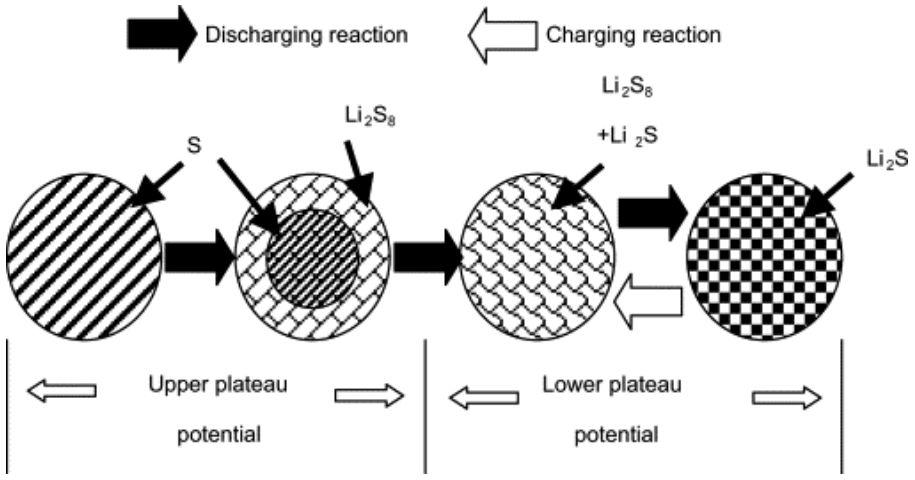

Figure 2.9. Model proposed for the electrochemical reactions of lithium/sulfur cell. Reprinted from Ref. [87] with permission from Elsevier.

Among all polymers, PVdF-HFP was found to meet all the basic requirements of a polymer electrolyte since it has a high dielectric constant ε = 8.4, the crystalline units of the vinylidene fluoride provide excellent chemical and mechanical stability and the amorphous hexafluoropropylene (HFP) units increase the plasticity of the membrane and yield high ionic conductivity [88-89].

Shin et al. [64] reported the fabrication of PVdF-HFP GPE using a ball-milling technique. Tetra-ethylene glycol dimethylether (TEGDME) was used as a plasticizer, $LiCF_3SO_3$, $LiBF_4$ and $LiPF_6$ as lithium salt and acetone as the solvent. This polymer electrolyte showed good mechanical properties and ionic conductivity of 4.99×10^{-4} S cm^{-1} at ambient temperature. The resulting GPEs were introduced into Li/S cells and the batteries delivered initial specific discharge and charge capacities of ~ 575 and 765 mAh g^{-1} at the current rate of 0.14 mA cm^{-2} at room temperature.

Wang et al. [63] prepared PVdF-HFP/SiO_2 porous membranes by a phase separation method using acetone/ethanol as solvent/non-solvent (Figure 2.5). The GPE showed an ionic conductivity of ~ 1.2×10^{-3} S cm^{-1} at room temperature (Figure 2.10). The electrochemical properties of this GPE were tested in Li/S battery cells with two different sulfur-based cathode materials-sulfur/active carbon (S/C) composite and sulfur/polyacrylonitrile (S/PAN) composite. The cell with S/C composite cathode exhibited a reversible capacity of 440 mAh g^{-1} after 25 cycles (Figure 2.11). However, the cell with S/PAN composite cathode exhibited an initial discharge capacity of 850 mAh g^{-1} and capacity of about 600 mAh g^{-1} after 50 cycles (Figure 2.12).

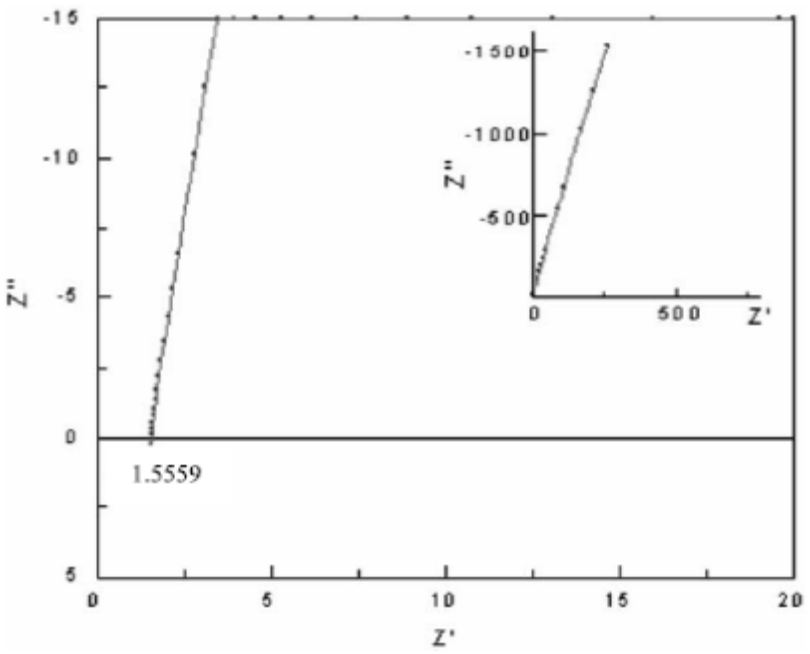

Figure 2.10. Impedance spectrum of SS/gel electrolyte/SS cell. Reprinted from Ref. [63] with permission from Elsevier.

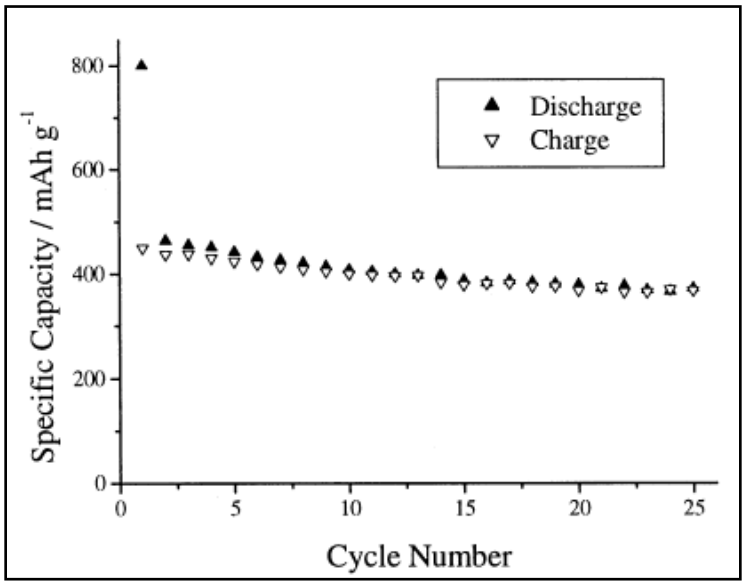

Figure 2.11. Cycling performance of the S/C composite cathode. Reprinted from Ref. [63] with permission from Elsevier.

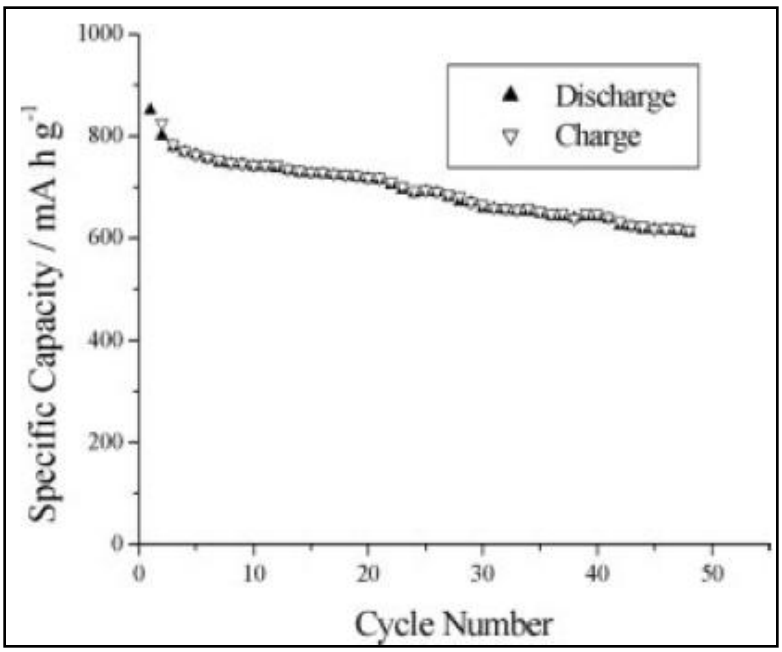

Figure 2.12. Cycling performance of the S/PAN composite cathode. Reprinted from Ref. [63] with permission from Elsevier.

Jin et al. used a simple phase separation process to prepare PVdF-HFP membrane with a highly porous structure (Figure 2.13) [90]. They reported that the homogeneously distributed micropores of the membrane had a diameter range of 3-5 μm, and the uniform and interconnected skeleton porous structure gave the membrane the ability to absorb enough electrolytes and act as a framework for lithium ion conduction. The GPE was then prepared by soaking the porous membrane in N-methyl-N-butylpyrrolidinium bis(trifluoromethanesulfonyl) imide ionic liquid. The resulting GPE showed good thermal stability, high electrochemical stability (>5.0 V vs. Li/Li+) and good interfacial stability with lithium metal electrode. The Li/S cell assembled using this GPE delivered an initial discharge capacity 1217 mAh g^{-1} and maintained a capacity of 818 mAh g^{-1} after more than 20 cycles at a current density of 50 mA g^{-1}.

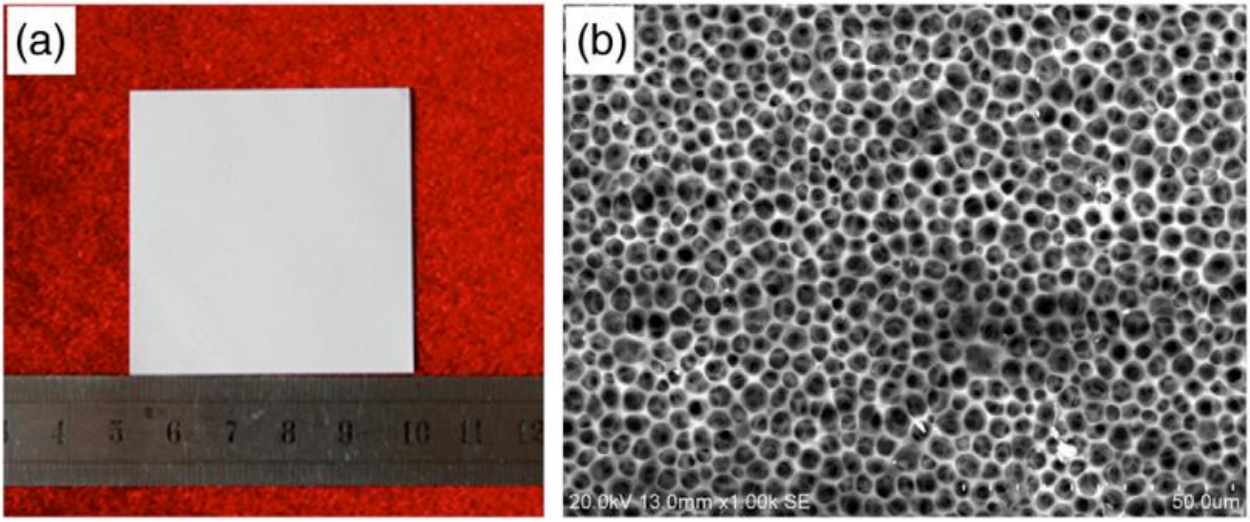

Figure 2.13. Photograph (a) and SEM image (b) of PVdF-HFP porous membrane. Reprinted from Ref. [90] with permission from Elsevier.

In summary, gel polymer electrolytes consist of a liquid trapped in a porous polymer membrane. Their ionic conductivity depends strongly on the properties of the liquid electrolyte provided that the membrane is composed of connected micropores that can act as channels for lithium ion conduction. If the prepared membrane does not have a connected microporous structure, the transfer of lithium ions mainly occurs in the polymer membrane [91]. For this reason, modification of the structure of the polymer to achieve highly porous membranes with small pore size is one of the most important strategies to improve lithium transport and ion conductivity of GPEs in Li/S batteries. This can be achieved by optimizing preparation method and modification of the polymer matrix, such as blending, copolymer and cross-linking, compounding and adding nanoparticles.

2.2 Scope of this work

High-energy lithium/sulfur batteries provide much promise, but also have many challenges. In general, poor cycle life is the main drawback of Li/S batteries, mainly due to the dissolution of lithium polysulfides into the electrolyte. To overcome this problem, this study focuses on the electrolytes for rechargeable Li/S batteries.

Two approaches have been considered for this purpose. First, fabrication of an effective gel polymer electrolyte by modifying the pore size and its distribution to enhance the uptake and retention of electrolyte and suppress polysulfide migration. Second, we focus on the introduction of a fluorinated liquid electrolyte into the Li/S battery cell to suppress the dissolution of lithium polysulfide and improve its cycle life. As results will show, the Li/S cell showed a better cycle performance using these approaches. However, problems associated with Li/S batteries could not be solved solely by modifying the electrolyte. Combined with advances in the anode and cathode, the development of an effective electrolyte with high conductivity and compatibility can offer a promising future for Li/S batteries.

Chapter 3

Electrochemical performance of lithium/sulfur battery with polymer nanocomposite electrolytes[1]

3.1 Introduction

Two types of nano-layered silicates, sodium montmorrilonite (Na^+-MMT) and organically modified montmorrilonite (OMMT) [92] were incorporated into a PVdF-HFP matrix to fabricate highly porous nanocomposite membranes with small and uniformly distributed pores to improve the retention of the liquid electrolyte in the membrane and therefore prevent the release of electrolyte during cycling.

3.2 Experimental

3.2.1 Preparation of polymer electrolytes

PVdF– HFP (Kynar Flex 2801, 12 wt% HFP) was used with Na^+-montmorillonite (Na^+-MMT) and organically modified montmorilonite (OMMT, 30B), purchased from Southern Clay and kept in oven at 473 K for one week prior to testing. Acetone was used as a solvent and tert-butyl methyl ether (extra pure, Acros Organics) was used as a non-solvent. Microporous polymer nanocomposite films were prepared by a phase inversion technique using acetone/ether as solvent/non-solvent. PVdF–HFP and nano-layered silicates (2.5 wt%) were dissolved in acetone by mechanical stirring overnight. This was followed by ultrasonic sonication for 1 h to form a homogenous casting solution at a PVdF–HFP concentration of 4 wt% at room temperature. Tert-butyl methyl ether (10 wt% based on the amount of acetone) was added further to this solution and left agitating until the solution was homogeneous. The resulting solution was poured onto a clean aluminum weighing pan. After complete evaporation of acetone and ether, a white and opaque microporous membrane formed. Finally, the membrane was dried at 80 $^{\circ}$C in a vacuum oven for 24 h to remove any further traces of acetone and ether. A similar preparation method was adopted for preparation of the microporous PVdF-HFP membrane without incorporation of nano-layered silicates.

[1] Data presented in this chapter was published in Ref. [115].

3.2.2 Preparation of sulfur/polyacrylonitrile/$Mg_{0.6}Ni_{0.4}O$ composite cathode

Nanosized $Mg_{0.6}Ni_{0.4}O$ was synthesized by using the simple self-propagating high temperature synthesis method. 0.6 mol $Mg(NO_3)_2$ (98% purity, Sigma-Aldrich), 0.4 mol $Ni(NO_3)_2$ (98% purity, Sigma-Aldrich) and 3.5 mol glycine (Fisher Scientific, 98.5% purity) were dissolved in 100 mL deionized water. The solution was then heated to evaporate the excess water. The resulting viscous liquid ignited and underwent self-sustaining combustion to form ash composed of nickel and magnesium oxide. This was calcined at 700 ◦C in air for 6 h and pulverized to $Mg_{0.6}Ni_{0.4}O$ powder. To make the sulfur/PAN/$Mg_{0.6}Ni_{0.4}O$ ternary composite, sulfur (100-mesh particle size powder, Sigma-Aldrich), PAN and $Mg_{0.6}Ni_{0.4}O$ were mixed in a weight ratio of 4:1:0.25. This mixture was ball-milled (pulverisette 7, Fritsch) at 800 rpm for 2 h with ethanol as a dispersant and then dried in a vacuum oven at 65 ˚C for 3 h to remove the solvent. This was followed by a heat-treatment at 350 ˚C for 3 h in argon gas to allow sulfur to melt and react with the PAN [93-95]. The amount of active material in the heat treated composite was 47 wt%.

The S/PAN/$Mg_{0.6}Ni_{0.4}O$ composite cathode was prepared by mixing 80 wt% of S/PAN/$Mg_{0.6}Ni_{0.4}O$ composite, a conductor of 10 wt% acetylene black (99.5% purity,MTI) and a binder PVdF (Kynar, HSV900) dissolved in N-methyl-2-pyrrolidene (NMP) (≥99.5% purity, Sigma-Aldrich). The resultant slurry was then spread onto circular nickel foam (≥99% purity, MTI) of 1 cm diameter. This was left to dry in a vacuum oven for 12 h at 60 ◦C. The cathode electrode was pressed at 8 MPa using a hydraulic press to assure good contact.

3.2.3 Preparation of sulfur/carbon composite cathode

Ketjen black (KB, EC600JD) and sulfur in a weight ratio of 1:2 were mixed using an agitating mortar. This was followed by grinding the mixture in a planetary-type ball mill at a rotational speed of 450 rpm for 4 h. Then, the mixed powders were compressed under 8 MPa into a small pellet. Subsequently, the pellet was heated at 155 ˚C for 12 h in oven in order to melt the sulfur and allow the melted sulfur to diffuse into the pores of KB. Finally, the sample was kept at 300 ˚C for 2 h to evaporate sulfur remaining at the surface of KB. The cathode electrode was prepared by mixing 60 wt% S/KB composite, 20 wt% acetylene black (AB, MTI, 99.5% purity) as conductive agent and 20 wt% polyvinylidene fluoride (PVDF, Kynar, HSV900) as a

binder with NMP (Sigma-Aldrich, ≥99.5% purity) as a dispersant. The obtained slurry was then applied to an Al foil current collector and was dried in a drying oven at 70 ◦C for 12 h.

3.2.4 Characterization of the materials

The crystalline phases of the samples were characterized by using X-ray diffraction (XRD) analysis (D8 Discover, Bruker) equipped with Cu-Kα radiation. The porosity and morphology of the samples were investigated by using field emission scanning electron microscopy (FE-SEM) (Leo-1530, Zeiss). The samples were gold-sprayed prior to SEM measurements. The morphology and roughness of the surface of electrolyte membranes were examined using atomic force microscopy (AFM) (Molecular imaging, Agilent). The mechanical properties of the microporous polymer membranes were measured by an universal tensile machine (Instron model 3365) at a constant cross-head speed of 1 mm/min according to the ASTM D 638 method. The specimen dimensions were 50 mm × 5 mm× 80 μm. Thermal stability of the samples was examined by using differential scanning calorimetry-thermogravimetric analysis (DSC-TGA) (Q-600, TA instruments) using the temperature ramp mode at a heating rate of 10 ◦C min^{-1} from room temperature up to 600 ◦C in a N_2 atmosphere.

3.2.5 Electrochemical characterization

Electrochemical stability window of the polymer electrolytes was determined by running cyclic voltammetry at 0.2 mVs^{-1} between 0–5 V in three-electrode cell using stainless steel as the working electrode, lithium as both the counter and the reference electrodes and the polymer electrolyte using a Biologic potentiostat at 0.2 mVs^{-1} between 0–5 V. The Li/GPE/sulfur-based cathode coin cells were assembled in a glove box. The polymer electrolyte was inserted between the composite cathode and the lithium foil anode which were then sealed in a coin-type battery cell. For the S/PAN/$Mg_{0.6}Ni_{0.4}O$ composite cathode, the gel polymer electrolyte was obtained by soaking the polymer membrane in a 1M $LiPF_6$ dissolved in a 1:1 (v/v) mixture of ethylene carbonate (EC) and diethylene carbonate (DEC). When a S/C composite cathode was used, the gel polymer electrolyte was obtained by soaking the polymer membranes in a liquid electrolyte consisting of a 1M lithium bistrifluoromethanesulfonamide (LiTFSI) (Aldrich, 99.95%) dissolved in tetraethylene glycol dimethyl ether (Aldrich, 99% purity). AC impedance spectroscopy was performed at room temperature with a potentiostat (VMP3, BioLogic) over the

frequency range from 1 Hz to 100 KHz. A galvanostatic charge/discharge test was carried out within a voltage range of 1–3 V at a discharge rate of 0.2 C (1C = 1672 mAh g^{-1}).

3.3 Results and Discussion

When the non-solvent tert-butyl methyl ether is added into the PVdF–HFP/acetone or PVdF-HFP/nanoparticle/acetone solution, precipitation occurs. At low non-solvent contents, the polymer still remains dissolved and the solution is homogenous. However at sufficiently high non-solvent contents, the polymer will precipitate. After complete evaporation of the solvent and non-solvent, a porous dry membrane is obtained. During the evaporation process, the formerly transparent film gradually becomes opaque due to the formation of microcellular foam within the membrane.

Hydrophobic nano-layered silicates interact with hydrophobic polymers. Therefore, it is expected that PVdF-HFP can easily interact with organically modified montmorillonite (OMMT) and probably form an intercalated or exfoliated structure. On the other hand, the presence of hydrated Na^+ between the galleries makes the Na^+-MMT hydrophilic, so that hydrophilic polymers can mix with the OMMT without having to modify the silicate hosts. Dispersion of Na^+-MMT in hydrophobic matrixes is difficult and only low amounts of these nanoparticles can interact and possibly intercalate or exfoliate in the PVdF-HFP matrix. A 2.5 wt% of nanoclay was selected for preparation of the nanocomposites. Figure 3.1 shows the XRD patterns for the pristine nanoparticles, PVdF-HFP and their nanocomposites. As shown, the pristine OMMT and Na^+-MMT nanoclays show intensive peak at around 5° and 8°, respectively. However, for both nanocomposite samples these peaks disappear, which is consistent with an exfoliated nanoparticle morphology in both of these systems.

The morphology and pore distribution of the membranes were examined by SEM (Figure 3.2). By incorporation of nanoparticles, the pore size decreases but the pore numbermand its uniformity increases (Figure 3.2). An appropriate amount of porosity is necessary to uptake sufficient amounts of a liquid electrolyte and maintain good conductivity. However, in the case of a highly porous membrane, the pores cannot hold the liquid electrolyte solution effectively during cycling of the battery cell. Therefore, high porous membranes with small and uniformly distributed pore size and good mechanical stability are required for Li/S batteries.

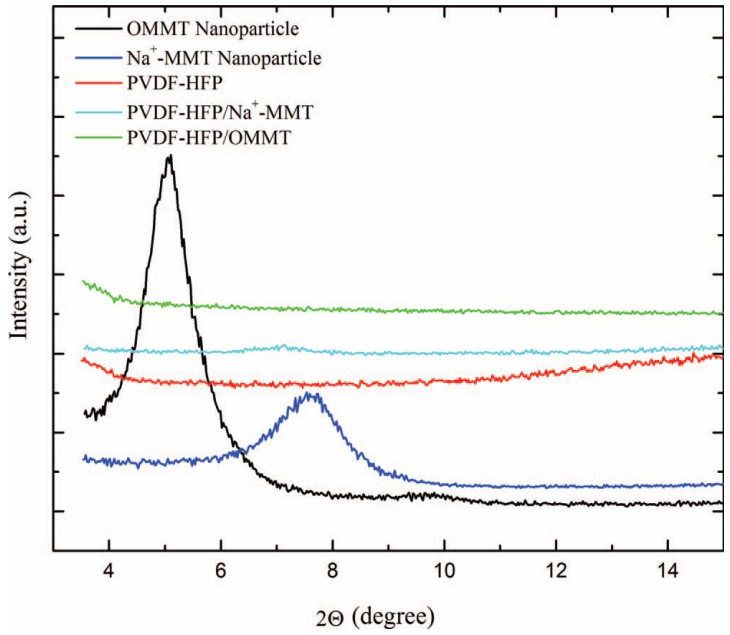

Figure 3.1. XRD patterns obtained for the OMMT, Na^+-MMT, PVdF-HFP, PVdF-HFP/30B OMMT, and PVdF-HFP/Na^+-MMT samples.

Surface morphology, roughness and pore size of the polymer membranes were examined by AFM to obtain images shown in Figures 3.3 and 3.4. From the SEM images, it was concluded that incorporation of nanoparticles reduces the pore size of the membranes. AFM topographic images further display the microstructures of the surface of membranes. The PVdF-HFP membrane has rougher surface than that of nanocomposite membranes. Roughness in height mode for PVdF-HFP, PVdF-HFP/Na^+-MMT, and PVdF-HFP/OMMT membranes are 139 nm, 79 nm, and 131 nm, respectively. By incorporation of Na^+-MMT nanoparticles, the surface roughness decreases, which can be attributed to the decrease in pore size and pore number. On the other hand, roughness of the PVdF-HFP/OMMT membrane is almost the same as that of pure PVdF-HFP membrane. Hence, from both SEM and AFM images it can be concluded that incorporation of organically-modified nanoparticles results in having a highly porous membrane with smaller and more uniformly distributed pores.

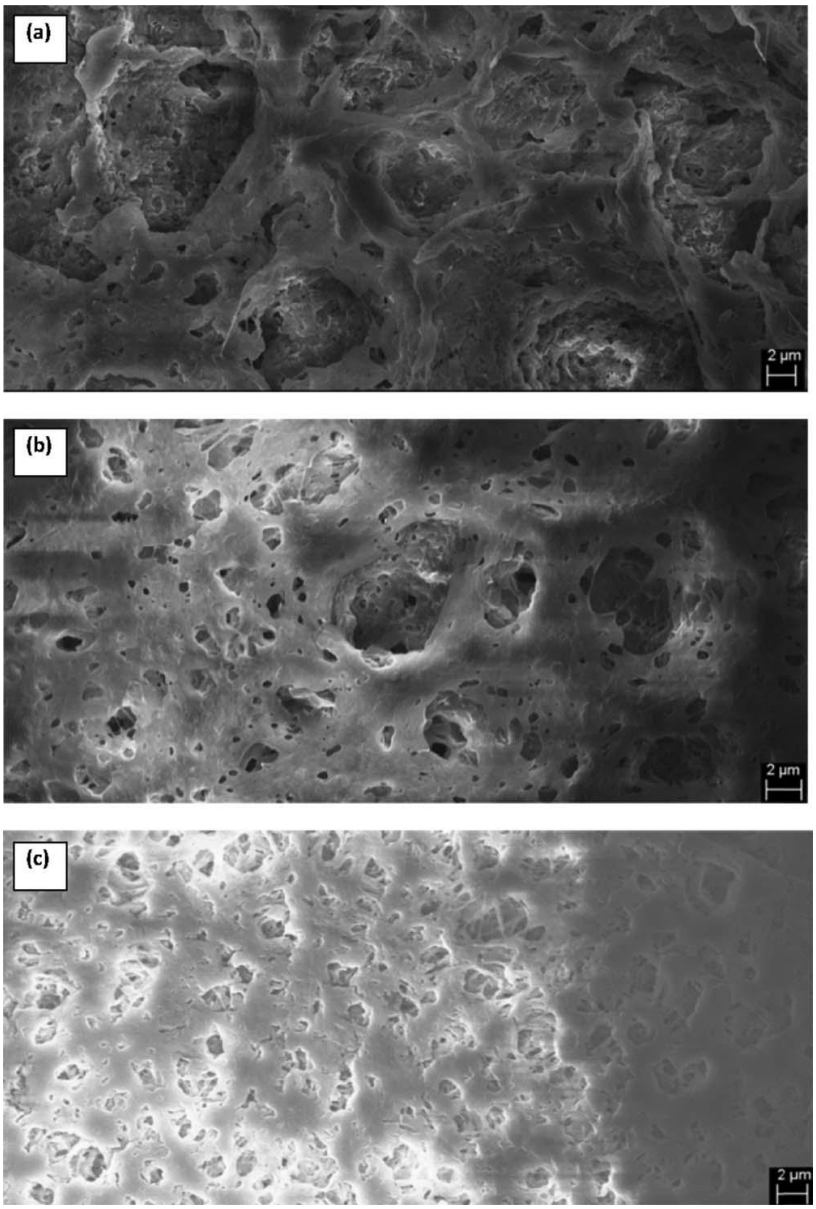

Figure 3.2. SEM images of three different samples at the same magnification, (a) PVdF-HFP, (b) PVdF-HFP/Na^+-MMT, (c) PVdF-HFP/OMMT.

In order to evaluate the tensile strength of microporous membranes, stress-strain curves for all the samples were obtained by using uniaxial stress-strain tests as presented in Figure 3.5. Tensile strength of the membranes increases by incorporation of nanoparticles and PVdF-HFP/OMMT nanocomposite membrane has the highest mechanical strength due to its smaller and uniformly distributed pores, as proved by SEM and AFM images.

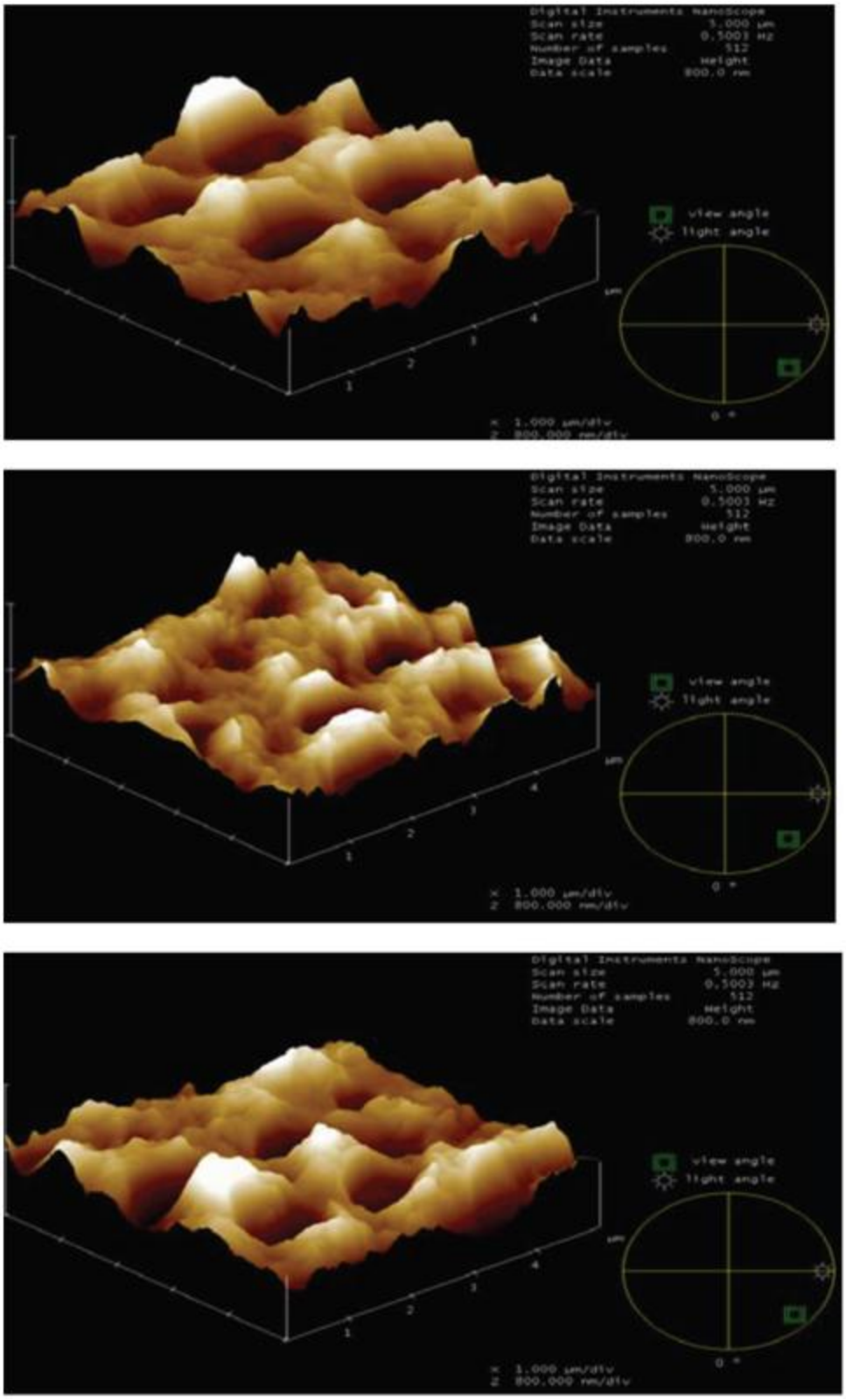

Figure 3.3. AFM topographic images of three different samples, (a) PVdF-HFP, (b) PVdF-HFP/Na^+-MMT, (c) PVdF-HFP/OMMT.

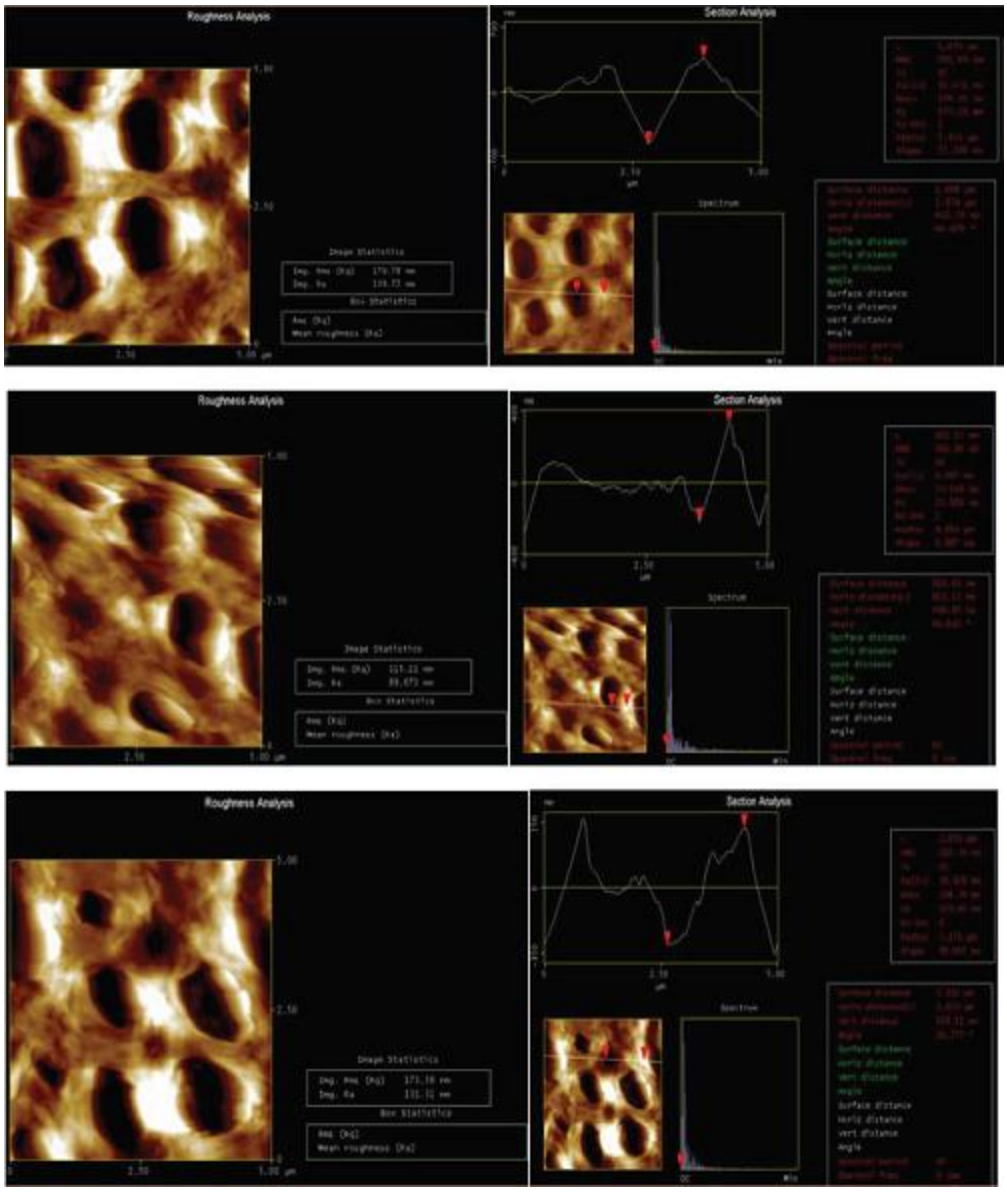

Figure 3.4. Roughness and pore size analysis of three different samples, (a) PVdF-HFP, (b) PVdF-HFP/Na^{+}-MMT, (c) PVdF-HFP/OMMT.

Thermogravimetric analysis and the corresponding heat flow curves obtained for the electrolyte membranes are presented in Figures 3.6. The melting temperature of PVdF-HFP is 159 ◦C [96]. It can be seen that GPEs are thermally stable almost up to 90 ◦C. A significant weight loss at temperature ranging between 100–200 ◦C was observed for all of the electrolyte membranes, reflecting the decomposition of the liquid electrolyte held in porous structure.

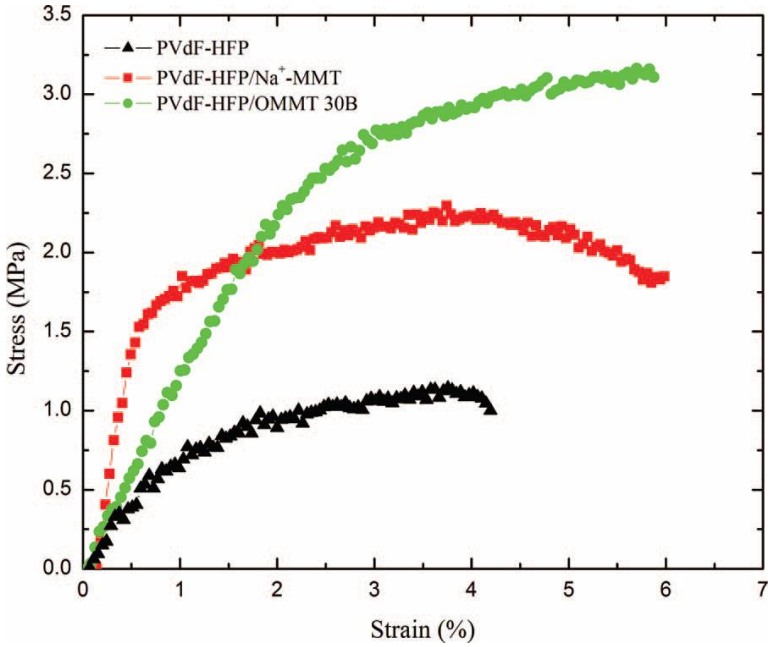

Figure 3.5. Tensile strength of microporous PVdF-HFP, PVdF-HFP/Na^+-MMT, and PVdF-HFP/OMMT membranes.

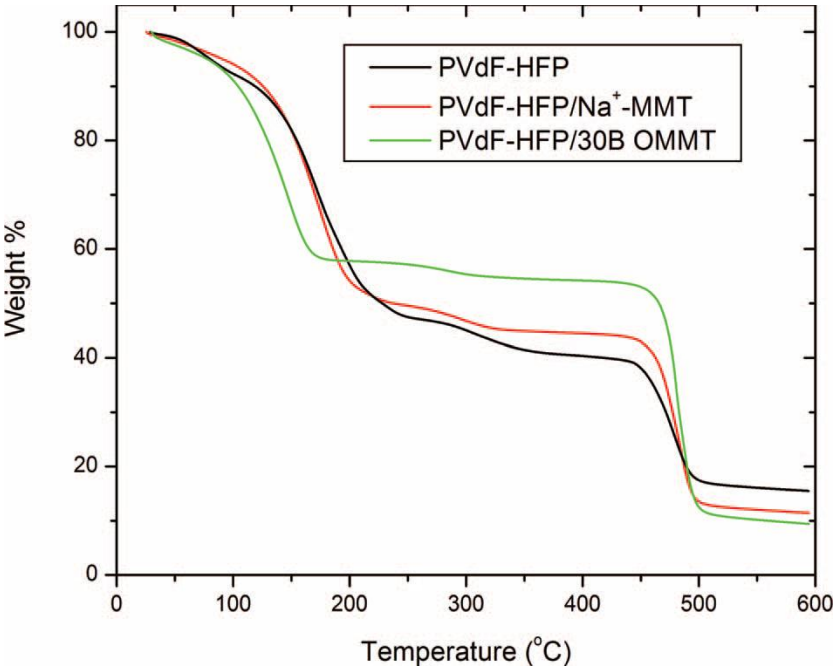

Figure 3.6. Thermogravimetric analysis obtained for PVdF-HFP, PVdF-HFP/Na^+-MMT, and PVdF-HFP/OMMT gel polymer electrolytes.

In order to determine the conductivity of the polymer electrolytes, AC impedance spectroscopy was carried out on a stainless steel/GPE/stainless steel cell. The Nyquist plots at room temperature (25 $^{\circ}$C) are presented in Figure 3.7. As shown in this figure, a linear relationship exists between the real part and the imaginary part of the impedance spectra for all the samples. The resistance of the electrolyte can be determined from the intersection of the Nyquest spectrum at the real axis. Ionic conductivity values for PVdF-HFP, PVdFHFP/Na^{+}-MMT, and PVdF-HFP/OMMT electrolyte membranes are measured to be 5.8, 7.0, and 4.9 mS/cm, respectively. These values indicate high ionic conductivity of the membranes prepared by this combination of solvent/non-solvent system.

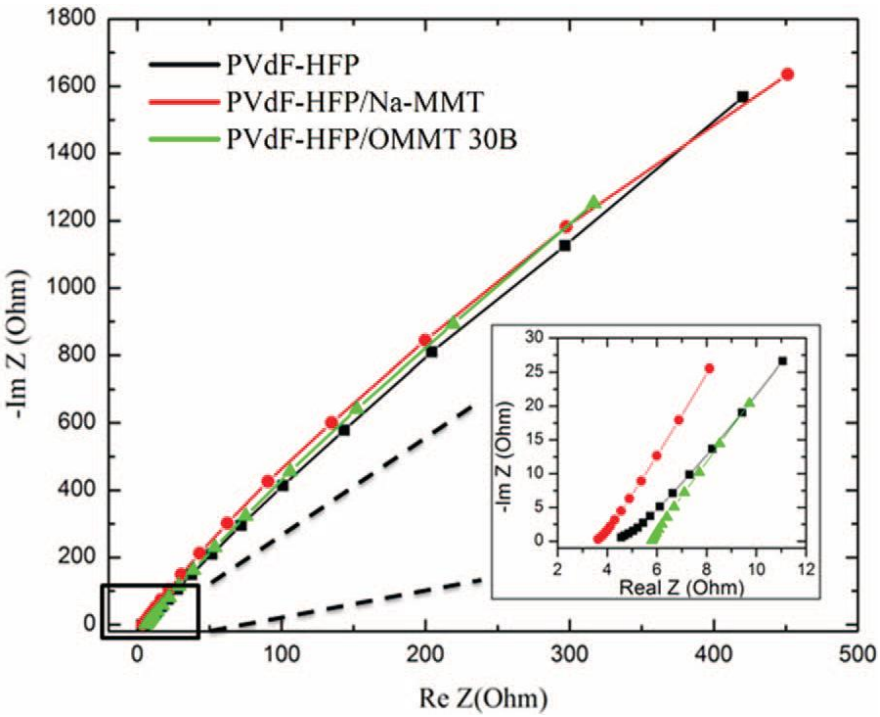

Figure 3.7. Impedance spectra of the electrolyte membranes.

The polymer electrolyte system must have high electrochemical stability in order to be implemented in commercial lithium-ion batteries. Generally, current–voltage measurements are used to determine the operating voltage window of the polymer electrolyte. Cyclic voltametry results of the polymer electrolytes are shown in Figure 3.8. As can be seen, the anodic stability of all of the polymer electrolytes for is up to 4.8 V, indicating the electrochemical decomposition would not occur below 4.8 V.

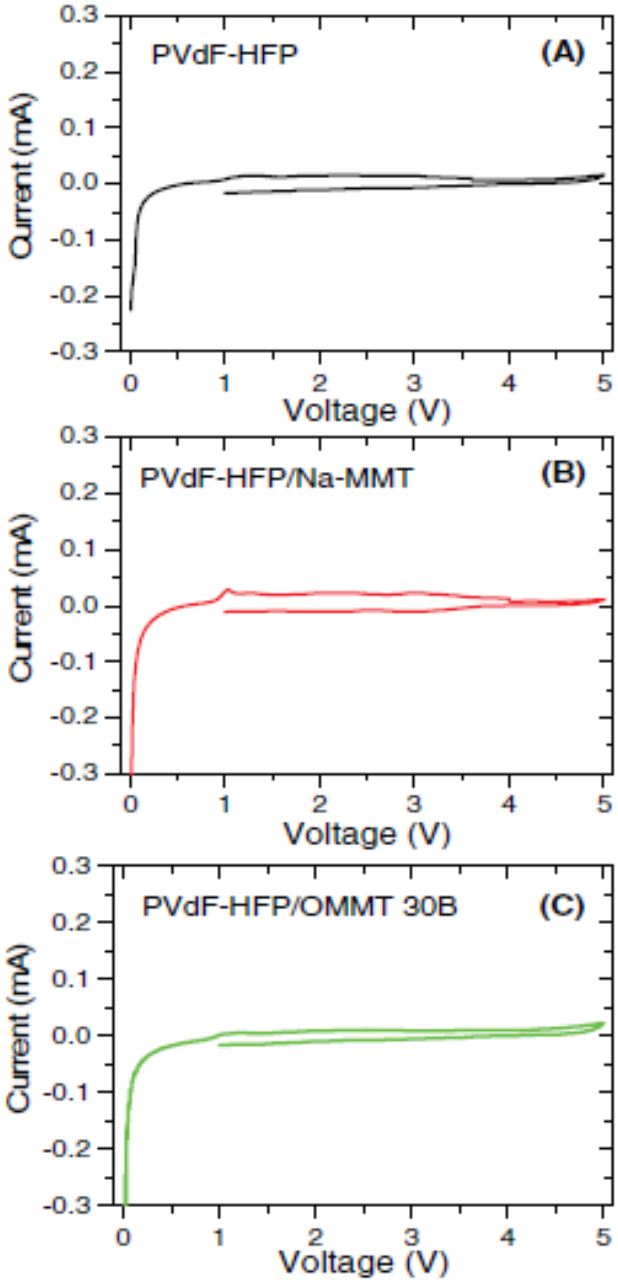

Figure 3.8. CV graphs at 0.05 C for the first cycle of Li-GPE-stainless steel cell with (A) PVdF-HFP, (B) PVdF-HFP/Na^{+}-MMT, and (C) PVdF-HFP/OMMT.

In order to prepare the sulfur-based cathode material, sulfur, polyacrylonitrile (PAN) and $Mg_{0.6}Ni_{0.4}O$ were mixed and ball milled. It has been reported that the addition of nanosized $Mg_{0.6}Ni_{0.4}O$ powder in sulfur based cathodes can improve the Li/S cell performance by absorbing the intermediate polysulfides formed during electrochemical reactions within the cell

[97]. $Mg_{0.6}Ni_{0.4}O$ powder was produced by the self-propagation high-temperature synthesis (SHS) method [98] The XRD analysis was carried out to investigate the possible structural changes due to the possible interactions of $Mg_{0.6}Ni_{0.4}O$ with other cathode components. These patterns for the starting components S, PAN, $Mg_{0.6}Ni_{0.4}O$ and ternary composite cathode material are shown in Figure 3.9. Compared with $Mg_{0.6}Ni_{0.4}O$, the PAN/S/ $Mg_{0.6}Ni_{0.4}O$ ternary composite shows sharp peaks of $Mg_{0.6}Ni_{0.4}O$ with reduced peak intensity. However, peaks assigned to elemental sulfur have disappeared in the S/PAN/$Mg_{0.6}Ni_{0.4}O$ ternary composite, which indicates that sulfur is no longer crystalline in the ternary composite [99].

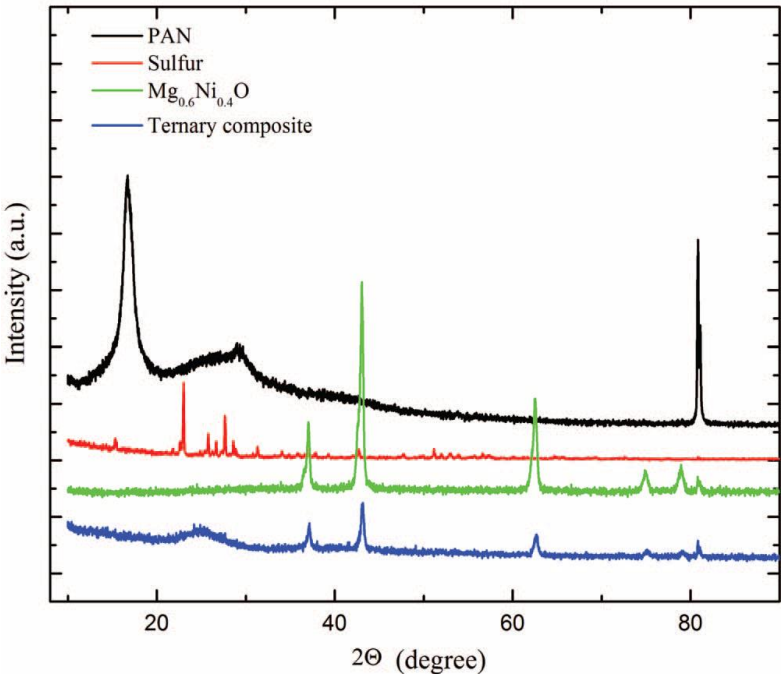

Figure 3.9. XRD spectra of sulfur, PAN, $Mg_{0.6}Ni_{0.4}O$, and the S/PAN/$Mg_{0.6}Ni_{0.4}O$ ternary composite.

The morphology of the ternary composite cathode is shown in Figure 3.10. As can be seen, the ternary composite consists of nanosized primary particles and a very rough surface which could be beneficial for the contact and interaction between the electrode and the electrolyte, and therefore be highly favorable for ion diffusivity and electrochemical performance of the battery cell.

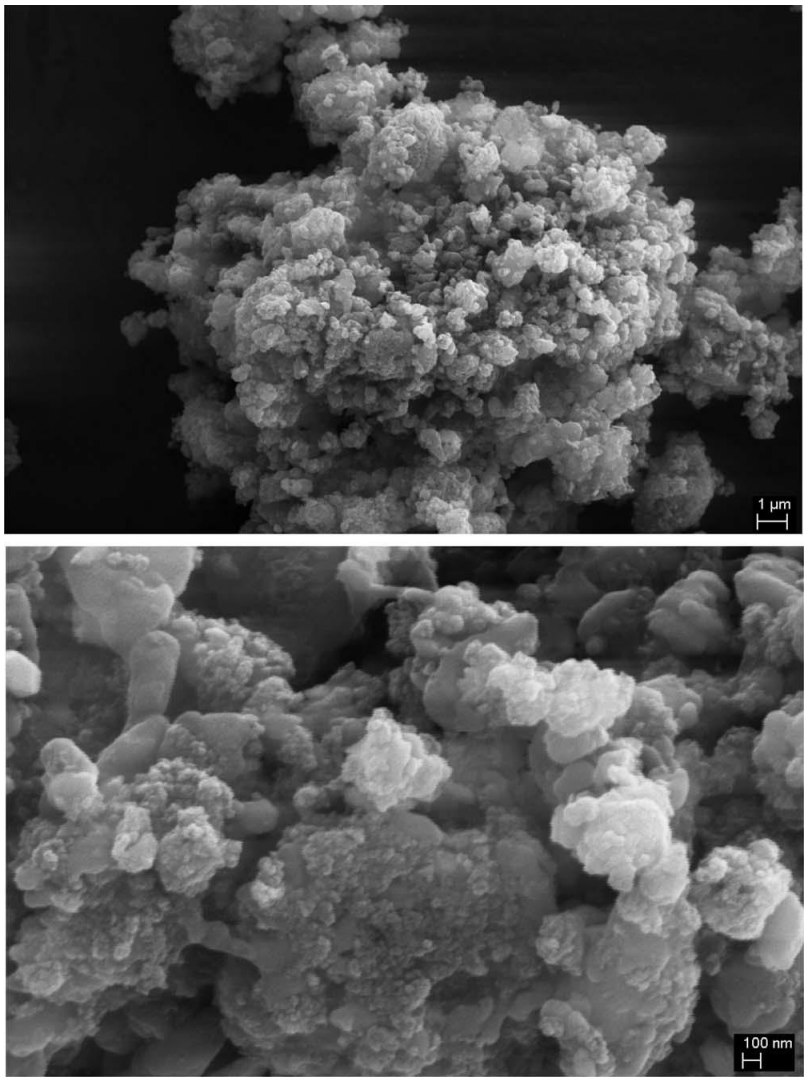

Figure 3.10. SEM images of S/PAN/$Mg_{0.6}Ni_{0.4}O$ ternary composite at two different magnifications.

Performance of the Li-GPE-ternary composite battery cells was investigated at room temperature. Charge-discharge profiles of a cell containing the PVdF-HFP/OMMT nanocomposite electrolyte, are shown in Figure 3.11. The battery performance in terms of discharge capacity versus cycle number for over 300 cycles is presented in Figure 3.12. Within the first discharge process, these batteries delivered capacities of 1622, 1546, and 1507 mAh g^{-1}_{sulfur} or 616, 588, 573 mAh $g^{-1}_{composite}$ respectively. In their second discharge process, they delivered capacity of 930, 880, 620 mAh g^{-1}_{sulfur} or 354, 335, 236 mAh $g^{-1}_{composite}$. As can be seen, discharge capacity increases by incorporation of both types of nanoparticles. However, the cell assembled with the PVdF-HFP/OMMT nanocomposite electrolyte exhibits a higher initial discharge capacity and better capacity retention. It has been reported [24] that the choice of

organic solvent plays a crucial role in the electrochemical performance of sulfur-based cathodes. In S/PAN cells with carbonate-based electrolytes, a small amount of soluble polysulfides are formed. As a result, polysulfide shuttle can be prevented to some extent, leading to higher efficiency. In contrast, ether-based electrolytes dissolve polysulfides and enables migration of polysulfides to the lithium anode surface and loss in active mass during cycling of the battery cell.

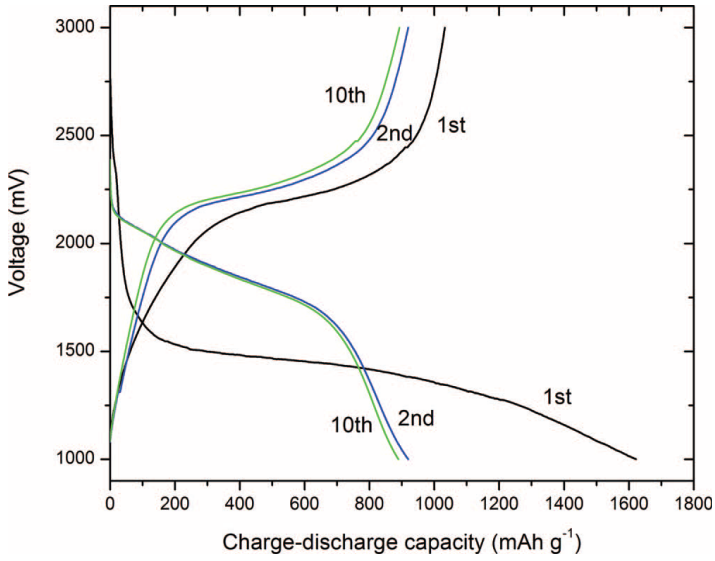

Figure 3.11. Charge-discharge profiles of the Li-GPE-ternary composite cathode battery at room temperature and a C/5 rate and 1–3 V voltage range. PVdF-HFP/OMMT electrolyte membrane is the one used in this cell.

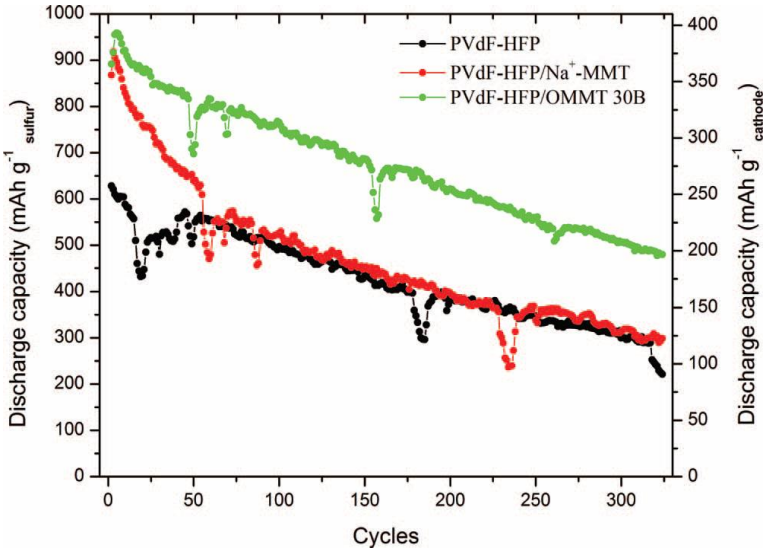

Figure 3.12. Discharge capacity vs. cycle number of Li-GPE-ternary composite cathode cells with different polymer electrolyte membranes (25◦C, 0.2 C-rate, 1–3 V).

In order to further evaluate the performance of gel polymer electrolyte membranes in preventing the shuttle phenomenon, they were embedded in ether-based electrolyte solutions and were tested in Li/S batteries with sulfur/carbon composite as the cathode. Figure 3.13 (top) presents the charge–discharge curves for the first cycle of these cells with gel polymer electrolytes. All systems exhibit characteristic potential profiles of charge–discharge of sulfur cathodes with two potential plateaus of the electrochemical activity due to the multiple electrochemical reactions in these cells [45,100]. Discharge capacity and Coulombic efficiency versus cycle number of these cells are also shown in Figure 3.13 (bottom). One can see from this figure that the cyclability and Coulombic efficiency of the cell assembled by PVdF-HFP/OMMT nanocomposite electrolyte is remarkably enhanced compared with the other cells. This cell retains about 65% of its initial capacity over 80 cycles, while the discharge capacity of the other cells fades more drastically upon cycling. This improvement is ascribed to the improved liquid electrolyte upholding of this polymer electrolyte favored by the addition of organically modified nanoparticles, hence preventing release of electrolyte solution and controlling dissolution of polysulfides during cycling of the cell. This improvement could also be attributed to the suppression of the shuttle effect by the small pore size and uniformly distributed porous structure of this membrane, which reduce the diffusion of polysulfides to the anode side and promote reaction reversibility of the cathode, positively affecting its Coulombic efficiency. The stable interfacial characteristics promoted by the nanoparticles may also contribute to the improved capacity retention.

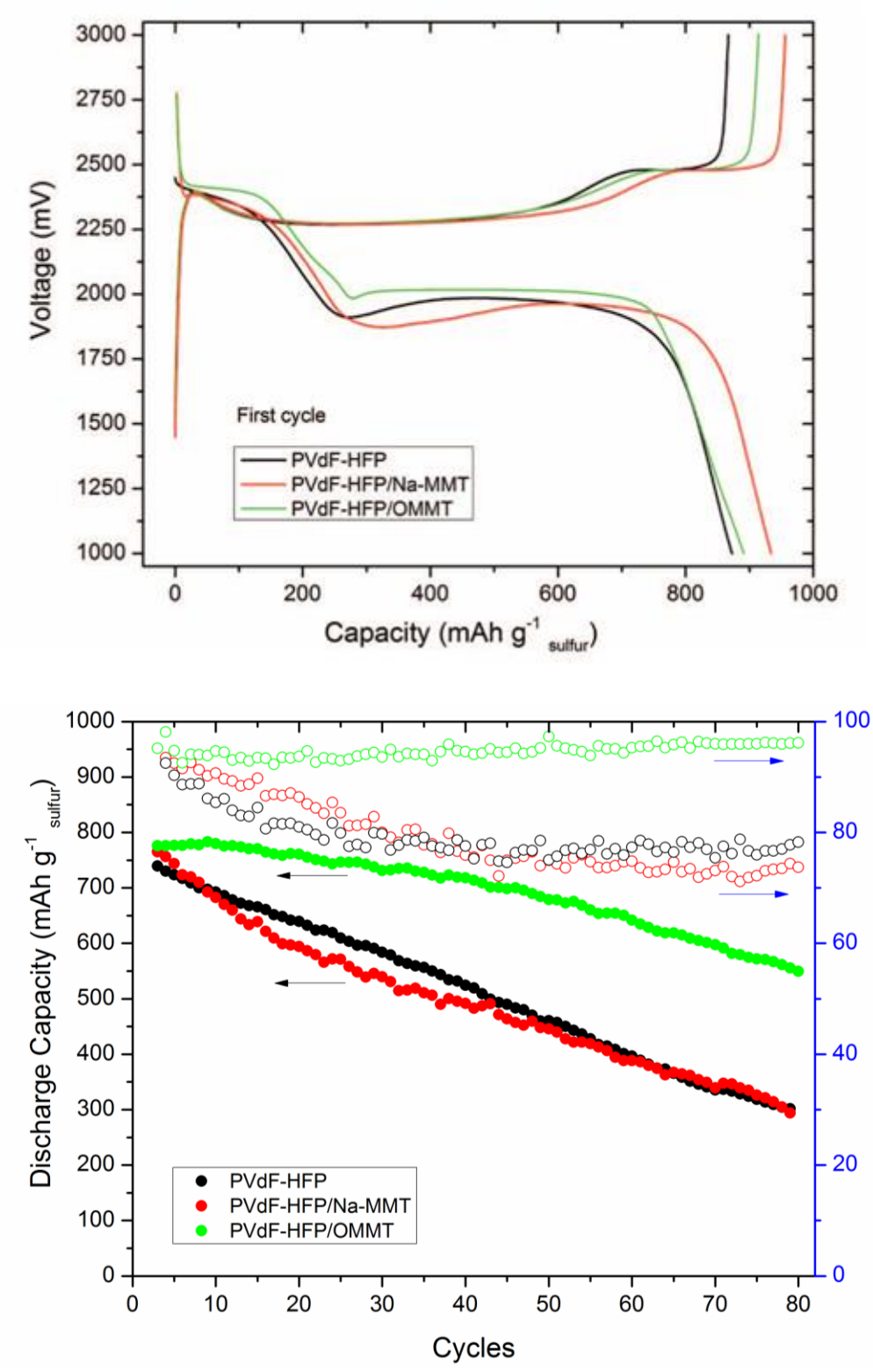

Figure 3.13. (top) Charge-discharge profiles for the first cycle, (bottom) discharge capacity and Coulombic efficiency versus cycle number for Li-S/C cells with different polymer electrolyte membranes (25◦C, 0.2 C-rate, 1–3 V).

3.4 Conclusions

In this chapter, fabrication and characterization of PVdF-HFP/silicate nanocomposite electrolytes and their application to Li/S batteries were investigated. The phase inversion method using acetone/tert-butyl methyl ether as solvent/non-solvent was used to fabricate highly porous electrolyte membranes. AC impedance spectroscopy and cyclic voltammetry revealed high ionic conductivity and electrochemical stability of the membranes; ionic conductivity as high as 4–7 mS/cm and electrochemical stability of up to 4.8 V were obtained at room temperature. The Li/S battery cells assembled by PVdFHFP/OMMT nanocomposite electrolyte showed a higher discharge capacity and improved capacity retention compared to the other cells. It is evident that active mass loss is satisfactorily controlled during the cycling. It seems that small pore size and uniform pore distribution of the PVdF-HFP/OMMT membrane prevent electrolyte release during cycling, which can control the dissolution of polysulfides and suppress active mass loss and hence overcome one of the major obstacles preventing the practical development of Li/S batteries.

Chapter 4

Synthesis of PVdF-HFP/Functionalized PMMA Electrolytes for Lithium/Sulfur Battery[2]

4.1 Introduction

As mentioned earlier, blending has been considered to be an effective method for modifying GPEs with desired properties; however, achieving such an electrolyte often requires an addition of high amounts of another polymer, which adversely affects the electrochemical properties of the PVdF-HFP matrix. In this part of the study, functionalized poly(methyl methacrylate) (PMMA) was synthesized and blended in low amounts with PVdF-HFP to form a GPE. This simple idea was prompted by the belief that addition of small amounts of a compatible functional polymer bearing some random inorganic domains into PVdF-HFP would promote pore frmation in the host polymer membrane and immobilize high amounts of electrolyte solution during cycling of a battery cell.

4.2 Experimental

The functionalized poly (methyl methacrylate) was synthesized by polymerization of methylmethacrylate (MMA) and methacryloxypropyltrimethoxysilane (MPTMS) at 343K via a free radical method using AIBN as the initiator following a procedure reported by Sanchez et al [101]. A porous polymer membrane consisting of PVdF– HFP (Kynar Flex 2801, 12 wt. % HFP) and functionalized PMMA (weight ratio: 75/25) was prepared by the phase separation method using acetone as solvent and tert-butyl methyl ether (extra pure, Acros Organics) as non-solvent. A free-standing gel polymer electrolyte film was obtained by soaking the membrane in a 1 M LiPF6 dissolved in a 1:1 (v/v) mixture of ethylene carbonate (EC) and diethylene carbonate (DEC) for 30 min.

The sulfur/polyacrylonitrile (S/PAN) composite was prepared by mechanically mixing sulfur (Sigma-Aldrich) and PAN (Sigma-Aldrich) in a weight ratio of 4:1 and heat treating at 300 °C for 3 h in a tubular furnace filled with Ar gas. The cathode electrodes of either $LiCoO_2$ or

[2] Data presented in this chapter was published in Ref. [116].

S/PAN were prepared by making a slurry containing the active material, binder (PVdF) and super-P carbon in NMP and then casting on a graphite foil. Both Li/S and Li/$LiCoO_2$ cells were assembled by sandwiching the GPE between the lithium metal anode and either the S/PAN or $LiCoO_2$ cathode.

4.3 Results and discussion

Size exclusion chromatography (SEC) and ^1H NMR were used to characterize the synthesized polymer. Responses of two detectors (refractive index and viscometer DP) as a function of retention volume obtained from SEC measurement along with the schematic structure of the synthesized polymer are shown in Figure 4.1. SEC revealed a polymer with Mn = 26066 g mol^{-1} and PDI = 1.96. ^1H NMR was recorded at room temperature on a Brucker DRX 300 spectrometer to confirm the presence of trimethoxysilane groups on the polymer and the corresponding spectrum is shown in Figure 4.2. The following peaks are observed- δH: 3.9 (OCH_2), 3.5 (OCH_3), 1.2 (CH_2Si), 0.5–2 (CH_2, CH_3, $CH_2CH_2CH_2$). Two peaks assigned to the OCH_2 and CH_2Si indicate the successful synthesis of functionalized PMMA containing trimethoxysilane groups.

Differential scanning calorimetry (DSC) and thermogravimetric analysis (TGA) experiments were used to measure the glass transition temperature and thermal stability of the f-PMMA. Results from the TGA depicted in Figure 4.3 (top), show that there is no major mass loss for the temperature up to 230 ^oC, indicating that f-PMMA is stable at lower temperatures. From the DSC curve in Figure 4.3 (bottom), glass transition temperature is measured to be ~100 ^oC.

The functionalized PMMA was then introduced into a PVdF-HFP matrix (25/75 weight ratio) in order to establish a membrane with numerous small, uniformly distributed pores. A polymer electrolyte of PVdF-HFP was also prepared to be used as a control sample. Scanning electron microscopy images for these two polymer membranes are shown in Figure 4.4(A) and (B). A porous membrane with a non-uniform pore size distribution is obtained for PVdF-HFP, which should promote the uptake of high amounts of liquid electrolyte solution, but poor retention during cycling of the battery. However, in the case of the new polymer electrolyte, the pore size decreases while their number and uniformity increase, which should improve the electrolyte solution retention and promote stability of the GPE morphology during cycling.

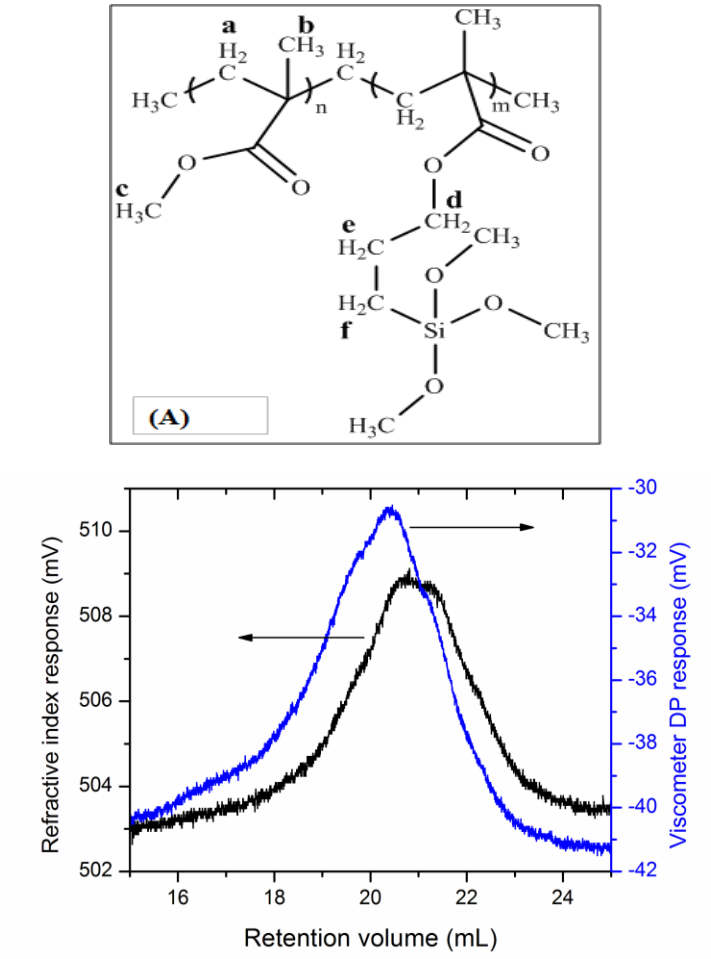

Figure 4.1. (top) Schematic structure and (bottom) Size exclusion chromatography of the functionalized PMMA.

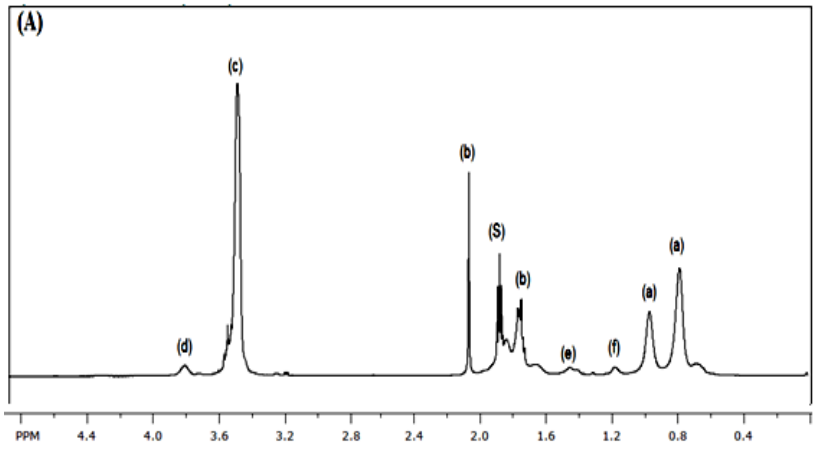

Figure 4.2. ^{1}H NMR spectrum of the functionalized PMMA

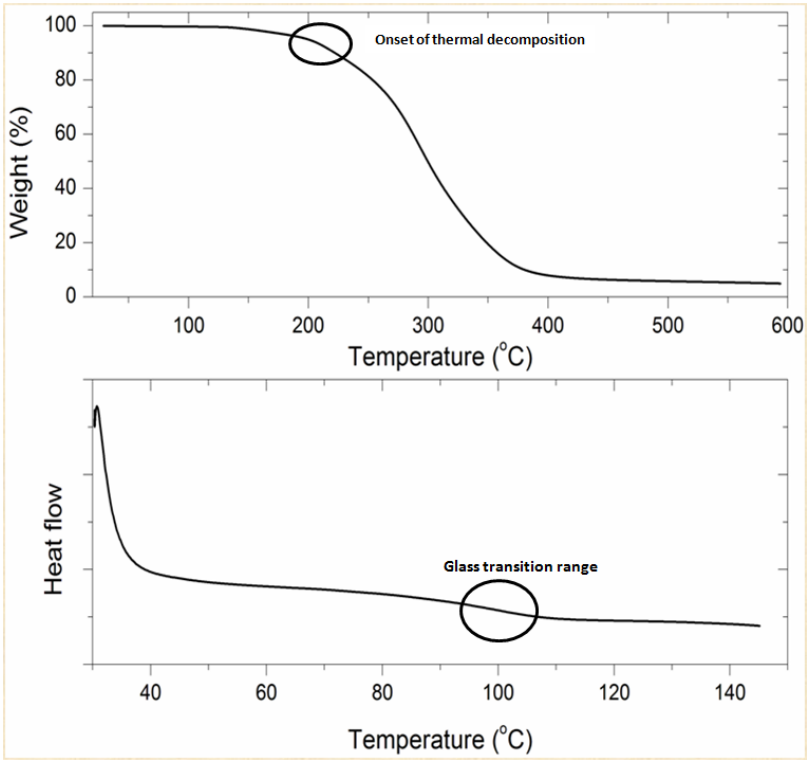

Figure 4.3. (top) TGA and (bottom) DSC curves for the functionalized PMMA.

A free-standing polymer electrolyte was then obtained by soaking the membrane in 1 M $LiPF_6$ dissolved in a 1 : 1 (v/v) mixture of ethylene carbonate (EC) and diethylene carbonate (DEC) for 30 min. Hereafter, this polymer electrolyte is referred to as the modified gel polymer electrolyte, with the acronym mGPE. Also, we refer to the PVdF-HFP electrolyte, as the control gel polymer electrolyte (cGPE). The electrolyte uptake was calculated using the following equation: uptake = $(W- W_0)/W_0 * 100\%$, where W and W_0 are the mass of soaked and dry membranes. The average electrolyte uptake of mGPE and cGPE were 124% and 131%, respectively.

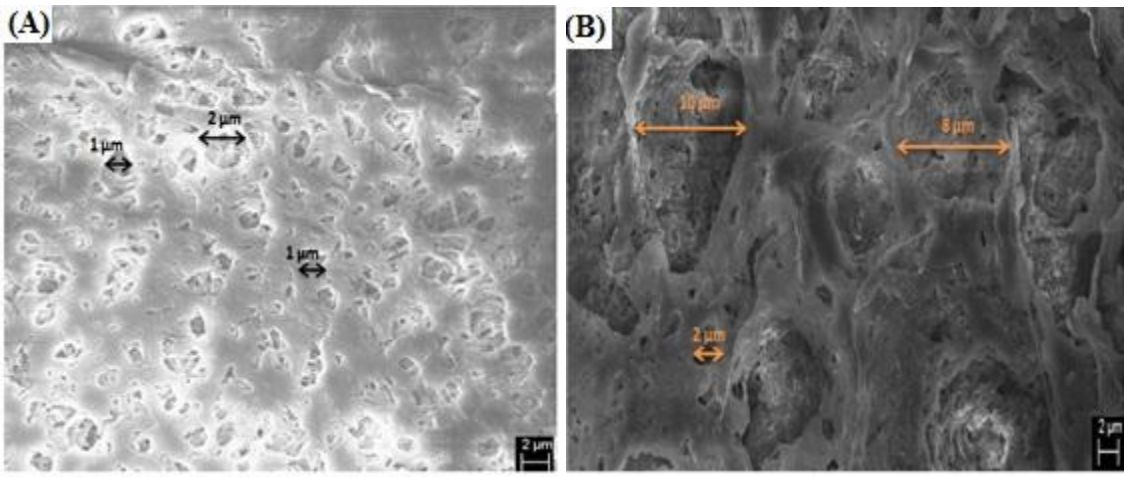

Figure 4.4. (A) and (B) SEM images of the new polymer electrolyte and PVdF-HFP membrane, respectively.

A Linear sweep voltammery graph for lithium metal/GPE/stainless steel is shown in Figure 4.5(top). A rise in current is observed around 4.8V (vs. Li/Li^+) and the current continues to increase with increasing potential. This indicates that electrochemical decomposition would not occur below 4.8V. Figure 4.5(bottom) shows the complex impedance plot of the stainless steel/GPE/stainless steel cell at room temperature. The ionic conductivity value is measured to be 4.7 mS/cm. Such a high ionic conductivity can be attributed to the good electrolyte uptake by the polymer electrolyte.

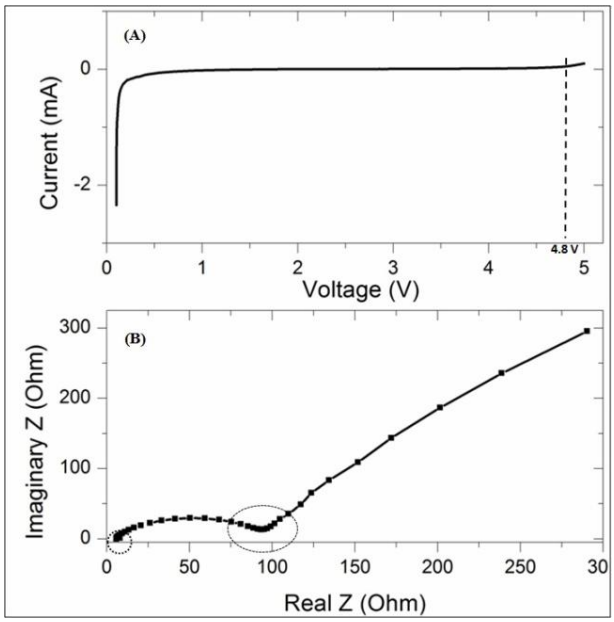

Figure 4.5. Linear sweep voltammetry at a scan rate of 5 mV/s, and room temperature complex impedance plot of the GPE.

4.3.1 Li/GPE/$LiCoO_2$ cell

Here, we first test the gel electrolyte performance by assembling a lithium battery containing $LiCoO_2$, a very well-known cathode active material and then performance of the gel polymer electrolyte in a lithium/sulfur cell. Figures 4.6 and 4.7 show typical charge–discharge profiles and cycle life for a Li/$LiCoO_2$ cell assembled with the mGPE at a constant current of 0.2C. This cell delivers an initial discharge capacity of 140 mAh g^{-1} based on the weight of $LiCoO_2$ active material. A discharge capacity of 132 mAh g^{-1}, 94% of the initial value, and columbic efficiency of almost 100% were obtained after 100 cycles. Such improved discharge capacity retention in a Li/mGPE/$LiCoO_2$ cell is better than that of 92% of a good GPE based on PVdF-HFP and core-shell structured $SiO_2(Li^+)$ particles recently reported by Kim et al. [102] indicating better performance of our GPE during cycling.

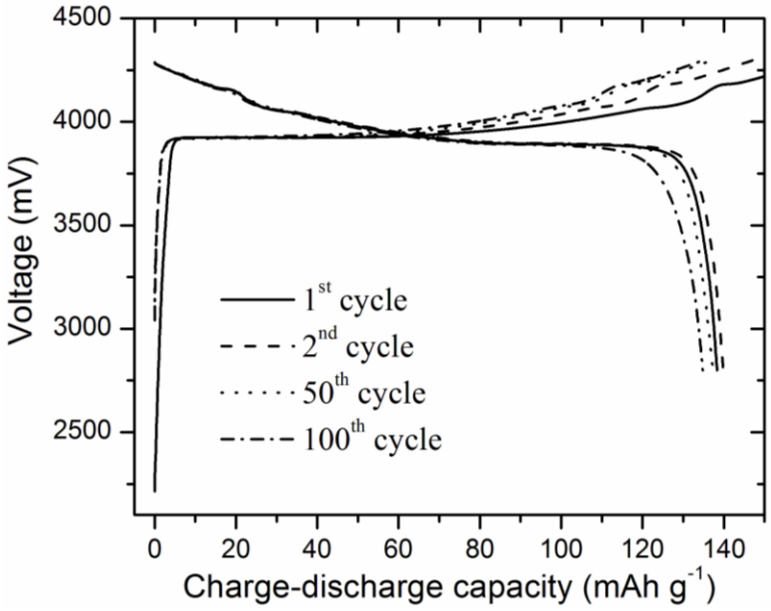

Figure 4.6. Charge–discharge curves for the $LiCoO_2$/mGPE/lithium metal cell at 0.2 C rate.

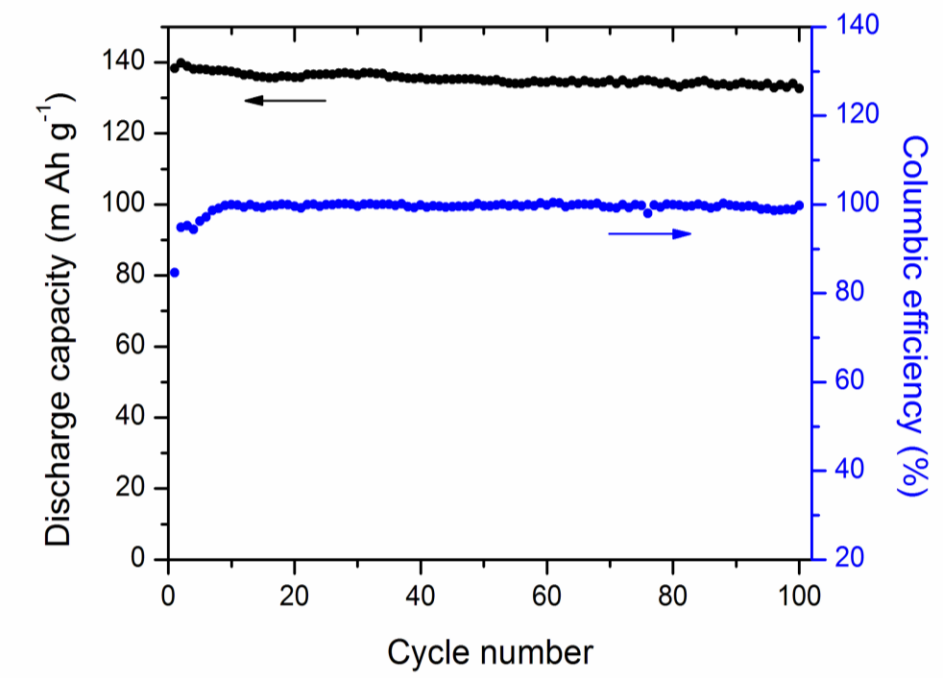

Figure 4.7. Cycle life of $LiCoO_2$/mGPE/lithium metal cell at 0.2 C rate.

4.3.2 Li/GPE/S cell

The electrochemical properties of these Li/S cells were investigated using coin-type cells (CR2032). Each cell was composed of a lithium metal anode, a sulfur-based cathode and an electrolyte, either a polymer electrolyte or a liquid electrolyte (a polypropylene separator (Celgard, USA) with 1 M $LiPF_6$ dissolved in a 1 : 1 (v/v) mixture of EC and DEC). AC impedance spectroscopy was performed on the cells at room temperature to yield the results shown in Figure 4.8. As expected, the Li–liquid electrolyte–S cell has the lowest ohmic resistance, but interestingly both the Li–mGPE–S and Li–cGPE–S cells also have low ohmic resistance indicating the ease of Li-ion transportation due to uptake of high amounts of liquid electrolyte solution by their porous membrane structure. However, Li–mGPE–S has the highest charge transfer resistance attributed to its slow reaction kinetics [103]. In the case of the Li–liquid electrolyte–S cell, reaction intermediates can easily diffuse through the separator resulting in fast reaction kinetics [104]. However, the unique morphology of the mGPE prevents migration of the reaction intermediates and causes accumulation of these intermediates in the cathode area,

which increases the polarization of the double layer and slows down the reduction rate of sulfur during electrochemical reactions.

Cyclic voltammetry curves for the first few cycles of the Li–mGPE–S cell are shown in Figure 4.9. A clear reduction peak is observed at ~1.7 V followed by a shoulder near 2 V due to multistep electrochemical reactions of sulfur with Li^+ ions. The peak at ~2.5 V is assigned to the oxidation reaction within the cell. As can be seen, a small shift in the oxidation peak is observed in the fifth cycle, which is possibly due to the formation of a solid electrolyte interface (SEI) on the electrodes.

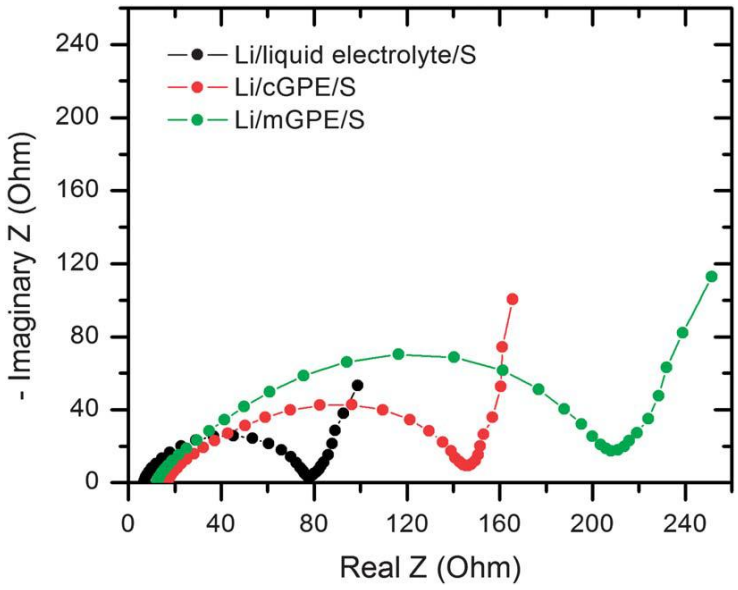

Figure 4.8. Complex impedance plots for all the cells.

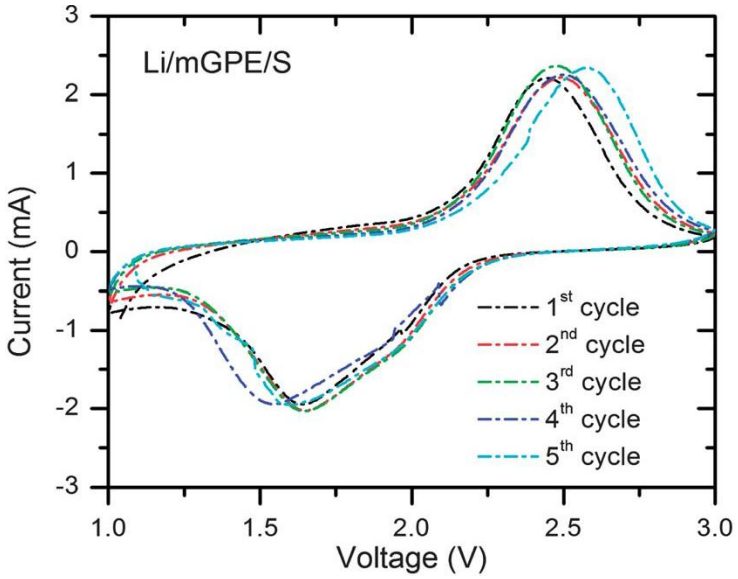

Figure 4.9. CV profiles for the Li–mGPE–S cell.

The initial profiles of the galvanostatic charge–discharge test are shown in Figure 4.10. All the cells show almost the same initial discharge capacity. However, the Li–mGPE–S cell has a slightly smaller initial charge capacity, which is attributed to the slower kinetics of the electrochemical reaction in the cell. An interesting point in this figure is the higher discharge voltage of the Li–cGPE–S and Li–mGPE–S cells compared to the Li–liquid electrolyte–S cell. The sharp local minimum observed in the beginning of the discharge process is due to the precipitation of polysulfides in the cathode, which reduces the concentration of the reaction intermediates in the electrolyte and increases the discharge voltage [105]. Lack of such a local minimum in the discharge process of the Li–liquid electrolyte–S cell indicates that polysulfides can easily diffuse through the separator and their concentration would not reach the saturation threshold. On the other hand, the diffusion of polysulfides through the membrane is suppressed in the Li–mGPE–S and Li–cGPE–S cells. Therefore, their concentration can reach the saturation threshold and increase the discharge voltage. Moreover, the relatively earlier appearance of the sharp local minimum in the Li–mGPE–S cell shows the enhancement in blocking of the intermediate polysulfides in the cathode area in the case of mGPE as compared to cGPE.

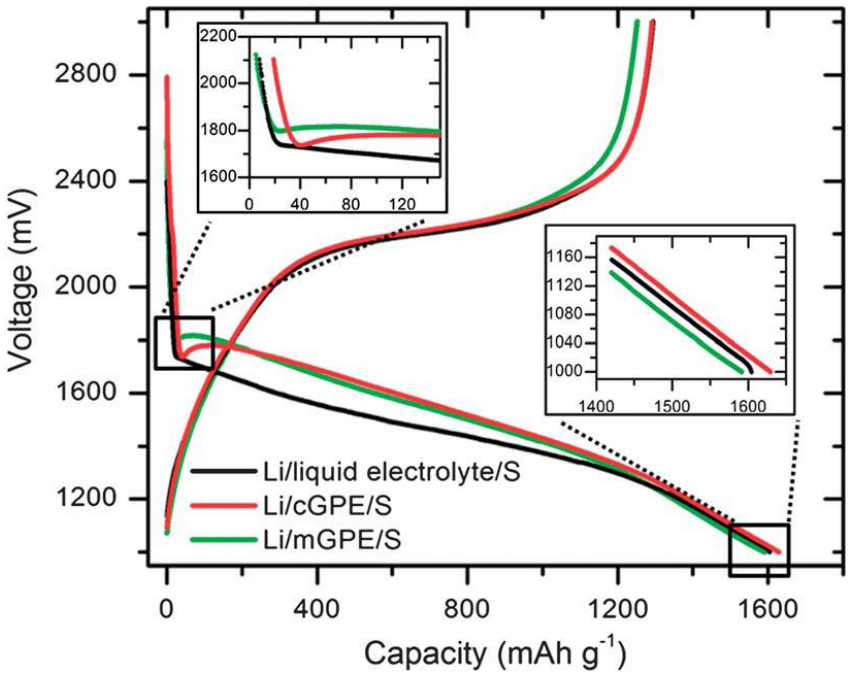

Figure 4.10. Initial charge–discharge profiles of the cells at 0.2 C rate.

Figure 4.11 shows cycle life of these cells. The Li–liquid electrolyte–S cell exhibits a discharge capacity of 1100 mAh g^{-1} after 40 cycles. Then, poor cyclability leads to a low capacity of 200 mAh g^{-1} after 100 cycles, which is about 15% of the initial value. However, the Li–cGPE–S cell capacity fading starts after the first few cycles. A capacity of about 400 mAh g^{-1} was obtained after 100 cycles, which is about 30% of the initial value. The active mass lost due to the dissolution of polysulfides into electrolyte solution and diffusion of these polysulfides through the membrane (shuttle effect) is the main reason of such poor capacity retention in both of the mentioned Li–S cells. In the case of the liquid electrolyte, it seems that the microporous separator (average pore size = 0.064 mm) can prevent migration of the dissolved polysulfides in the first 40 cycles. Afterwards, facile movement of these polysulfides through the separator and their deposition on the lithium metal surface leads to sharp capacity fading. For the cGPE, the electrolyte solution can be released from the membrane even in the first few cycles and the generated polysulfides can pass through big pores of the membrane resulting in the capacity fading. Since the polymer membrane is able to hold some of the electrolyte solution, the overall polysulfide dissolution and active mass loss is less than that of the Li–S cell with liquid electrolyte. In contrast, the Li–mGPE–S cell exhibits remarkably better capacity retention; a discharge capacity of 1050 mAh g^{-1} was obtained after 100 cycles, which is about 88% of the initial value. Such an enhancement in capacity retention is due to the unique porous configuration of the membrane, which holds the electrolyte solution and prevents dissolution of polysulfides during cycling (Figure 4.11).

4.4 Conclusions

In conclusion, acceleration of polysulfide dissolution into the excessive liquid electrolyte solution has been a limiting factor in developing polymer electrolytes for Li–S battery applications. The proposed GPE was capable of retaining the electrolyte solution and preventing polysulfide diffusion during cycling of the battery cell to improve the cycle performance of the sulfur-based electrode material. This new Li–S battery configuration enabled a stable discharge capacity of 1050 mAh g^{-1} to be achieved after more than 100 cycles. To our knowledge, this is the first work to fabricate a polymer electrolyte with a better performance over a long number of cycles as compared to conventional liquid electrolytes used in Li–S batteries.

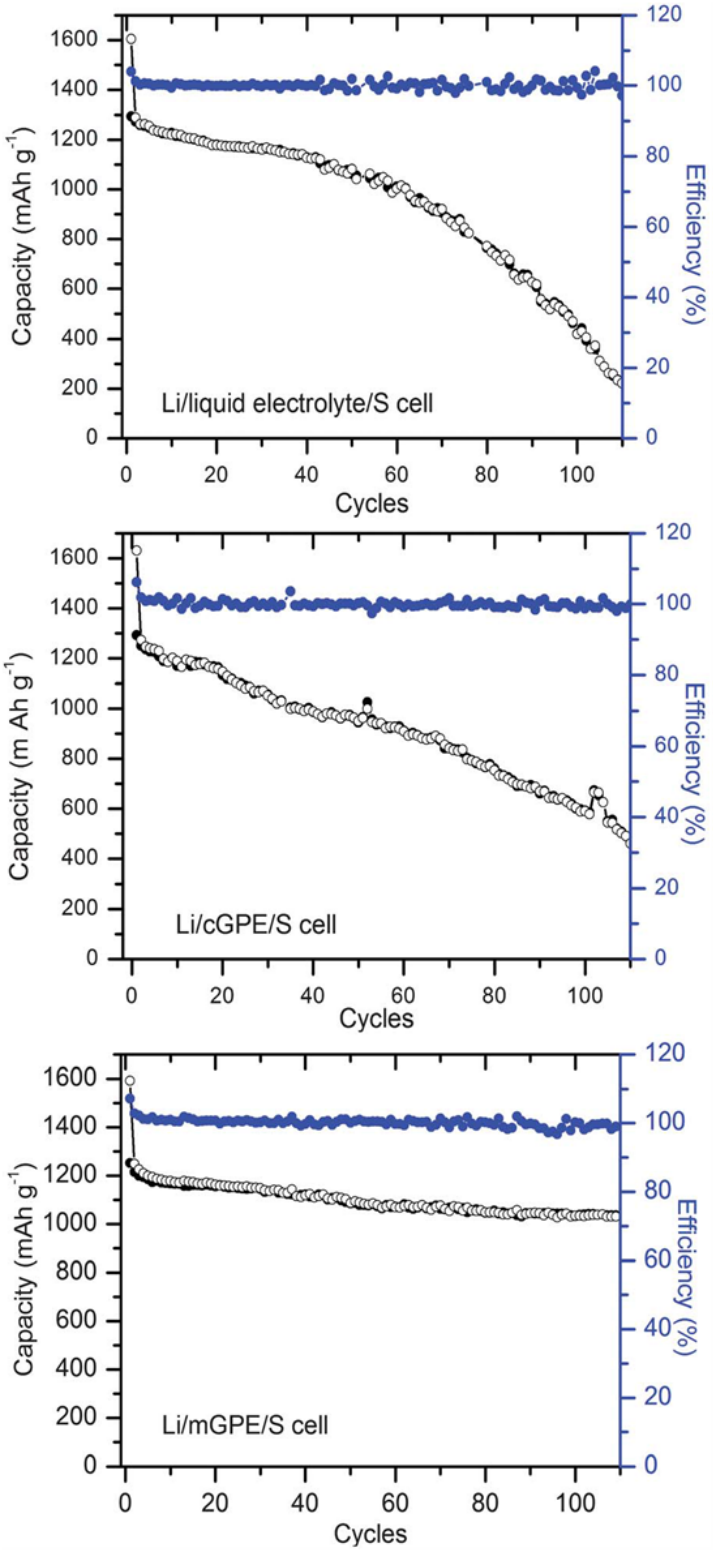

Figure 4.11. Charge–discharge versus cycles of the cells at 0.2 C rate. Charge capacity: solid symbols and discharge capacity: empty symbols.

Chapter 5

Synthesis of PVdF-HFP/functionalized PMMA/mesoporous silica composite electrolyte for lithium/sulfur batteries[3]

5.1 Introduction

As discussed, gel polymer electrolytes composed of poly(vinylidenefluoride-co-hexafluoropropylene) (PVdF-HFP) blended with functionalized-poly(methyl methacrylate) (PMMA) significantly improved performance of the battery cell in terms of specific capacity and cycle life. To further improve the battery performance, we synthesized mesoporous silica particles and incorporated them in the above-mentioned polymer blend. The electrolyte system comprised of a polymer matrix and mesoporous silica particles might evolve as an attractive alternative to immobilize the liquid electrolyte solution physically within a polymer/mesoporous silica structure. Furthermore, the mesoporous silica particles impart mechanical strength and facilitate lithium ion transfer within the pores. More importantly, mesoporous silica particles, which are inert to electrochemical reactions, can trap intermediate products within their porous structure to prevent them from shuttling between electrodes [7].

5.2 Experimental

5.2.1 Material preparation

Mesoporous silica (MPS) particles were synthesized by a simple procedure, as shown in Figure 5.1 [106]. A nonionic surfactant, Brij 56, was dissolved in a dilute HCl solution (pH = 1.5). Then, tetramethyl orthosilicate (TMOS) was added to the solution with mild stirring at room temperature. After 20 min, the homogenous and transparent solution was poured into a Teflon dish. After two days, a glassy monolith sample was obtained and dried at 40-100 ^{o}C in a vacuum oven for 24 h to remove all the residual solvents. Finally, the surfactant was removed by calcination in air atmosphere at 550 ^{o}C for 16 h.

[3] Data presented in this chapter was published in Ref.[117].

A functional poly(methyl methacrylate) (f-PMMA) was synthesized by free radical polymerization of methylmethacrylate (MMA) (0.1 mol) and methacryloxypropyltrimethoxysilane (MPTMS) (10 mmol) in tetrahydofuran (THF) using AIBN as the initiator following a procedure described in the previous chapter. MPS, poly(vinylidenefluoride-co-hexafluoropropylene) (PVdF-HFP) and f-PMMA were dissolved in acetone by mechanical stirring overnight. This step was followed by ultrasonication for 1 h to form a homogenous solution at room temperature. Then, tert-butyl methyl ether was added and mixture was agitated until the solution was homogenous. The resulting solution was poured onto a clean petri dish. After evaporation of acetone and ether, the electrolyte membrane was further dried at 65 ^{o}C in a vacuum oven for 24 h to remove any traces of the acetone and ether. The polymer electrolyte was finally obtained by soaking the membrane in 1 M $LiPF_6$ dissolved in a 1:1 (v/v) mixture of ethylene carbonate (EC) and diethylene carbonate (DEC) for 30 min. Hereafter, we refer to the composite polymer electrolyte using the acronym CPE.

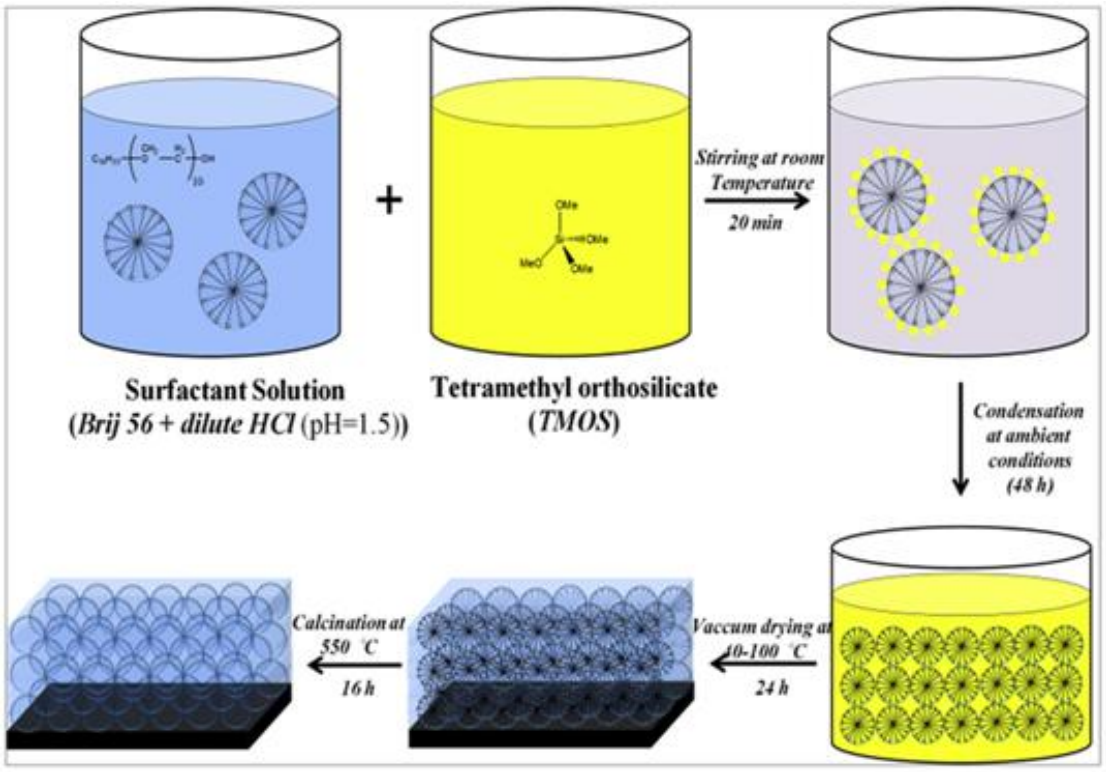

Figue 5.1. Schematic of the synthesis steps for mesoporous silica particles.

A sulfur/polyacrylonitrile (S/PAN) composite was chosen to be used as the cathode material. It has been reported that sulfur can either be distributed homogeneously in conductive PAN or can bind to the PAN matrix chains during heat treatment. This should significantly improve Li/S battery performance in terms of specific capacity and cyclability [62, 107-108]. However, the electrochemical properties of S/PAN composite cathodes are highly dependent on the preparation procedure. In order to obtain a good S/PAN cathode, a reaction between sulfur and PAN is necessary during heat treatment. This can be classified in three different temperature ranges:

1) Below 280 ^{o}C no reaction between S and PAN occurs. Sulfur remains in its elemental state (agglomerated poly (sulfur)). As a result, very poor electrochemical performance is obtained [109].

2) Between 280 and 450 ^{o}C, a reaction occurs between sulfur and PAN to form a composite that contains amorphous sulfur (nano-sulfur) distributed within the conductive polymer matrix and polymer chains with S-S_x ($0 < x < 6$) bonds on the sides [24,107]. This composite exhibits a high initial capacity, which is reduced upon cycling due to lower electric conductivity of sulfur and formation of lithium polysulfides that are soluble in liquid electrolyte (polysulfide shuttle) [62].

3) Above 450 ^{o}C, a complete reaction between sulfur and PAN occurs to form a disulfur side-chain functioning in the electrochemical reactions. As a result, excellent cyclability but low capacity are achieved [107].

In this study, the composite cathode was prepared by ball-milling a mixture of sulfur (Sigma-Aldrich) and PAN (Sigma- Aldrich) in a weight ratio of 3:1. This process was followed by heat treatment at 300 ^{o}C for 3 h in a tubular furnace filled with Ar gas. The amount of active material in the heat-treated S/PAN composite was 42%. The final sulfur-based cathode material was then prepared by mixing 80 wt% of S/PAN composite, 10 wt% acetylene black (99.5% purity, MTI), and 10 wt% PVdF (Kynar, HSV900) dissolved in N-methyl-2-pyrrolidene (NMP) (99.5% purity, Sigma-Aldrich). The sulfur mass loading of the electrode was about 2 mg cm^{-2}.

5.2.2 Characterization of the materials

The morphology of the samples was investigated by using field emission scanning electron microscopy (FE-SEM) (Leo-1530, Zeiss). The samples were gold-sprayed prior to SEM measurements. Nitrogen adsorption/desorption isotherms were measured at 77 K with a surface area analyzer (ASAP 2020). Prior to the measurements, the samples were degassed at 300 ^{o}C for at least 24 h. The Brunauer-Emmett-Teller (BET) method was used to calculate the specific surface area. The Barrett-Joyner-Halenda (BJH) model was also used to calculate the pore size and volume. The electrochemical properties were investigated using coin-type cells (CR2032) with a lithium metal anode, a sulfur-based cathode and composite polymer electrolyte. A Li/S battery cell with liquid electrolyte (a polypropylene separator (Celgard, USA) with 1 M $LiPF_6$ dissolved in 1:1 (v/v) mixture of EC and DEC) was also prepared to be used as a control sample. AC impedance spectroscopy was performed on the Li/S batteries cells with a VMP3 potentiostat (BioLogic) over the frequency range from 0.1 Hz to 1 MHz at room temperature. The cycling performance of the cells was investigated at room temperature on an Arbin BT2000 battery testing system in galvanostatic mode with cut-off voltages of 1.0 V and 3.0 V.

5.3 Results and discussion

Figures 5.2(A) and (B) show the pore size distribution and the nitrogen adsorption/desorption isotherm curves of the MPS particles. From the data, the following values are obtained: a BET surface area of 804.15 m^2 g^{-1}, pore volume of 0.86 cm^3g^{-1} and pore size of 3.83 nm. The scanning electron microscopy (SEM) images of the MPS particles at two different magnifications are shown in Figure 5.2(C) and (D). These images reveal that the synthesized silica is composed of spherical particles with diameters of between 200 and 400 nm, with no strict long-range order. Scanning electron microscopy images for the composite polymer membrane are shown in Figure 5.3. The electrolyte membrane has a thickness of about 100 mm. As can be seen, a porous membrane with small and uniformly distributed pores was obtained which would improve the electrolyte solution retention and promote the stability of the GPE morphology during cycling. Moreover, small and uniformly distributed pores might increase the mechanical stability of the polymer electrolyte.

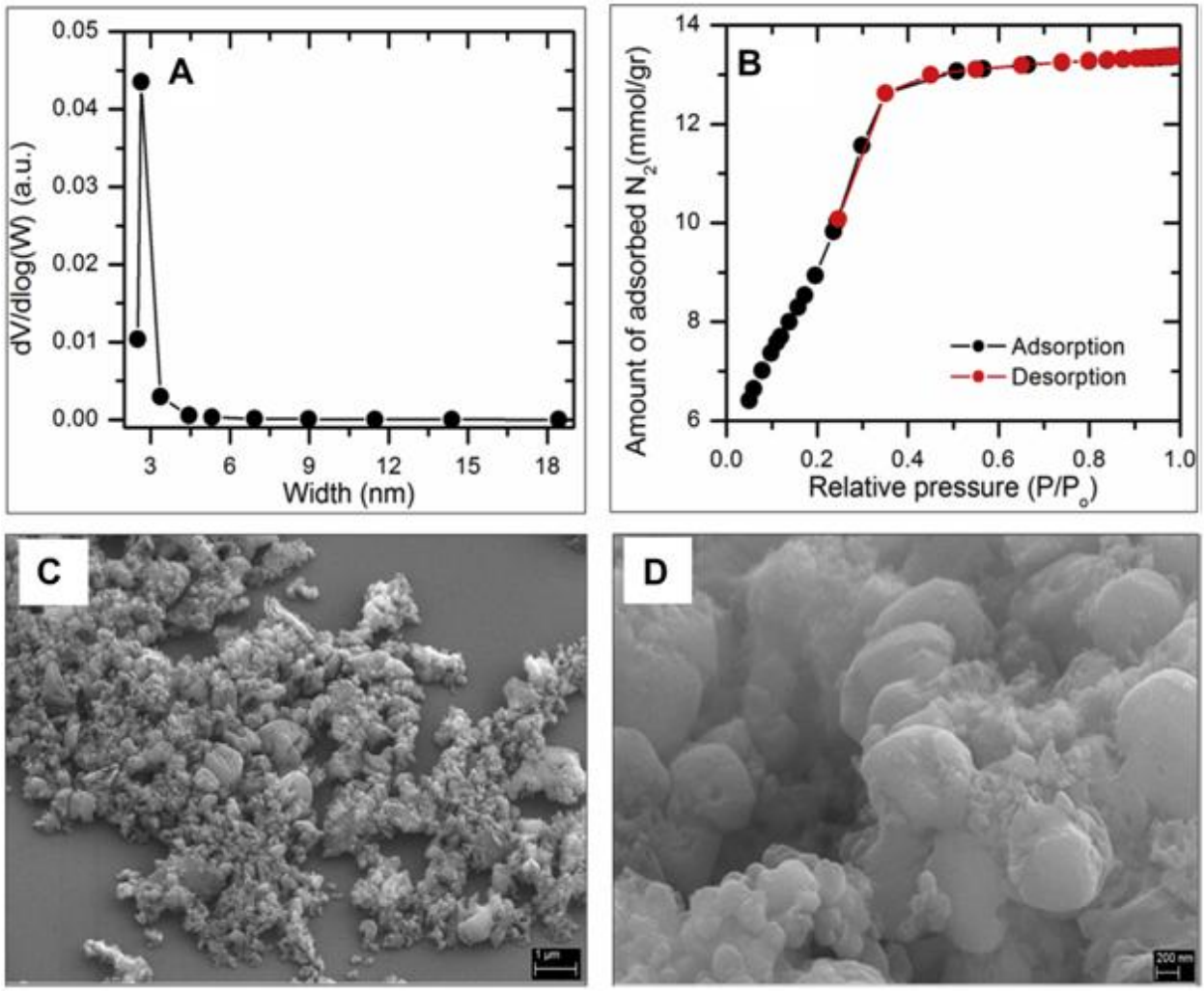

Figure 5. 2. Characterization of the synthesized particles; (A) nitrogen adsorption/desorption isotherm, (B) BJH pore size distribution graphs, (C) and (D) SEM images at low and high magnifications.

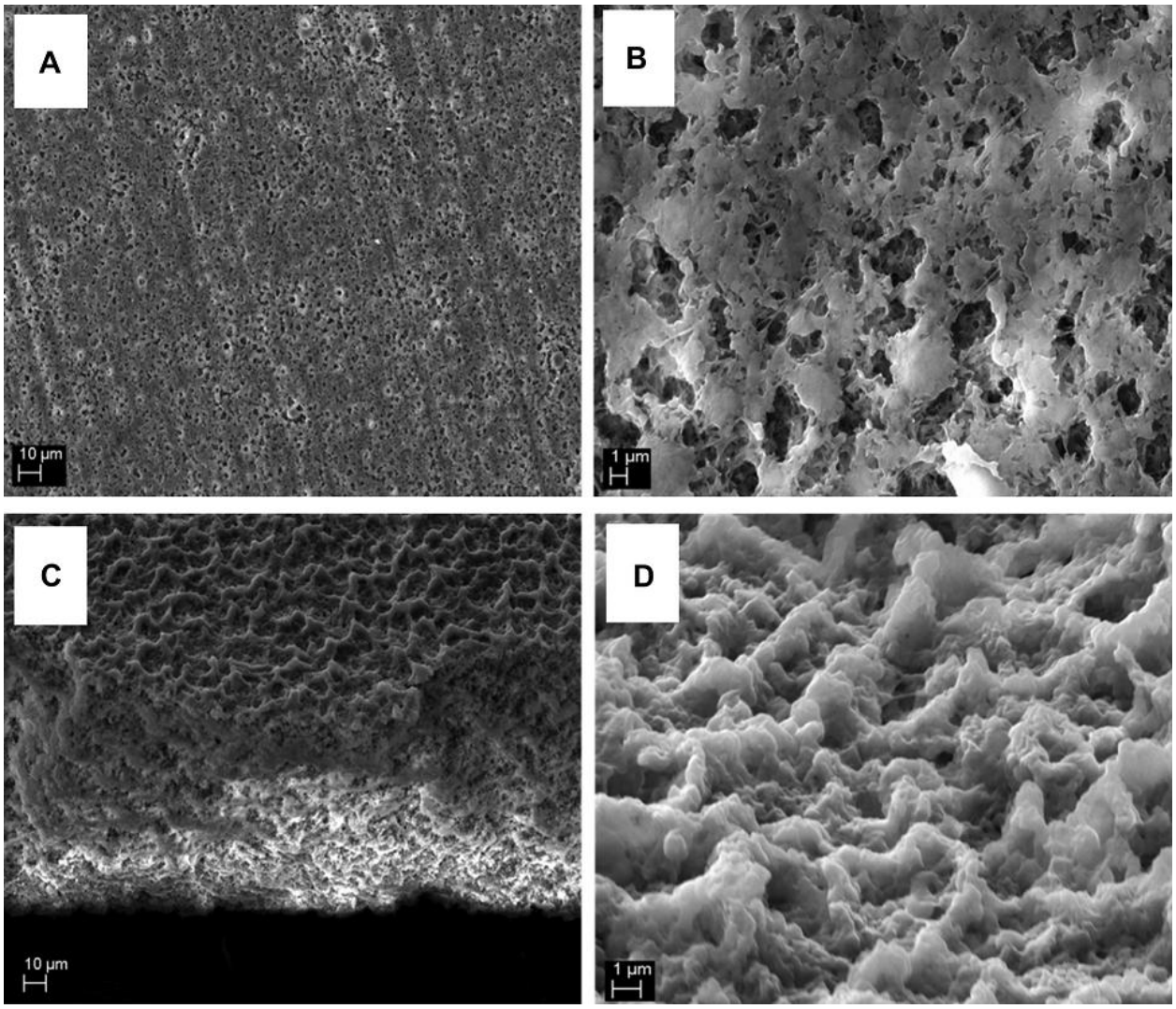

Figure 5.3. SEM images of the surface and cross-section of the composite polymer electrolyte.

Figure 5.4 presents the Nyquist plots of these battery cells obtained from AC impedance spectroscopy at the end of each cycle (i.e., end of the charge process) to characterize the effect of aging. Both cells exhibit low bulk (ohmic) resistance indicating the ease of lithium ion transportation within these cells. Furthermore, both fresh cells exhibit a high charge transfer resistance, which remarkably decreases upon initial cycling. In the case of Li/ liquid electrolyte/S cell, a stable charge transfer resistance is observed after the second cycle. However, the Li/CPE/S cell shows higher charge transfer resistance compared to the other cell that consistently increases upon cycling. This trend in charge transfer resistance of the Li/CPE/S cell is attributed to its slow reaction kinetics. In this case, diffusion of the generated polysulfides through the

electrolyte membrane is hindered, resulting in accumulation of these intermediate products in the cathode area and slowing the electrochemical reactions during cycling [105].

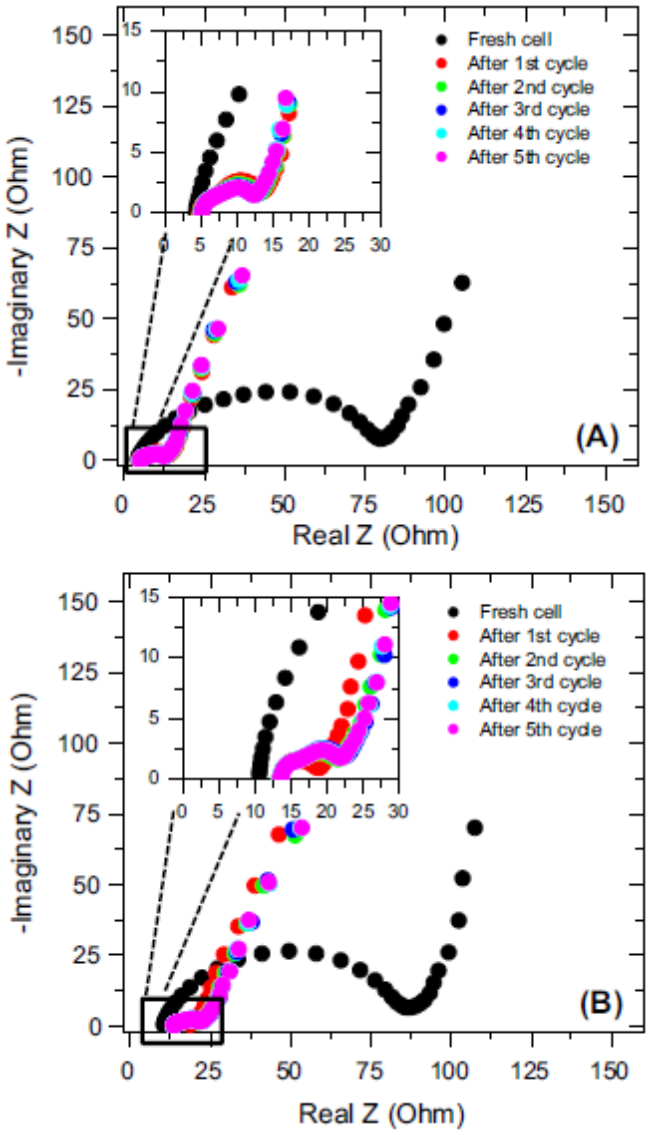

Figure 5. 4. Complex impedance plots for the first few cycles of (A) Li/liquid electrolyte/S and (B) Li/CPE/S battery cells.

Figure 5.5 shows galvanostatic charge/discharge cycles for both Li/S cells. The Li/liquid electrolyte/S exhibits an initial discharge capacity of 1610 mAh g^{-1} and initial charge capacity of about 1300 mAh g^{-1} based on the weight of sulfur active material. The values for the Li/CPE/S are 1648 mAh g^{-1} and 1277 mAh g^{-1}, respectively. Achieving such a high initial capacity values indicate a nearly complete reaction between lithium and sulfur due to high ionic conductivity of

both of the electrolytes used in these batteries, which supplies sufficient lithium ions for further electrochemical reactions with sulfur and results in the improved capacity of the cell [60]. Figure 5.6 presents the variation of discharge capacity with cycle number for these battery cells. As can be seen, the Li/liquid electrolyte/S cell exhibits a stable cyclability only up to 40 cycles. Then, poor cyclability leads to a drop in capacity to about 400 mAh g^{-1} sulfur or 135 mAh g^{-1} composite after 100 cycles. The active mass loss due to the dissolution of polysulfides into electrolyte solution and diffusion of these polysulfides through the separator (shuttle effect) is the main reason for such poor capacity retention in the Li/liquid electrolyte/S cell [110]. In contrast, the Li/CPE/S battery cell exhibits remarkably better capacity retention; a discharge capacity of 1143 mAh g^{-1} sulfur or 385 mAh g^{-1} composite was obtained after 100 cycles.

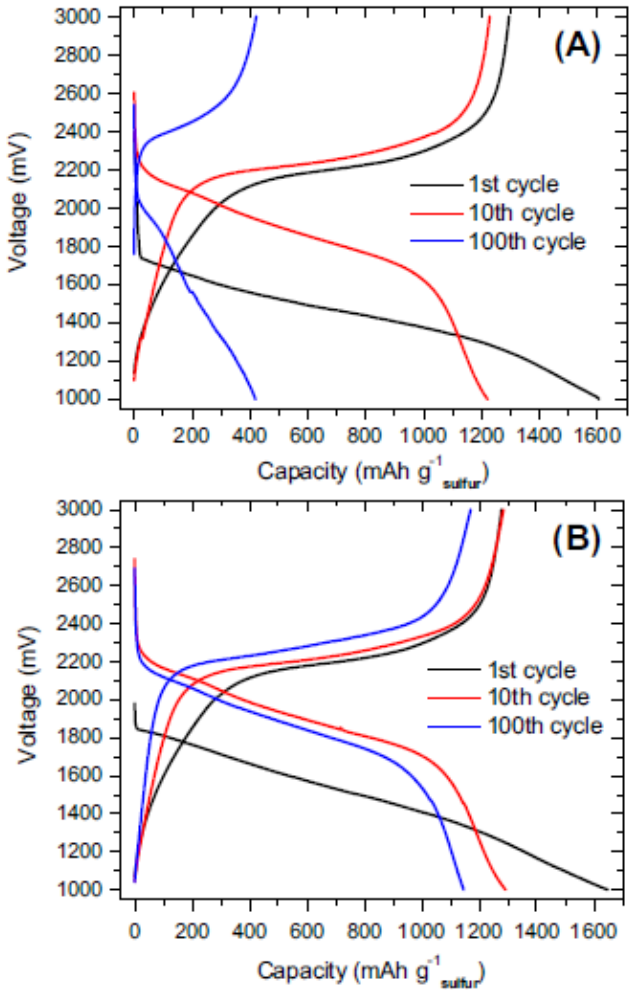

Figure 5.5. Charge/discharge curves of (A) Li/liquid electrolyte/S and (B) Li/CPE/S battery cells at 0.2 C.

To understand the reason for the improved electrochemical performance of the Li/CPE/S cell, the morphology of the two sides of the composite electrolyte after a few cycles was investigated by SEM equipped with an energy-dispersive X-ray (EDX) spectroscopy. Measuring the amount of sulfur deposited on the surface of either electrolyte or lithium metal can be considered a powerful tool to determine active mass loss during cycling. After opening the cell, we did not observe any electrolyte solution in the battery indicating the ability of the electrolyte membrane to retain the solution during cycling. Also, no agglomerated phase on the lithium metal surface was apparent. SEM images for the two sides of the composite electrolyte together with the EDX signals and S mapping are shown in Figure 5.7. The content of S in Figure 5.7(A) is 1.38 atomic %, while this value in Figure 5.7(B) is 0.03%.

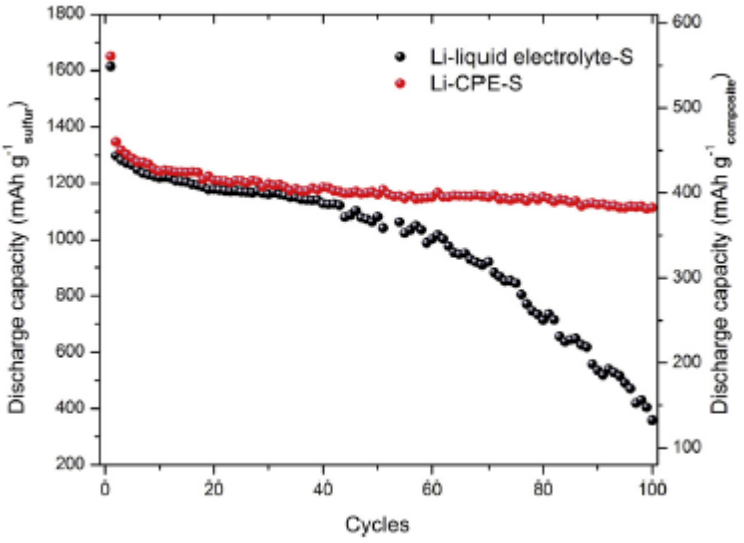

Figure 5.6. Discharge capacity versus cycles of the battery cells at 0.2 C rate.

It seems that physical immobilization of the liquid electrolyte solution within the composite membrane containing mesoporous particles can promote electrolyte retention and retard dissolution of polysulfides during cycling. Also, the migration of generated polysulfides through the electrolyte membrane is effectively hindered to suppress the shuttle effect. The combination of these effects leads to achieving such a high and stable capacity for the Li/S battery cell after long cycling.

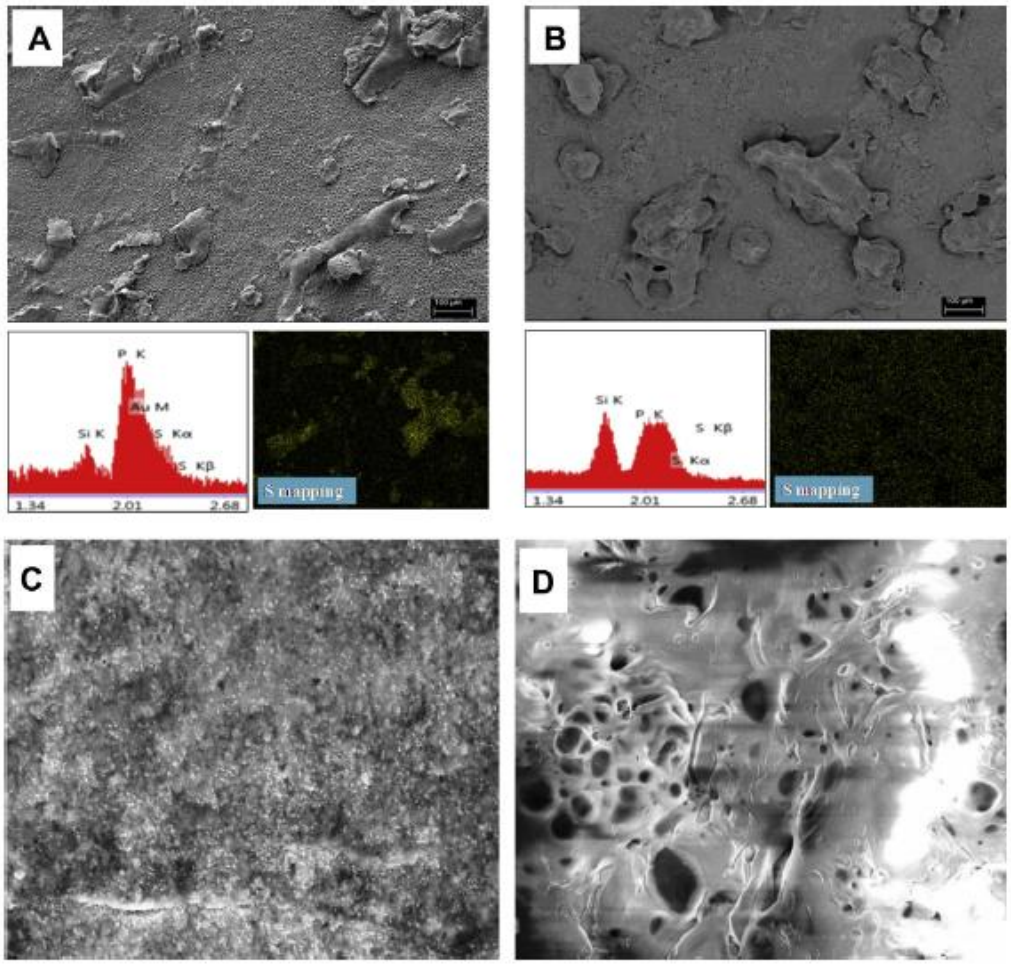

Figure 5.7. SEM and EDX results for two sides of the composite electrolyte after 25 cycles. (A) The side in contact with sulfur-based cathode, and (B) the side in contact with lithium metal. Scale bar = 100 mm, (C) and (D) SEM images of fresh lithium metal, and lithium metal after cycling.

5.4 Conclusions

A novel composite polymer electrolyte based on a polymer matrix and mesoporous silica particles was prepared and used in high performance Li/S batteries. Mesoporous silica particles were synthesized by a simple procedure. The resultant composite electrolyte displayed exceptional electrochemical properties of low ohmic resistance and relatively high charge transfer resistance, indicating the ease of Li^+ ion transportation and suppression of polysulfide shuttling between lithium anode and sulfur-based cathode. As a result, a high and stable discharge capacity of 1143 mAh g^{-1} was obtained after more than 100 cycles.

Chapter 6

Fabrication and characterization of a fluorinated electrolyte for high-energy and low-cost lithium-sulfur battery with a sulfur/hardwood charcoal composite cathode material[4]

6.1 Introduction

As mentioned earlier, to overcome the drawbacks of Li/S batteries, a large number of studies have focused on increasing the electronic conductivity of sulfur by encapsulating sulfur molecules with conducting materials, such as porous carbon or conductive polymers, which enables them to become electrically wired and electrochemically active. Conductive polymers such as polyacrilonitrile (PAN) and polypyrrole (PPY) are usually used to prepare sulfur-polymer composites. Although sulfur/polymer composites generally improve the cycling performance of Li/S cells, a large amount of the conductive polymer should be mixed into the cathode in all of these composites, resulting in low sulfur content of the electrode (<50 wt%). As a result, the pursuit of this strategy seems to be more academic than practical. On the other hand, a sulfur/carbon (S/C) composite potentially offers higher loading of sulfur. A few recent studies have reported application of activated carbon with high porosity and surface area in preparing sulfur composite cathodes.

In this part of this study, we aim to fabricate and characterize a feasible electrolyte choice for a Li/S battery cell with a sulfur-activated hardwood charcoal composite cathode material. Activated hardwood charcoal (AHC) is an odorless, tasteless and nontoxic powder derived from chips and sawdust with a high surface area (1400-1800 m^2/g), which can be used in poultices for external treatment of localized inflammation, infection and pain. Moreover, AHC is completely safe, even for oral use, allowing it to be added to animal food for treating poisons, infections and foul odors. Owing to its high porosity, specific surface area and good electrical conductivity, AHC may provide a unique scaffold to embed sulfur and improve the electronic conductivity of sulfur active material. Utilization of AHC, an inexpensive and abundant source of carbon, can significantly lower the final cost of the battery preparation.

[4] Data presented in this chapter was published in Ref. [118].

First, we will fabricate and test the effect of utilization of a polymer electrolyte membrane on the performance of this composite cathode material. As results will show, the resultant Li/S battery demonstrates improved electrochemical performance in terms of discharge capacity retention and cycle life as compared to its conventional counterparts.

In the second part of this chapter, a fluorinated liquid electrolyte will be employed in this high-energy and low-cost Li/S cell and the electrochemical properties will be studied in detail. Very recently, researchers have considered addition of a fluorinated solvent into the electrolyte solution to suppress the dissolution of lithium polysulfide and prevent the shuttle effect [32,111]. The resulting Li/S battery showed improved cyclability and Coulombic efficiency only over a very limited number of cycles, which was too small for any possible practical applications. In order to be relevant, Li/S batteries have to demonstrate a cycle life as long as that of lithium-ion batteries. In this study, we aim to utilize the same strategy in order to stabilize sulfur-activated hardwood charcoal composite, a low-cost and environmentally benign cathode material, with a prolonged cycle life.

6.2 Experimental

6.2.1 Materials preparation

An activated hardwood charcoal (AHC) powder purchased from *buyactivatedcharcoal.com* was pre-heated at 800 ^{o}C for 3 h. BET analysis confirmed the pore volume and specific surface area of the AHC to be 1.12 cm^3g^{-1} and 1747.3 m^2 g^{-1}, respectively. A mixture of sulfur (100-mesh particle size powder, Sigma-Aldrich) and AHC powder in a weight ratio of 10:4 was used to prepare the S–AHC composite by employing a solution processing method [31]. First, sulfur powder was dissolved in dimethyl sulfoxide (DMSO) at 120 ^{o}C by vigorously stirring for 2 h. Then, the AHC powder was added to the solution and dispersed by stirring for 4 h. This was followed by gradually cooling the mixture to room temperature overnight as it was stirred. During cooling, the dissolved sulfur molecules recrystallized in the highly porous structure of the AHC to form a sulfur–carbon composite. Finally, the composite powder was washed with ethanol and milli-Q water several times and then dried in a vacuum at 100 ^{o}C to evaporate ethanol, water and residual DMSO.

The porous polymer membrane was prepared as follows. Poly(vinylidene fluoride) (PVdF) was dissolved in acetone/dimethyl formamide (7:3, w/w) by ball milling at 380 rpm for 3 h, and was left to settle for 5 min to remove air bubbles before casting. Then, the solution was cast by a doctor blade on a glass mold and was kept at room temperature for 2 min for solvent evaporation and then it was immersed in milli-Q water bath for 1 h for phase inversion to generate micropores. The resulting membrane was vacuum dried at 80 °C overnight to remove water and any remaining solvent trace.

6.2.2 Characterization of the materials

X-ray diffraction (XRD) patterns were obtained on a D8 Discover Bruker instrument equipped with Cu-Kα radiation. SEM images were taken using a field emission scanning electron microscopy (FE-SEM) (Leo-1530, Zeiss). The samples were gold-sprayed prior to SEM measurements. The interior morphology of the samples was further studied using transmission electron microscopy (TEM, CM10, Philips). The state of sulfur in the S–AHC composite was studied by UV−vis absorption spectroscopy (Ultrospec 4300 Pro) with 1 nm resolution on powders dispersed in ethanol through ultrasonication for 3 h. Thermogravimetric analysis (TGA) was carried out using a DSC-TGA (Q-600, TA instruments) at temperature ramp mode with a heating rate of 10 ^{o}C min^{-1} at N_2 gas atmosphere. Nitrogen adsorption–desorption isotherms were measured at 77 K with a Surface Area Analyzer (ASAP 2020). Prior to the measurements, the samples were degassed at 300 C for at least 24 h. The Brunauer–Emmett–Teller (BET) method was used to calculate the specific surface area. The Barrett–Joyner–Halenda (BJH) model was also used to calculate the pore size and volume.

6.2.3 Electrochemical characterization

The S-AHC cathode electrode was prepared by mixing of wt% S-AHC composite, 20 wt% acetylene black (AB, MTI, 99.5% purity) as conductive agent, 10 wt% polyvinylidene fluoride (PVDF, Kynar, HSV900) as a binder and NMP (Sigma-Aldrich, ≥99.5% purity) as a dispersant. The obtained slurry was then applied to an Al foil current collector and dried in a drying oven at 70 °C for 12 h. The polymer electrolyte was obtained by soaking the porous membrane in a liquid electrolyte, consisting of a 1M lithium bistrifluoromethane sulfonamide (LiTFSI) (Aldrich, 99.95%) dissolved in in 1:1 v/v 1,2-dimethoxyethane (DME) and 1,3-dioxolane (DOL). The electrochemical properties were investigated using coin-type cells

(CR2032). Each cell was composed of a lithium metal anode, a sulfur-based composite cathode and an electrolyte, either a polymer electrolyte or a liquid electrolyte (a polypropylene separator (Celgard, USA) with 1 M LiTFSI dissolved in a 1 : 1 (v/v) mixture of DME/DOL). Hereafter, we refer to the polymer electrolyte with the acronym PE. Also, we refer to the liquid electrolyte as the acronym LE. A galvanostatic charge/discharge test was carried out within a voltage range of 1-3 V, at a discharge rate of 0.2 C (1C= 1672 mAh g^{-1}). Cyclic voltammetry measurements were done at a scanning rate of 0.1 mV s^{-1}.

The electrochemical properties the Li/S cells with the fluorinated electrolyte were also investigated using coin-type cells (CR2032). Each cell was composed of a lithium metal anode, a sulfur-based composite cathode and an electrolyte consisting of a polypropylene separator (Celgard, USA) with 1 M LiTFSI dissolved in a 1 : 1 (v/v) mixture of 1,3-dioxolane (DOL) and1,1,2,2-tetrafluoroethyl-2,2,3,3-tetrafluoropropyl ether (TTE). 1 M LiTFSI dissolved in a 1 : 1 (v/v) mixture of DOL and 1,2-dimethoxyethane (DME) was used as reference electrolyte solution. A galvanostatic charge/discharge test was carried out within a voltage range of 1.5-2.8 V at a discharge rate of either 0.1 C or 0.3 C (1 C = 1672 mAh g^{-1}). Cyclic voltammetry measurements were done at a scanning rate of 0.05 mV s^{-1}.

6.3 Results and discussion

6.3.1 Characterization of S-AHC composite cathode

The morphology of S-AHC composite was experimentally studied using XRD, DSC, TGA, SEM, TEM and BET. Figure 6.1(top) shows the XRD spectra of pristine sulfur, AHC and S-AHC composite. The pattern observed for pristine sulfur matches very well with the standard of orthorhombic phase sulfur while the pattern of the S-AHC composite shows a broad diffraction peak at ~25^{o} and low intensity diffraction peaks of crystal sulfur, which could be an indication recrystallization of sulfur into the internal pores or surface of AHC particles. Figure 6.1(bottom) shows the DSC curves for sulfur, AHC powder, and S-AHC composite. Pristine sulfur shows two sharp endothermic peaks at 110 ^{o}C and 120 ^{o}C arising from the phase transition and melting of the elemental sulfur. However, the S-AHC composite shows only one endothermic peak with lower intensity at 115 ^{o}C attributed to the melting of nano-sized elemental sulfur [31]. SEM and TEM images for AHC and S-AHC composite powders at two magnifications are shown in Figures 6.2 and 6.3, respectively. These images show the high

surface area and pore volume of the AHC powder. The as-prepared S-AHC composite aggregates have a particle size of a few hundred nanometers. Moreover, BET results confirmed that the specific surface area of AHC powder was reduced from 1747.3 to 541.17 m^2 g^{-1} and particle size increases from 3.43 to 11.08 nm when the S-AHC composite is formed. Results of EDX mapping for both sulfur (S) and carbon (C) are also shown in Figure 6.2. These results point out that sulfur is either embedded in the micropores of the AHC particles or deposited on its surface and distributed uniformly within the composite. During the composite preparation process, sulfur was dissolved and uniformly mixed with AHC matrix. Later in the cooling process, sulfur re-crystallized and was homogenously distributed in the matrix. As a result, the crystal size of sulfur was considerably reduced after this dissolution and re-crystallization process, allowing the formation of a S-AHC composite containing small sulfur crystals.

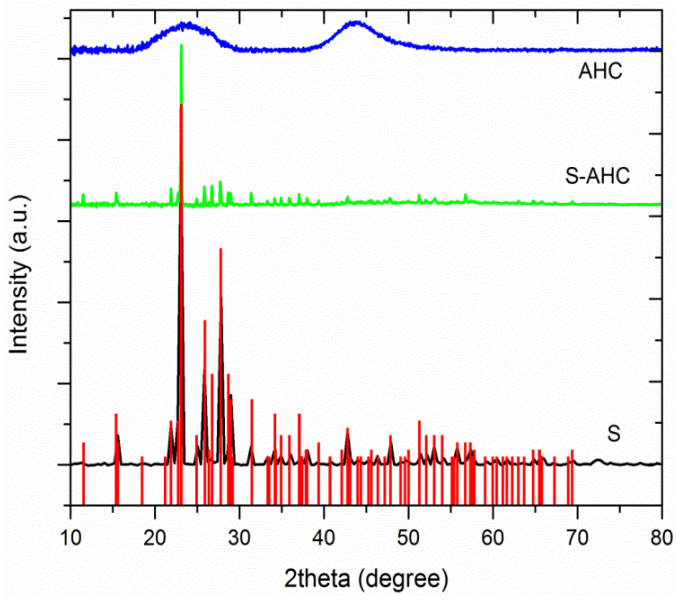

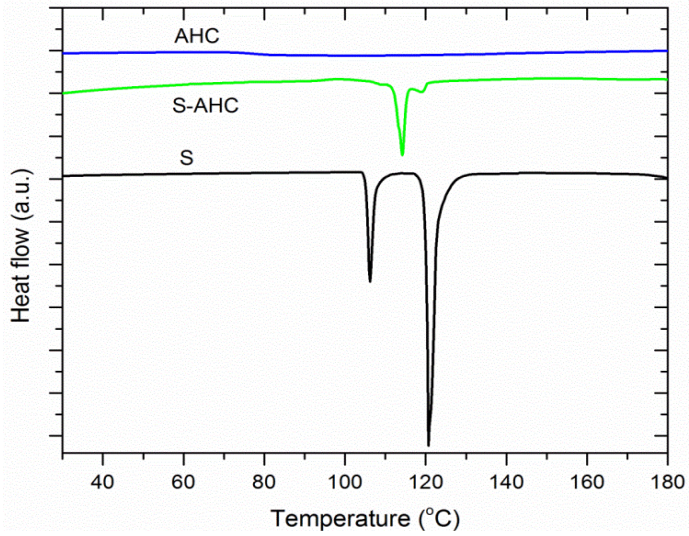

Figure 6.1. XRD patterns (top) and DSC curves (bottom) for elemental sulfur, activated hardwood charcoal, and the S-AHC composite

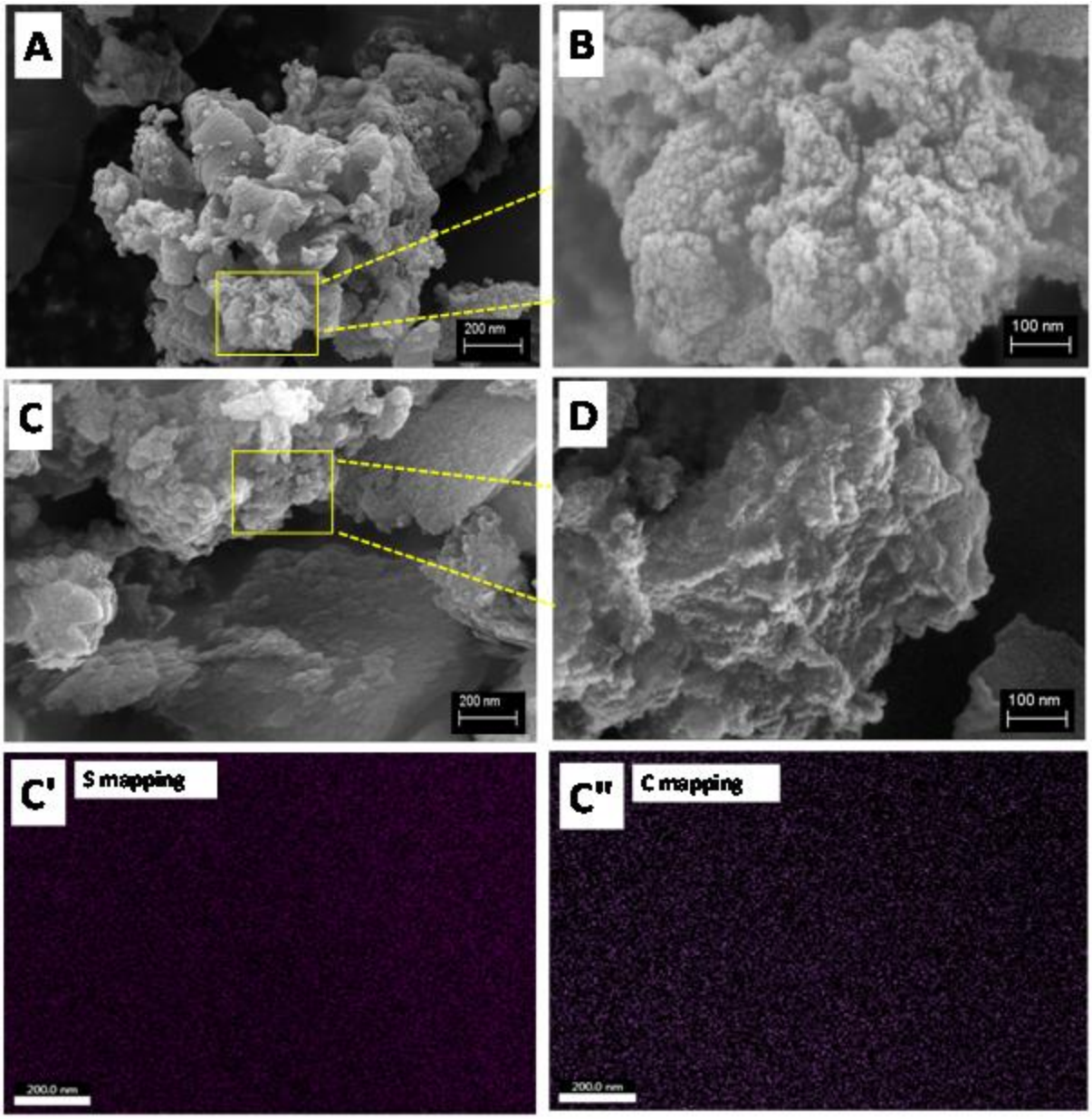

Figure 6.2. SEM images for (A,B) AHC powder, and (C,D) S-AHC nanocomposite powder at two different magnifications. (C', C") show the S mapping and C mapping of the S-AHC nanocomposite.

Thermogravimetric analysis (TGA) was used to determine the sulfur content in the S-AHC composite (Figure 6.4). Since sulfur is stable up to 220 ^{o}C, the rapid weight loss at 220-310 ^{o}C indicates a very rapid decomposition and fast migration of degradation products from the remaining mass. However, the weight loss of the S-AHC composite occurs in the range of 220-380 °C with a mass remaining of 35 wt%. Above 380°C, no further weight change was observed.

This shows that S-AHC composite contains 65 wt% sulfur, which is higher than the previously reported work [31]. This is due to the high surface area and porosity of activated hardwood charcoal (AHC) that offers higher loading of sulfur compared to conventional carbon sources.

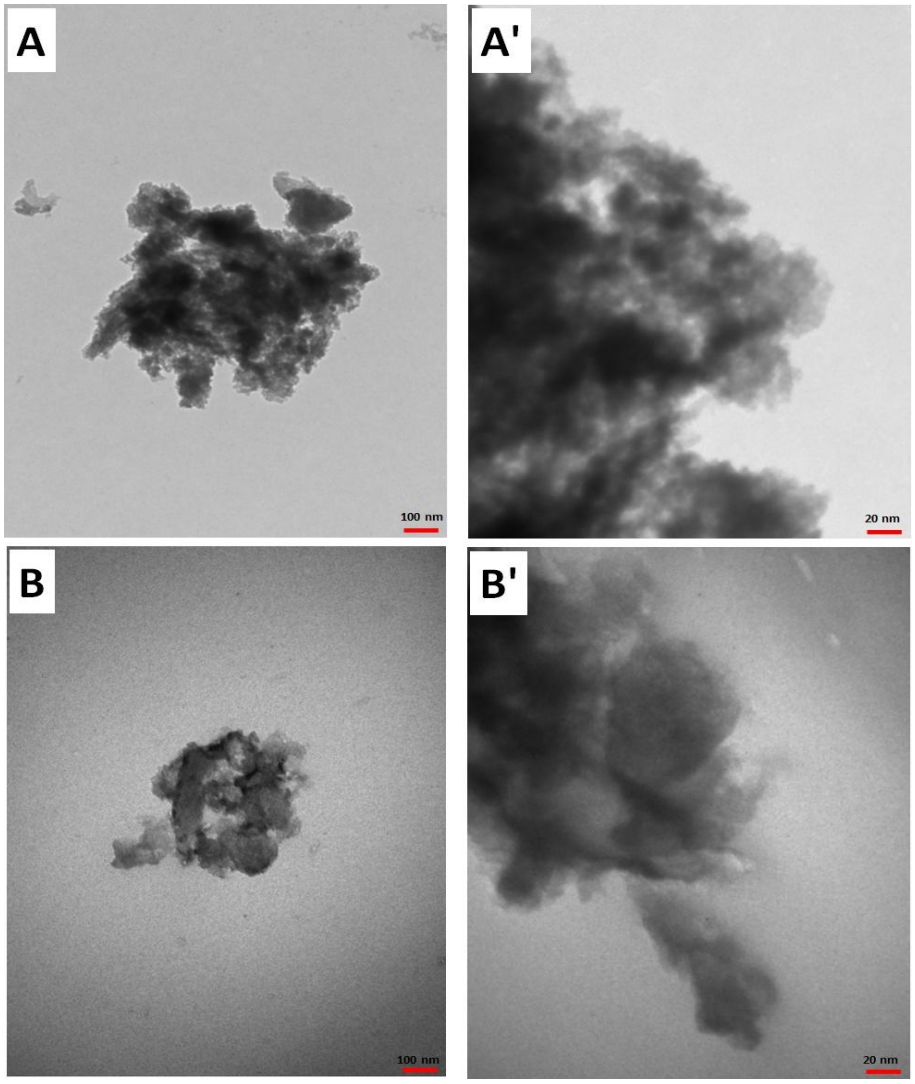

Figure 6.3. Bright field TEM image of (A, A') AHC, and (B, B') S-AHC composite at two magnifications

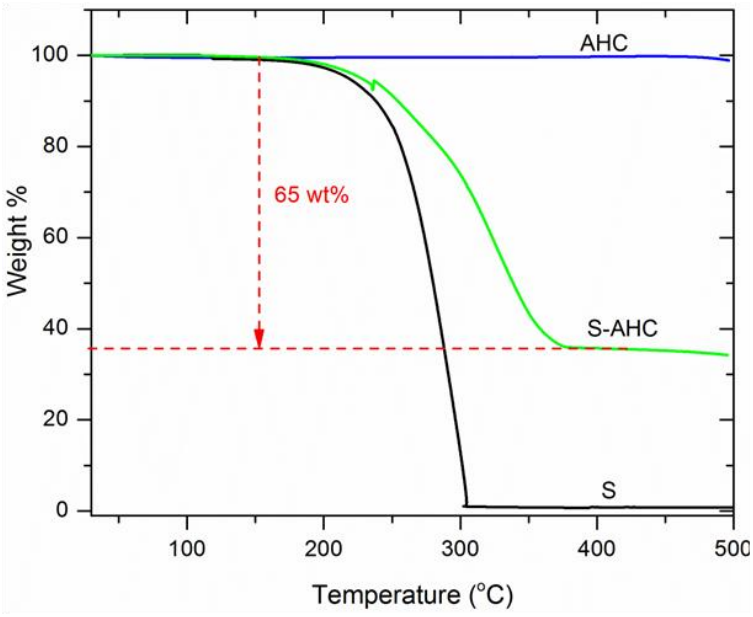

Figure 6.4. Thermogravimetric analysis graphs for sulfur, activated hardwood charcoal, and S-AHC composite

UV-Vis spectroscopy was used to study the state of sulfur within the composite. Figure 6.5 shows the obtained spectra for pristine sulfur, AHC powder and S–AHC composite. AHC shows no absorption peak while pristine sulfur shows a broad absorption peak between 200-350 nm, which is attributed to the elemental sulfur. As can be seen, the S–AHC composite has a similar absorption spectrum as S, indicating that no chemical reaction takes place between sulfur and AHC under this synthesis condition and that sulfur inside the micropores or on the surface of AHC powder remains in its elemental state.

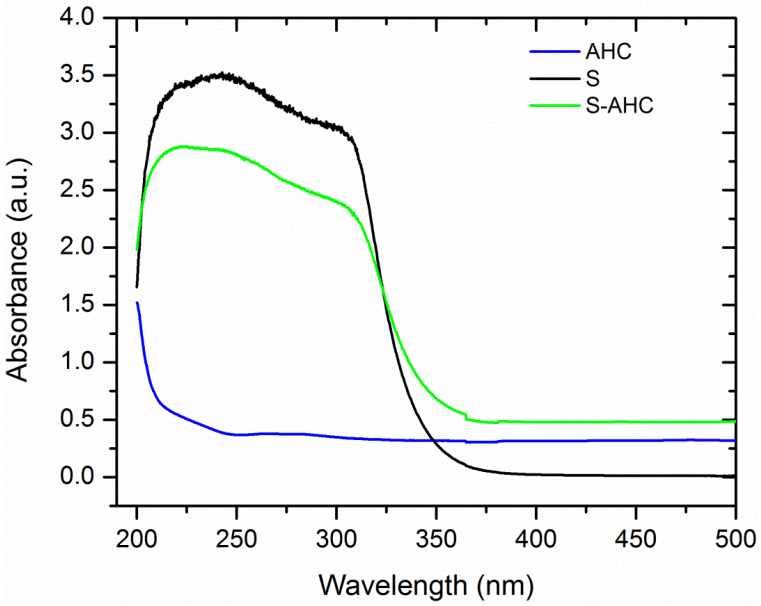

Figure 6.5. UV-vis spectra of sulfur, AHC, and S-AHC composite

As a comparison, Ketjenblack (KB, AkzoNobel, EC-600 JD), a commonly used porous carbon with high specific surface area of 1400 m^2 g^{-1}, was used as a matrix to prepare a S-KB composite according to the same solution processing method. The content of sulfur in S-KB composites was determined by thermal gravimetric analysis (TGA) to be about 61 wt% (Figure 6.6) which is lower than that of S-AHC composite. Apparently, AHC powder can effectively encapsulate higher amounts of sulfur in its micropores leading to a higher sulfur content of this composite. Charge-discharge profiles and the cycling properties of the S-AHC and S-KB electrodes are presented in Figure 6.7. From this figure, the S-AHC electrode delivers considerably higher discharge capacity than S-KB. It seems that using AHC with high pore size and specific surface area as a scaffold for sulfur is an effective approach to enhance the sulfur active material utilization in the cell and achieve higher capacities.

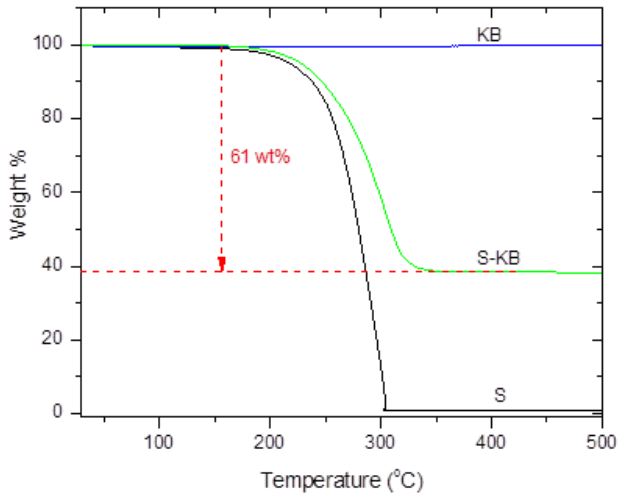

Figure 6.6. TGA curves for sulfur, Ketjenblack (KB), and S-KB composite

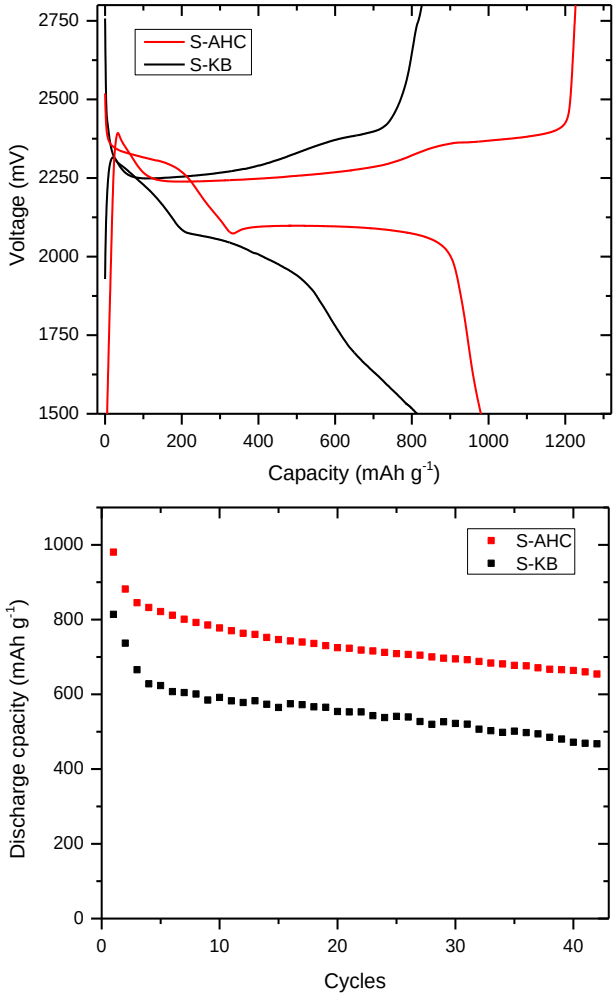

Figure 6.7. (top) Charge–discharge profiles of the first cycle and (bottom) cycle life for S-AHC and S-KB cathode composites at 0.2 C and 1.5-2.8 V voltage range.

6.3.2 Electrochemical performance of the high-energy and low-cost Li/S battery with a polymer electrolyte

A scanning electron microscopy image of the thin PVDF membrane is shown in Figure 6.8. The electrolyte membrane had a thickness of about 35 μm. Despite being this thin, the film membrane exhibited reasonably good tensile strength and mechanical stability for handling preparation of the battery cell. As the SEM image shows, a highly porous membrane with very small pore size (a few hundred nanometers) was obtained, which would immobilize the liquid electrolyte solution in contact with the sulfur cathode during electrochemical reactions of the battery cell.

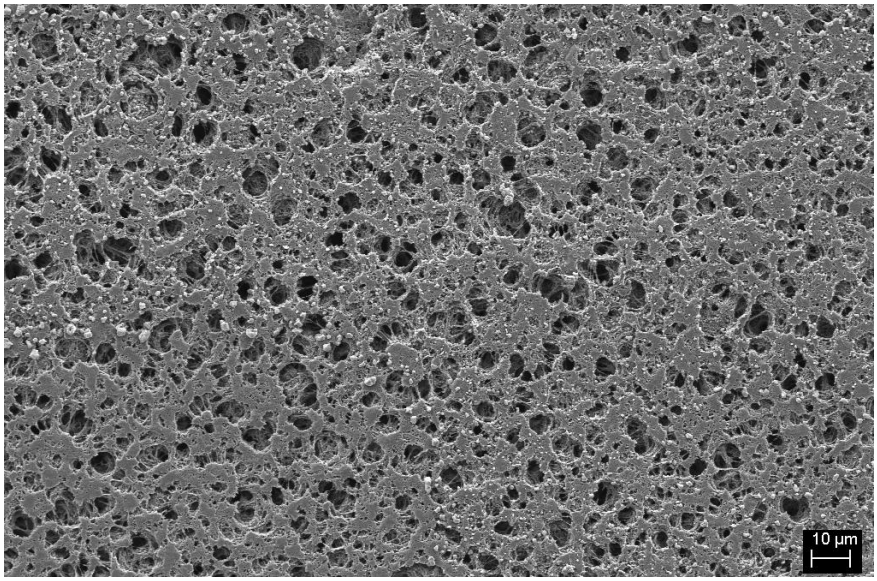

Figure 6.8. SEM image for the porous PVDF-based electrolyte membrane

AC impedance spectroscopy was performed on the Li/S-AHC cell with a potentiostat (VMP3, BioLogic) over the frequency range from 0.1 Hz to 0.1 MHz at room temperature to yield the results shown in Figure 6.9. As expected, the control battery cell has a lower ohmic resistance indicating easier lithium ion conduction in this cell. Interestingly, the modified cell has higher charge transfer resistance (R_{ct}) attributed to the slow reaction kinetics within this cell. In this case, dissolution and diffusion of the generated intermediate polysulfides into the electrolyte are hindered, resulting in accumulation of these intermediate products in the cathode area and slowing the electrochemical reactions between the electrodes during cycling. The slower reaction

kinetics of the modified Li/S battery cell is further proved in the cyclic voltammograms (Figure 6.10). Smaller reduction and oxidation peaks are observed in the Li/PE/S compared to the control Li/S cell is an indication of slower reaction kinetics in this cell.

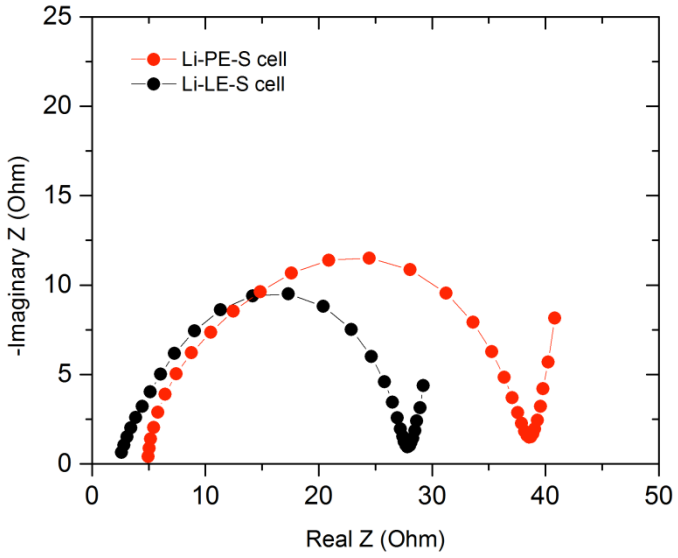

Figure 6.9. AC impedance spectroscopy for both cells at room temperature

Figure 6.11 shows the galvanostatic charge-discharge profiles of the first cycle for both Li/S cells. In these profiles, two discharge plateaus are observed (at 2.4 and 2.1V) matching well with the two reduction peaks in the CV curves in Figure 6.10. These plateaus are attributed to the reduction of elemental sulfur to produce high-order lithium polysulfides followed by their further reduction to form Li_2S [112,113]. Both cells deliver a similar initial discharge capacity of about 1060 mAh g^{-1}. However, the modified battery cell has an initial charge capacity of 1088 mAh g^{-1} compared to the 1234 mAh g^{-1} for the control cell. As can be seen, the control battery cell has an obviously longer charge plateau cell (Figure 6.11). This difference is mainly due to the high solubility of the lithium polysulfides produced during the first discharge into the liquid electrolyte solution. These soluble species diffuse to the lithium metal anode during the charge process, allowing their direct reaction with lithium metal anode and a longer charge process of the battery cell.

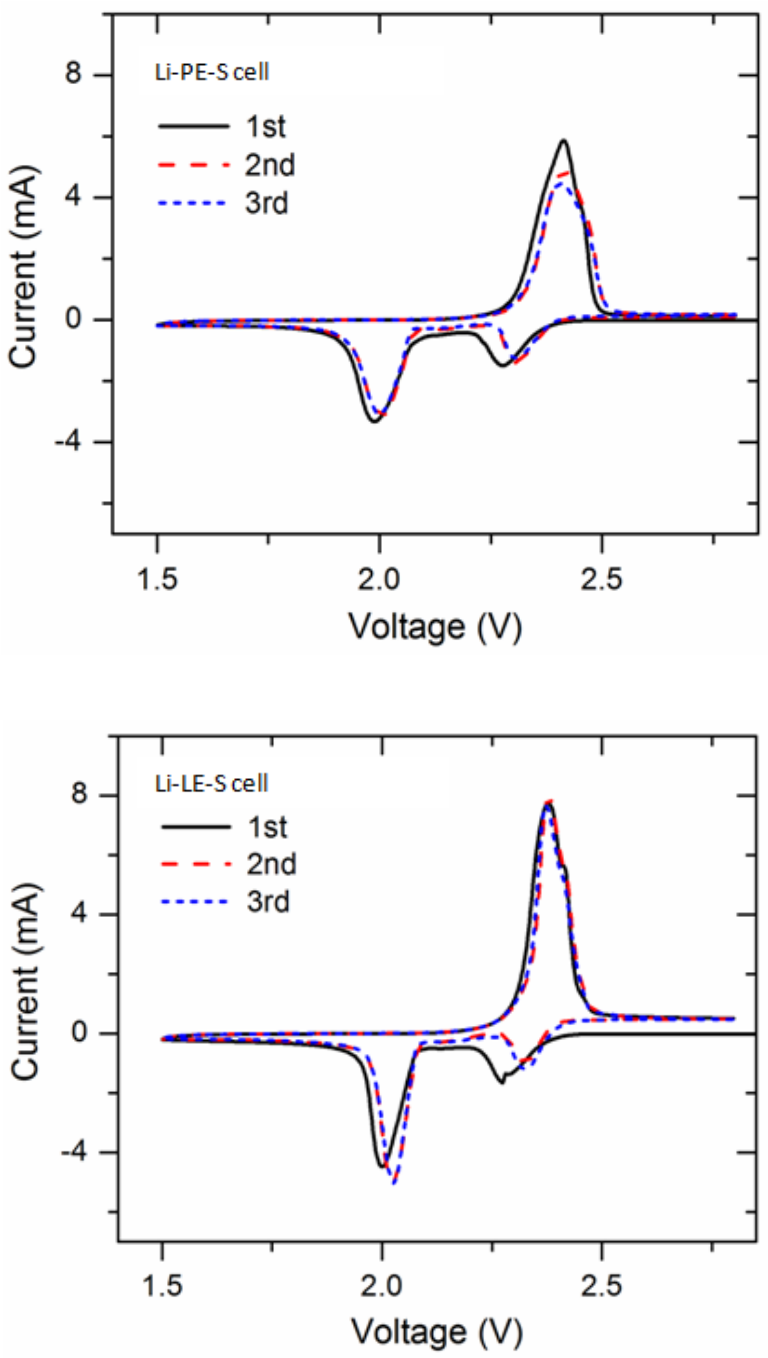

Figure 6.10. Cyclic voltammetry of the cells at a scan rate of 0.1 mV s^{-1} and voltage range of 1.5- 2.8 V.

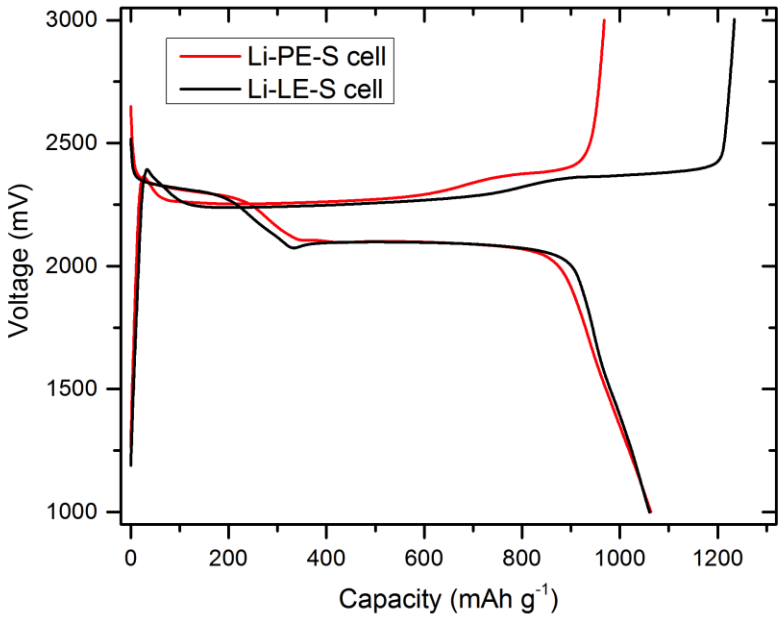

Figure 6.11. Charge–discharge profiles for both cells at 0.2 C and 1-3 V voltage range

Figure 6.12 presents the variation of discharge capacity and Coulombic efficiency with cycle number for these cells. For the control cell, discharge capacity decreases rapidly upon cycling. Such a poor cyclability and low Coulombic efficiency are attributed to the presence of the shuttle phenomenon of soluble lithium polysulfides during the charge and discharge processes within this cell, which reduces the discharge capacity and increases the charging capacity of Li/S batteries [114]. In contrast, the modified cell shows improved cyclability and higher Coulombic efficiency, delivering capacity of about 400mAh $g^{-1}$and maintaining a Coulombic efficiency of 90% after 250 cycles. However, it should be pointed out that in spite of the improved Coulombic efficiency and cyclability due to the suppressed shuttling of polysulfide, the delivered discharge capacities are lower than the previous report [31]. This can be attributed to the lower ionic conductivity of gel polymer electrolytes, as compared to liquid electrolytes, which supplies less lithium ions for the electrochemical reactions with sulfur and results in the lower capacity of the cell [115].

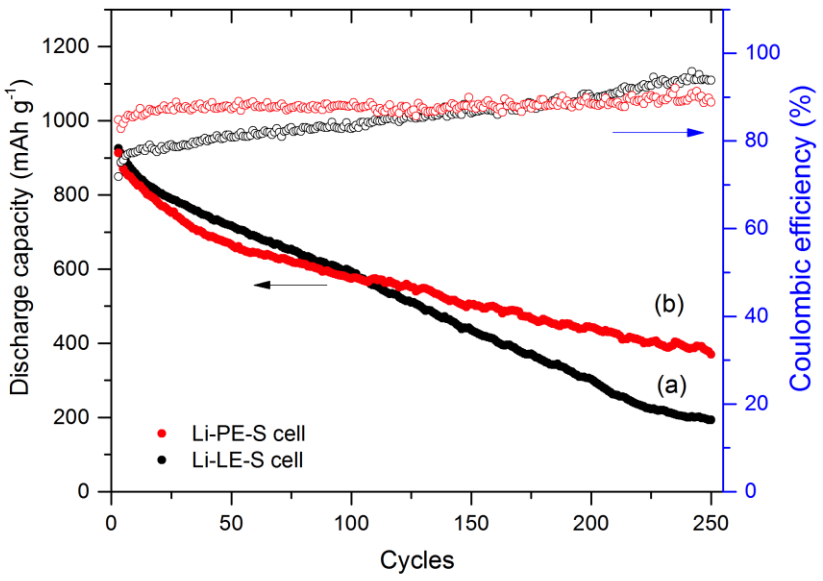

Figure 6.12. Cycle life for both cells at 0.2 C and 1-3 V voltage range

To understand the reason for the improved electrochemical performance of the modified Li/S cell, morphology of the electrolyte membrane and lithium metal anode before and after a few cycles was investigated by SEM. After opening the cell, we did not observe any electrolyte solution in the battery indicating the ability of the electrolyte membrane to retain the solution during cycling. Also, no evidence of an agglomeration phase on the lithium metal surface. The obtained SEM images are shown in Figure 6.13. It seems that physical immobilization of the liquid electrolyte solution within the electrolyte membrane can promote the electrolyte retention and retard dissolution of polysulfides during cycling. Also, the migration of generated polysulfides through the electrolyte membrane is effectively hindered to suppress the shuttle phenomenon.

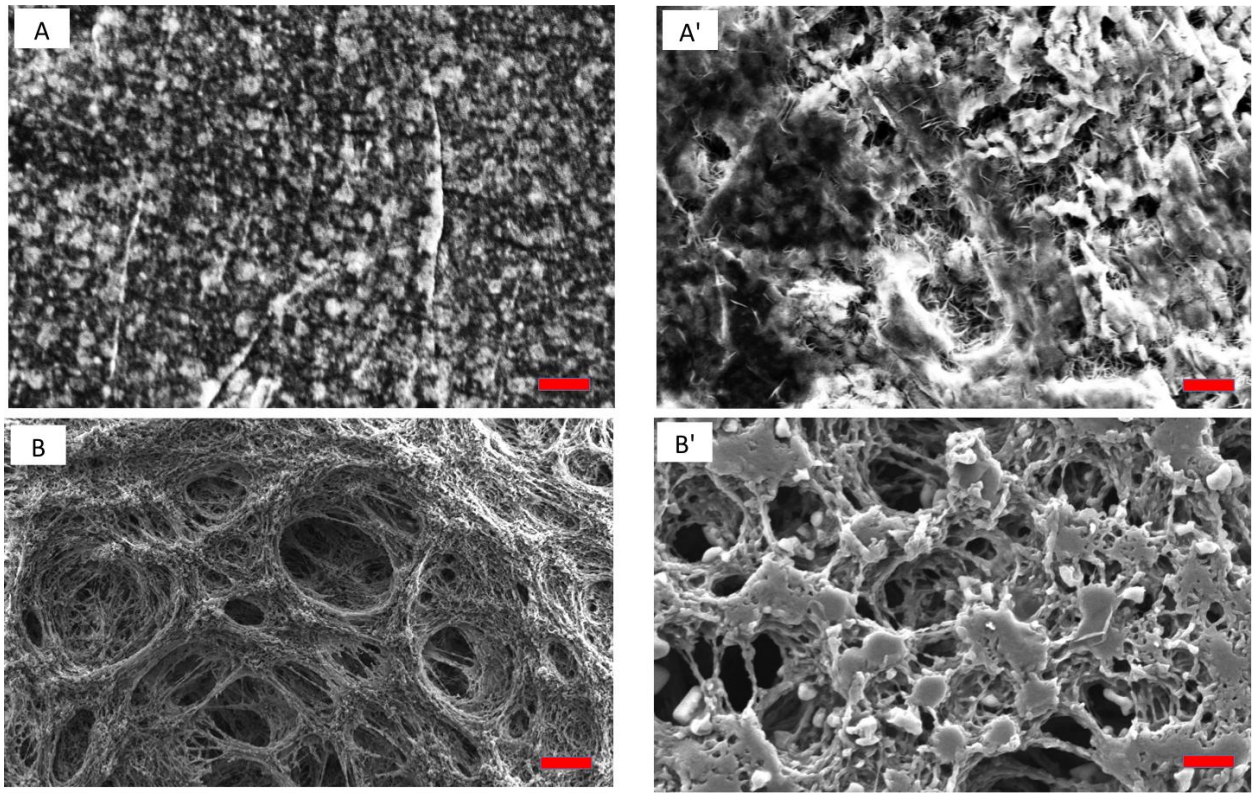

Figure 6.13. SEM images of (A, A') lithium metal and (B, B') polymer electrolyte membrane, before and after 25 cycles. Scale bar = 1 ηm.

6.3.3 Electrochemical performance of the high-energy and low-cost Li/S battery with a fluorinated electrolyte

Figure 6.14 shows the variation of capacity and Coulombic efficiency with cycle number for this Li/S battery cell. An initial discharge capacity of 1260 mAh g^{-1} (based on the sulfur mass in the composite cathode) is obtained. A stable discharge capacity of 800 mAh g^{-1} and a Coulombic efficiency of 97% are obtained after 100 cycles at 0.1 C, indicating very good cyclability of this battery cell. To compare the improvement in the electrochemical performance, a Li-S cell with the conventional electrolyte solution (1 M LiTFSI in DOL/DME) was also tested under the same testing condition to be used as a reference. Capacity retention and cycling efficiency versus cycles for these two Li/S cells are shown in Figures 6.15 and 6.16. The Li/S cell using the reference electrolyte solution shows low Coulombic efficiency and its capacity decreases rapidly over cycling. A discharge capacity of 230 mAh g^{-1} and Coulombic efficiency of 80% are obtained after 300 cycles. Such a poor cyclability and low efficiency are attributed to

the dissolution of lithium polysulfide intermediates into the electrolyte resulting in a severe active mass loss and shuttle reactions of these soluble species during the charge and discharge processes. In contrast, the Li/S cell with the new electrolyte solution shows significantly improved cyclability and higher Coulombic efficiency, delivering a capacity of about 600 mAh g^{-1} and maintaining a Coulombic efficiency of 97% after 300 cycles.

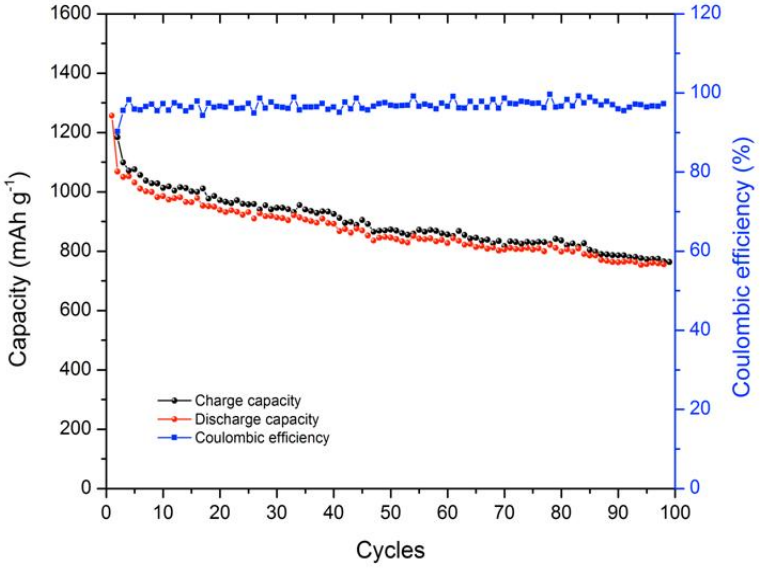

Figure 6.14. Cyclic performance and Coulombic efficiency of the Li-S cell with the fluorinated electrolyte at a 0.1 C rate and 1.5-2.8 V voltage range.

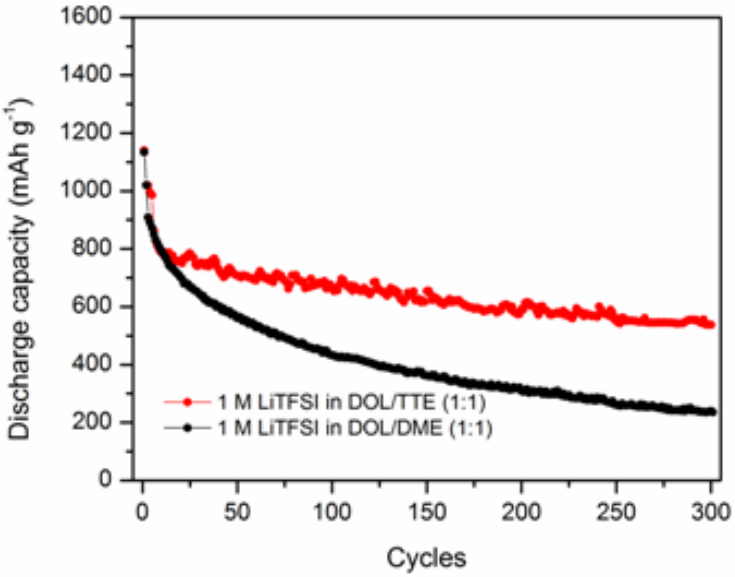

Figure 6.15. Comparison of the cyclic of two Li-S cells with different electrolytes at 0.3 C rate and 1.5 - 2.8 V voltage range.

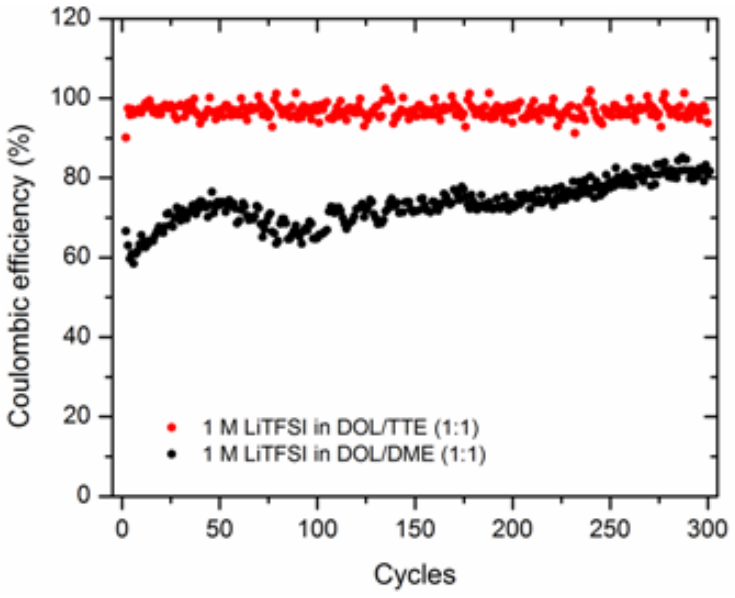

Figure 6.16 Comparison of Coulombic efficiency of two Li-S cells with different electrolytes at 0.3 C rate and 1.5 - 2.8 V voltage range.

Cyclic voltammetry (CV) measurements were used to identify the electrochemical properties of both cells, and the results are presented in Figure 6.17. For the cell with the reference electrolyte, typical characteristics of multistep electrochemical reactions between sulfur and lithium ions are observed by two oxidation peaks at 2.3 and 2.05 V, together with corresponding reduction peak at 2.35 V. On the other hand, the cell with the fluorinated electrolyte exhibited a relatively different trend, as the two oxidation peaks are located at 2.25 and 1.8 V. Moreover, the reduction peak is located at above 2.4 V, and a small shoulder is observed at a voltage slightly below 2.4 V. These shifts in the oxidation peaks toward lower potential and in the reduction peak toward higher potential in the cell with the fluorinated electrolyte indicates lower ionic conductivity arising from lower concentration of dissolved polysulfides in this electrolyte. Another noticeable difference in the CV graphs is the lower altitude of the reduction and oxidation peaks in the cell with the fluorinated electrolyte compared to the reference electrolyte, which is an indication of slow reaction kinetics in this cell, most probably because of lower concentrations of polysulfides.

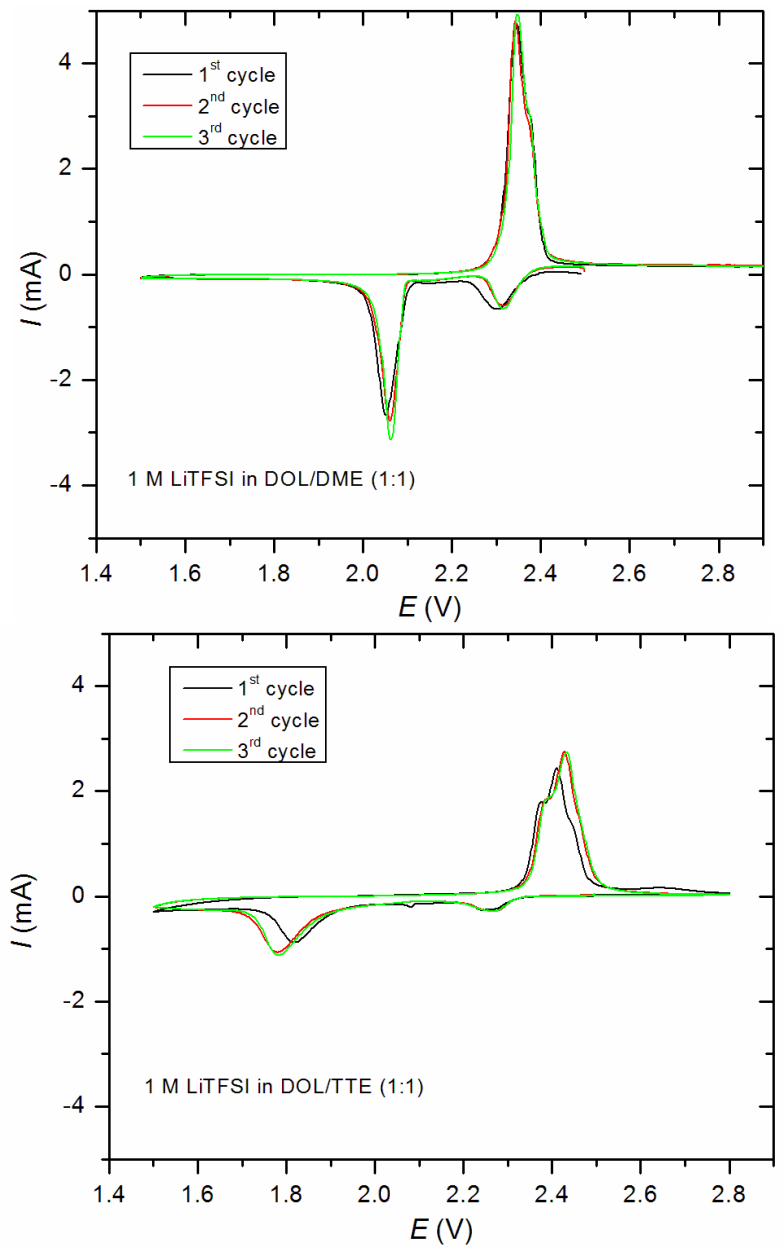

Figure 6.17. Cyclic voltammetry of both Li-S cells at a scanning rate of 0.05 mV s^{-1}.

Galvanostatic intermittent titration technique (GITT) experiments were also conducted with a BioLogic electrochemical instrument to further study the electrochemical reactions as a function of depth of discharge. The cells were discharged at a slow current rate of 0.05 C (83.6 mA g^{-1}) in the voltage range of 2.5- 1.5 V. Then, AC impedance spectroscopy was performed at each point with different depth of discharge (DOD). The impedance spectra were collected at room temperature with amplitude of 10 mV in the frequency range of 1 MHz to 100 mHz. As

shown in Figure 6.18, a notable difference in the impedance spectroscopy versus DOD of these cells was observed. Although both cells show almost the same ionic and charge transfer resistance values at the beginning of the discharge, the ionic resistance of the cell with the conventional electrolyte decreases as discharge process proceeds, which is directly related to the increase in the concentration of dissolved lithium polysulfides in the electrolyte. At points 2 and 3 of DOD, concentration of dissolved polysulfides reaches its highest value [113] and at the end of discharge (points 4-8 in DOD) concentration of these dissolved species begins to decrease. This trend in the ionic resistance is in good agreement with the minimum ionic conductivity theory as a function of concentration [113]. The impedance spectra also shows that the charge transfer resistance decreases between points 2 and 3 of DOD, due to the fast reaction kinetic of high-order polysulfides [113] and increases again at the end of discharge due to slow kinetics of low-order polysulfides. Furthermore, the deformation of impedance spectra at points 4-7 of DOD indicates the non-uniform precipitation of low-order polysulfides across the cathode [113-114], which might be one of the reasons to the fast fade in cyclability of this cell.

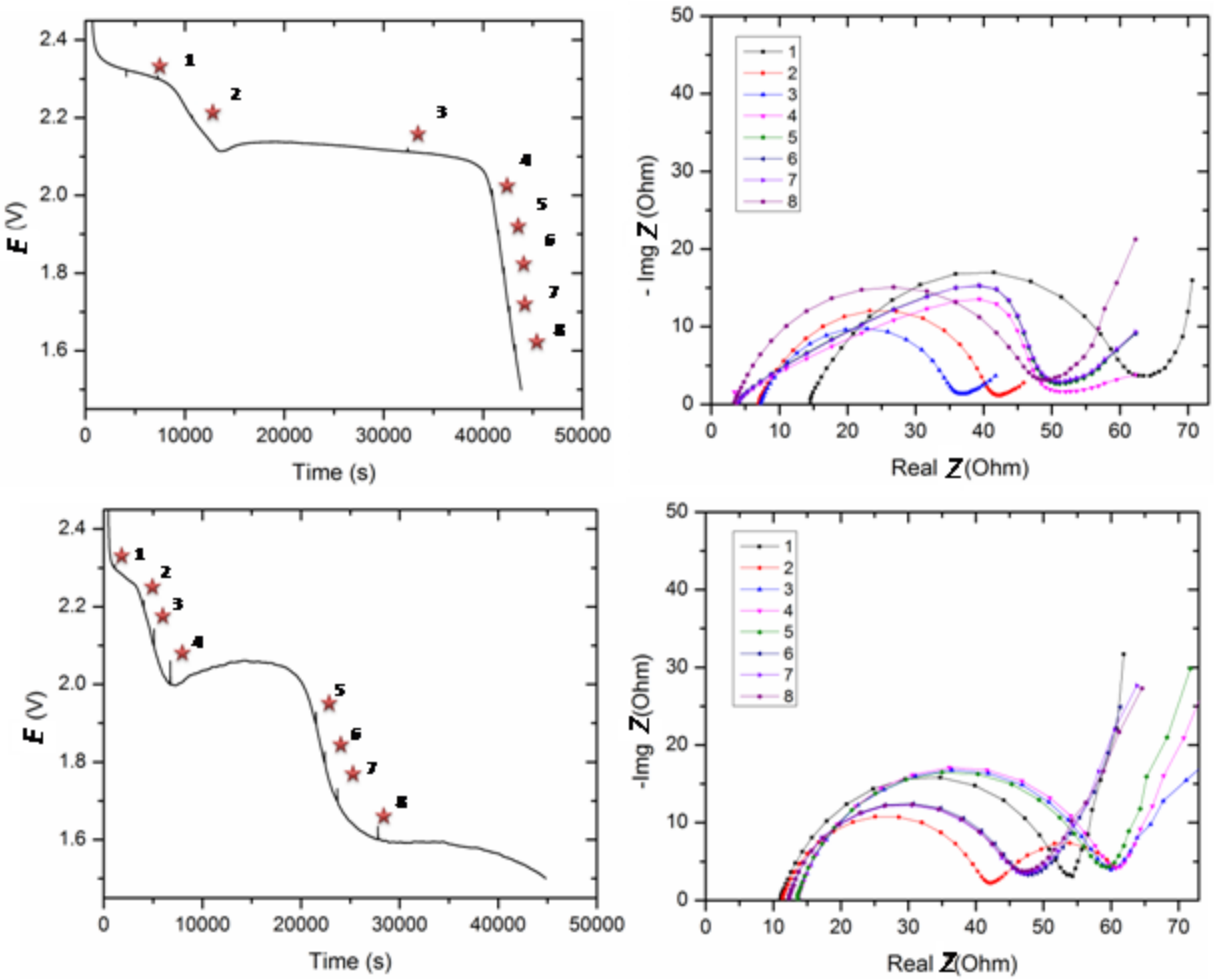

Figure 6.18. GITT and AC impedance spectroscopy results obtained at the first discharge process for the Li-S cell with two different liquid electrolytes. 1 M LiTFSI in DOL/DME (1:1) (top), and 1 M LiTFSI in DOL/TTE (bottom).

The voltage profile for the cell with the fluorinated electrolyte does not completely follow the typical two-plateau profile commonly observed for sulfur-carbon composite cathodes. The first and second plateaus are shorter than those of the reference cell. However, the ratio of second plateau to first one is almost identical for both cells. For this cell, the first voltage plateau is ascribed to the reduction of elemental and high-order polysulfides. But due to the low concentration of elemental sulfur and high-order polysulfides, the potential drops more quickly to the plateau, which is related to the reduction of low-order polysulfides. The third observed plateau might be related to a solid phase reduction [115] or a liquid phase one at low voltages due to the very slow dissolution of active material and very low concentration of dissolved polysulfides.

Interestingly, the cell with the fluorinated electrolyte shows a relatively small increase in its ionic resistance during the discharge process, which is consistent with less dissolution of lithium polysulfides into this liquid electrolyte. This phenomenon is also reflected by the larger shift in the second reduction peak in the CV of this cell. The voltage profile also points out that the fast kinetics of high-order polysulfides reduce the charge transfer resistance at point 2 of DOD, while the coexistence of two phases of active material (high-order polysulfides and low-order ones) and discontinuous phase of high volume fraction of elemental sulfur produces a second semicircle in impedance spectra. The points 3-5 in DOD of the new cell can be compared to the points 4-7 of DOD in the reference cell, as the charge transfer resistivity increases. However, the impedance spectra do not show any deformation. This is because of the small relaxation time of these small precipitated particles [114] that cannot be seen in this frequency range. One important note is that although cell voltage plateau and impedance spectra of these two cells are quite different, the delivered capacity is almost identical.

Changes in the morphology of S-AHC cathode electrode in the Li/S cell with the fluorinated electrolyte after the first cycle were studied through scanning electron microscopy. Figure 6.19 (A) shows the SEM image of the pristine S-AHC electrode. At the end of the first discharge process, large flakes of crystal-like discharge products (Li_2S_2 and/or Li_2S) are deposited on the surface of the cathode electrode (Figure 6.19 (B)). However, after the first charge process, all of the deposited discharge products disappear and the charged electrode shows morphology similar to the pristine cathode (Figure 6.19 (C)), which indicates the full reversibility of electrochemical reaction occurring in this Li-S cell. This was further proved by analysing the surface of the electrode by energy-dispersive X-ray spectroscopy (EDX), in which the pristine electrode and fully charged one show similar EDX spectra (Figure 6.19 (A', C').

These results indicate that dissolution of lithium polysulfides into the fluorinated liquid electrolyte is prevented; hence active mass loss and parasitic side reactions are eliminated to improve the cyclability and Coulombic efficiency of the Li/S cell.

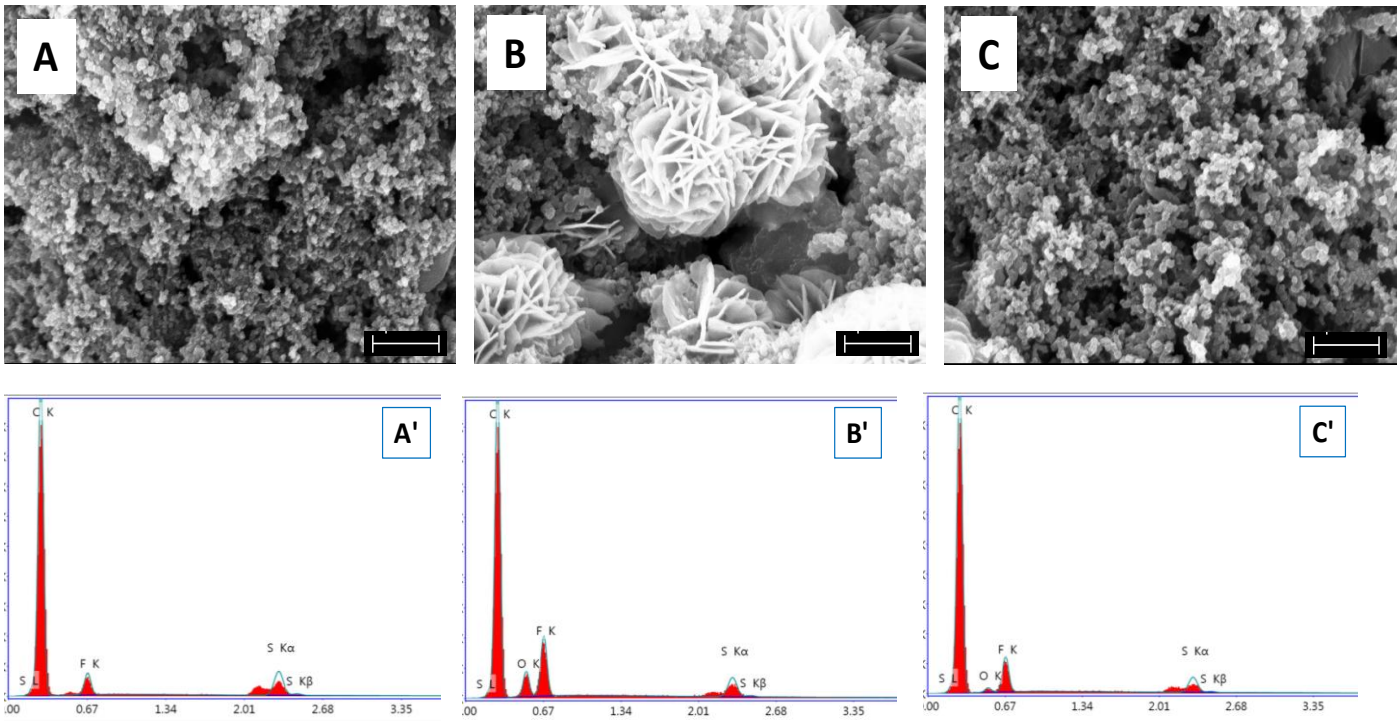

Figure 6.19. SEM images and EDX spectra of pristine S-AHC electrode (A, A'), discharged S-AHC electrode (B, B'), and charged S-AHC electrode (C, C').

6.4 Conclusions

A low-cost, high-energy sulfur-based composite cathode was prepared by mixing sulfur with activated hardwood charcoal through a simple solution processing method. The effect of two different electrolyte systems on the electrochemical performance of this cathode electrode was studied in detail. First, a polymer electrolyte was fabricated and utilized in this cell. The resultant Li/S battery delivered a high initial discharge capacity of 1060 mAh g^{-1} at 0.2C and exhibited improved cycling characteristics; discharge capacity of 400 mAh g^{-1} and Coulombic efficiency of 90% were obtained after 250 cycles. Second, a fluorinated liquid electrolyte was employed and the obtained Li/S cell delivered a high initial discharge capacity of 1260 mAh g^{-1} and exhibited discharge capacity of 800 mAh g^{-1} after 100 cycles at 0.1 C. We further demonstrated the improved cycling performance of this battery cell by comparing the obtained results with a reference liquid electrolyte commonly used in Li/S batteries. This new Li/S cell maintained stable discharge capacity of 600 mAh g^{-1} and Coulombic efficiency of 97% after 300 cycles at 0.3 C, while the reference cell delivered discharged capacity of 230 mAh g^{-1} with an

efficiency of 80%. Considering the improved cycling performance of the Li/S cell demonstrated in this work, this battery system seems to be a promising candidate for high-energy and low-cost energy storage systems.

Chapter 7

Conclusions and perspective towards future work

Environmental concerns associated with fossil fuels have triggered a search for alternative, clean and renewable energy sources. Attributed to their high energy density, rechargeable lithium ion batteries are among the most promising candidates of energy storage systems. Lithium ion batteries are the dominant power source for portable electronic devices, such as cell phones and laptops. However, for applications in hybrid or electric vehicles, significant improvements in energy density are still required. Among all lithium batteries, the lithium/sulfur cell has theoretical specific capacity of 1672 mAh g^{-1} and specific energy of 2600 Wh kg^{-1} when the complete reaction of sulfur and lithium is supposed. Sulfur is also cheap, abundant, and environmentally benign. However, it has been difficult to develop a practical Li/S battery due to the problems of low electrical conductivity of sulfur, active mass shuttling loss, and dissolution of polysulfides into liquid electrolyte. These drawbacks result in poor cycle life, low specific capacity, and low energy efficiency, thus severely limiting the overall application of Li/S batteries.

In recent years, extensive research has been carried out to develop Li/S batteries. However, most of the attentions have been focused on the optimization of sulfur cathode electrode neglecting the critical effect of the electrolyte. From the electrolyte perspective, besides deteriorating battery performance due to dissolving polysulfides, the use of liquid electrolytes raises some safety concerns since they are flammable and prone to leakage. Therefore, developing a feasible electrolyte alternative for Li/S batteries has been the center of this thesis.

Replacing liquid electrolytes with a gel polymer electrolyte provides advantages in simplified and flexible design and fabrication of Li/S batteries. Gel polymer electrolytes, consisting of solid matrices that provide mechanical strength, and embedded liquid electrolytes, can effectively reduce leakage of liquid electrolytes, while maintaining high lithium ion conduction. Therefore, in the first part of this thesis, different approaches for the preparation of gel polymer electrolytes were studied. PVDF-HFP was chosen as the matrix of polymer electrolyte membrane, and a few different methods were employed to modify the morphology of

the matrix in order to obtain a highly porous electrolyte membrane with small and uniformly distributed pores that possesses high absorption ability towards liquid electrolytes. The polymer membrane with absorbed liquid electrolyte presented a self-standing film with good mechanical properties and ionic conductivity values as high as 5 mS cm^{-1} at room temperature and electrochemical stability of up to 4.8V vs. Li^{+}/Li.

Sulfur/conductive polymer (S/PAN) composites were used as active cathode materials and were prepared via mechanical mixing and thermal treatment. The Li/S cell with PVdF-HFP/OMMT nanocomposite electrolyte delivered initial capacity of 1622 mAh g^{-1} and maintained a capacity of 500 mAh g^{-1} after 300 cycles. When the PVdF-HFP/functionalized PMMA electrolyte was used, the Li/S battery had an initial discharge capacity of 1600 mAh g^{-1} and a stable capacity of 1050 mAh g^{-1} after more than 100 cycles. Furthermore, utilization of PVdF-HFP/functionalized PMMA/mesoporous silica composite electrolyte resulted in an initial discharge capacity of 1648 mAh g^{-1} and a stable discharge capacity of 1143 mAh g^{-1} after more than 100 cycles.

In further studies, a high-energy and low-cost sulfur/hardwood charcoal composite cathode material was fabricated by a simple solution-based processing method. Results showed that gel polymer electrolytes cannot effectively prevent polysulfide dissolution and performance fading in this Li/S cell. However, when a fluorinated liquid electrolyte containing 1,1,2,2-tetrafluoroethyl-2,2,3,3-tetrafluoropropyl ether was employed, a significant improvement in the electrochemical performance of the Li/S cell was achieved. An initial discharge capacity of 1260 mAh g^{-1} (based on the sulfur mass in the composite cathode) is obtained. A stable discharge capacity of 800 mAh g^{-1} and a Coulombic efficiency of 97% are obtained after 100 cycles at 0.1 C. Moreover, this new Li/S cell maintained stable discharge capacity of 600 mAh g^{-1} and Coulombic efficiency of 97% after 300 cycles at 0.3 C, while the reference cell delivered discharged capacity of 230 mAh g^{-1} with an efficiency of 80%.

Although it is still necessary to further explore the effect of different electrolyte alternatives and electrolyte additives on the electrochemical properties of Li/S batteries, it is also vital to do research on the two other components of the Li/S battery, i.e. lithium metal anode and cathode, as well. For the cathode electrode, sulfur loading has to be increased considerably in order to improve the overall specific energy of the battery cell while maintaining good cycle life

and active material utilization. Such a high cell specific energy can be obtained only at elevated sulfur loadings (above 70%). If we want to explore the full potential of Li-S batteries, it is also necessary to find a proper anode material which has a comparable capacity and low plateau potential. A lithium metal-free anode should be developed to address all of the safety concerns and low cycling efficiency of the lithium metal anode.

In summary, many issues still remain unsolved in the way of practical development of Li/S batteries and intensive research efforts are needed to address them.

.

References

[1] Seh ZW, Li W, Cha JJ, Zhang G, Yang Y, McDowell MT, Hsu PC, Cui Y. Sulphur-TiO_2 yolk-shell nanoarchitecture with internal void space for long-cycle lithium-sulphur batteries. Nature Communications 2013; 4: 1-6.

[2] Cai K, Song MK, Cairns EJ, Zhang Y. Nanostructured Li_2S-C composites as cathode material for high-energy lithium/sulfur batteries. Nano Letters 2012; 12: 6474−6479.

[3] Li GC, Li GR, Ye SH, Gao XP. A Polyaniline-Coated Sulfur/Carbon Composite with an Enhanced High-Rate Capability as a Cathode Material for Lithium/Sulfur Batteries. Advanced Energy Materials 2012; 2:1238–1245.

[4] Guang H, Ji X, Nazar LF. High "c" rate Li-S cathodes: Sulfur imbibed bimodal porous carbons. Energy and Environmental Science 2011; 4: 2878-2883.

[5] Lin F, Wang J, Jia H, Monroe CW, Yang J, NuLi Y. Nonflammable electrolyte for rechargeable lithium battery with sulfur based composite cathode materials. Journal of Power Sources 2013; 223:18-22.

[6] Song MK, Cairns EJ, Zhang Y. Lithium/sulfur batteries with high specific energy: old challenges and new opportunities. Nanoscale 2013; 5: 2186-204.

[7] Ji X, Evers S, Black R, Nazar LF. Stabilizing lithium-sulphur cathodes using polysulphide reservoirs. Nature Communications 2011; 2:325-332.

[8] Ji X, Nazar LF. Advances in Li–S batteries. Journal of Materials Chemistry 2010; 20: 9821-9826.

[9] Mikhaylik YV, Akridge JR. Polysulfide Shuttle Study in the Li/S Battery System. Journal of The Electrochemical Society 2004; 151: A1969-A1976.

[10] Bruce PG, Freunberger S, Hardwick LJ, Tarascon JM. Li-O_2 and Li-S batteries with high energy storage. Nature materials 2012; 11: 19–29.

[11] Kolosnitsyn VS, Karaseva EV. Lithium-sulfur batteries: Problems and solutions. Russian Journal of Electrochemistry 2008; 44: 506–509.

[12] Kolosnitsyn VS, Karaseva EV, Amineva NA, Batyrshina GA. Cycling Lithium–Sulfur Batteries. Russian Journal of Electrochemistry 2002; 38: 329.

[13] Kolosnitsyn VS, Karaseva EV, Seung DY, Cho MD. Cycling a Sulfur Electrode in Mixed Electrolytes Based on Sulfolane: Effect of Ethers. Russian Journal of Electrochemistry 2002; 38:1314.

[14] Kolosnitsyn VS, Karaseva EV, Ivanov AL. Electrochemistry of a lithium electrode in lithium polysulfide solutions. Russian Journal of Electrochemistry 2008; 44: 564.

[15] Kolosnitsyn VS, Karaseva EV, Seung DY, and M. D. Cho. Cycling a Sulfur Electrode: Effect of Physicochemical Properties of Electrolyte Systems. Russian Journal of Electrochemistry 2003; 39 :1089.

[16] Barchasz C, Molton F, Duboc C, Leprêtre JC, Patoux S, Alloin F. Lithium/sulfur cell discharge mechanism: an original approach for intermediate species identification. Analytical chemistry 2012; 84: 3973–3980.

[17] Yin L, Wang J, Yang J, Nuli Y. A novel pyrolyzed polyacrylonitrile-sulfur@MWCNT composite cathode material for high-rate rechargeable lithium/sulfur batteries. Journal of Materials Chemistry 2011; 21: 6807-6810.

[18] Rauh RD, Abraham KM, Pearson GF, Surprenant JK, Brummer SB. A lithium/dissolved sulfur battery with an organic electrolyte. Journal of The Electrochemical Society 1979; 126: 523.

[19] Yamin H, Peled E. Electrochemistry of a nonaqueous lithium/sulfur cell. Journal of Power Sources 1983; 9: 28.

[20] Ji X, Lee KT, Nazar LF. A highly ordered nanostructured carbon-sulphur cathode for lithium-sulphur batteries. Nature Materials 2009; 8:500-506.

[21] Yuan L, Yuan H, Qiu X, Chen L, Zhu W. Improvement of cycle property of sulfur-coated multi-walled carbon nanotubes composite cathode for lithium/sulfur batteries. Journal of Power Sources 2009; 189:1141-1146.

[22] Wang JZ, Lu L, Choucair M, Stride JA, Xu X, Liu HK. Sulfur-graphene composite for rechargeable lithium batteries. Journal of Power Sources 2011; 196:7030-7034.

[23] Zhang B, Qin X, Li GR, Gao XP. Enhancement of long stability of sulfur cathode by encapsulating sulfur into micropores of carbon spheres. Energy & Environmental Science 2010; 3:1531-1537.

[24] Fanous J, Wegner M, Grimminger J, Andresen A, Buchmeiser MR. Structure-related electrochemistry of sulfur-poly(acrylonitrile) composite cathode materials for rechargeable lithium batteries. Chemistry of Materials 2011; 23:5024−5028.

[25] Chao ZS, Lan Z, Yu JH. Preparation and electrochemical properties of polysulfide polypyrrole. Journal of Power Sources 2011; 196:10263-10266.

[26] Fu YZ, Manthiram A. Core-shell structured sulfur-polypyrrole composite cathodes for lithium-sulfur batteries. RSC Advances 2012; 2:5927-5929.

[27] Zhang SS. Liquid electrolyte lithium/sulfur battery: Fundamental chemistry, problems, and solutions. Journal of Power Sources 2013; 231:153-162.

[28] Rao MM, Song XY, Cairns EJ. Nano-carbon/sulfur composite cathode materials with carbon nanofiber as electrical conductor for advanced secondary lithium/sulfur cells. Journal of Power Sources 2012; 205:474-478.

[29] Guo JC, Xu YH, Wang CS. Sulfur-Impregnated Disordered Carbon Nanotubes Cathode for Lithium–Sulfur Batteries. Nano Letters 2011; 11:4288-4294

[30] Wu F, Wu SX, Chen RJ, Chen S, Wang GQ. Electrochemical performance of sulfur composite cathode materials for rechargeable lithium batteries. Chinese Chemical Letters 2009; 20:1255-1258.

[31] Ryu HS, Park JW, Park J, Ahn JP, Kim KW, Ahn JH, Nam TH, Wang G, Ahn HJ. High capacity cathode materials for Li-S batteries. Journal of Materials Chemistry A 2013; 1:1573–1578.

[32] Azimi N, Weng W, Takoudis C, Zhang Z. Improved performance of lithium-sulfur battery with fluorinated electrolyte. Electrochemistry Communications 2013;37:96–99.

[33] Cheon SE, Ko KS, Cho JH, Kim SW, Chin EY, Kim HT. Rechargeable lithium sulfur battery. I. Structural change of sulfur cathode during discharge and charge. Journal of the Electrochemical Society 2003 ; 150 : A796-A799.

[34] Liang X, Wen Z, Liu Y, Wu M, Jin J, Zhang H, Wu X. Improved cycling performances of lithium sulfur batteries with $LiNO_3$-modified electrolyte. Journal of Power Sources 2011 ; 196 : 9839-9843.

[35] Choi JW, Kim JK, Cheruvally G, Ahn JH, Kim KW. Rechargeable lithium/sulfur battery with suitable mixed liquid electrolytes. Electrochimica Acta 2007 ; 52 : 2075.

[36] Chang DR, Lee SH, Kim SW, Kim HT. Binary electrolyte based on tetra(ethylene glycol) dimethyl ether and 1,3-dioxolane for lithium-sulfur battery. Journal of Power Sources 2002 ; 112 : 452-460.

[37] Kim S, Jung Y, Park SJ. Effects of imidazolium salts on discharge performance of rechargeable lithium-sulfur cells containing organic solvent electrolytes. Journal of Power Sources 2005, 152, 272-277.

[38] Choi JW, Cheruvally G, Kim DS, Ahn JH, Kim KW, Ahn HJ. Rechargeable lithium/sulfur battery with liquid electrolytes containing toluene as additive. Journal of Power Sources 2008; 183 : 441-445.

[39] Song JY, Wang YY, Wan CC. Review of gel-type polymer electrolytes for lithium-ion batteries. Journal of Power Sources 1999 ; 77 : 183-197.

[40] Wu YP, Zhang HP, Wu F, Li ZH. Polymer Lithium-Ion Batteries, Chemical Industry Press: Beijing, China, 2007.

[41] Xu JJ, Ye H. Polymer gel electrolytes based on oligomeric polyether/cross-linked PMMA blends prepared via in situ polymerization. Electrochemistry Communications 2005 ; 7 : 829-835.

[42] Venkatasetty HA. Solvents for lithium battery technology. Lithium battery technology. Ed, Venkatasetty, H. A. New York : John Wiley and Sons, 1-12 (1984).

[43] Wilkinson DP, Dahn JR. Electrolyte solution sequesting agents for electrochemical cells having carbonaceous electrodes. US patent no. 5130211. (1992)

[44] Nanjundiah C, Goldman JL, Dominey LA, Koch VR. Electrochemical stability of LiMF6 (M = P, As, Sb) in tetrahydrofuran and sulfolane. Journal of Electrochemical Society 1988; 135: 2914-2917.

[45] Wang H, Yang Y, Liang Y, Robinson JT, Li Y, Jackson A, Cui Y, Dai H. Graphene-wrapped sulfur particles as a rechargeable lithium-sulfur battery cathode material with high capacity and cycling stability. Nano Letters 2011; 11, 2644-2647.

[46] Liang X, Wen Z, Liu Y, Wu M, Jin J, Zhang H, Wu X. Improved cycling performances of lithium sulfur batteries with LiNO 3-modified electrolyte. Journal of Power Sources 2011; 196: 9839-9843.

[47] Jeddi K, Qazvini NT, Jafari SH, Khonakdar HA. Enhanced ionic conductivity in PEO/PMMA glassy miscible blends: role of nano-confinement of minority component chains. J. Polym. Sci. Part B: Polym. Phys., 48, 2065 (2010). Journal of Polymer Science, Part B: Polymer Physics 2010; 48: 2065-2071.

[48] Wright PV. Developments in polymer electrolytes for lithium batteries. MRS Bulletin 2002; 27:597-602.

[49] Hassoun J, Scrosati B. Moving to a solid-state configuration: A valid approach to making lithium-sulfur batteries viable for practical applications. Advanced Materials 2010; 22:5198-5201.

[50] Lightfoot P, Mehta MA, Bruce PG. Crystal structure of the polymer electrolyte poly(ethylene oxide)$_3$:$LiCF_3SO_3$. Science 1993; 262: 883-885.

[51] Chia F, Zheng Y, Liu J, Reeves N, Ungar G, Wright PV. Thick lamellar textures and high ambient conductivity in de-blended mixtures of low-dimensional systems of two polymers and Li salts. Electrochimica Acta 2003; 48: 1939-1951.

[52] Fauteux D, Massucco A, Mclin M, Van buren M, Shi J, Lithium polymer electrolyte rechargeable battery. Electrochim Acta 1995; 40: 2185-2190.

[53] Mayes J, Electrochem Soc., 146, 32 (1992).

[54] Cheradame J, Lenest JF, Maccallum JR, Vincent CA. Polymer Electrolyte Reviews; Elsevier: New York, 1,103 (1987).

[55] Owen JR, Chemistry and Industry, London, 71 (1988).

[56] Weston JE, Steele BC, Effects of inert fillers on the mechanical and electrochemical properties of lithium salt-poly(ethylene oxide) polymer electrolytes. Solid State Ionics 1982; 7: 75-79.

[57] Capuano F, Croce F, Scrosati B. Composite polymer electrolytes. Journal of the Electrochemical Society 1991;138: 1918-1922.

[58] Jeon BH, Yeon JH, Kim KM, Chung IJ. Preparation and electrochemical properties of lithium-sulfur polymer batteries. Journal of Power Sources 2002; 109: 89-97.

[59] Shin JH, Kim KW, Ahn HJ, Ahn JH. Electrochemical properties and interfacial stability of $(PEO)_{10}LiCF_3SO_3$-$TinO_{2n-1}$ composite polymer electrolytes for lithium/sulfur battery Materials Science & Engineering B 2002 ; 95 : 148-156.

[60] Jeong SS, Lim YT, Choi YJ, Cho GB, Kim KW, Ahn HJ, Cho KK.
Electrochemical properties of lithium sulfur cells using PEO polymer electrolytes prepared under three different mixing conditions. Journal of Power Sources 2007; 174: 745-750.

[61] Zhu X, Wen Z, Gu Z, Lin Z. Electrochemical characterization and performance improvement of lithium/sulfur polymer batteries. Journal of Power Sources 2005 ; 139 : 269-273.

[62] Yu JH, Park JW, Wang Q, Ryu HS, Kim KW, Ahn JH, Kang Y, Wang G, Ahn HJ.
Electrochemical properties of all solid state Li/S battery. Materials Research Bulletin 2012; 47: 2827-2829.

[63] Wang JL, Yang J, Wan CR. Sulfur composite cathode materials for rechargeable lithium batteries. Advanced Functional Materials 2003 ; 13 : 487-92.

[64] Shin JH, Jung SS, Kim KW, Ahn HJ. Preparation and characterization of plasticized polymer electrolytes based on the PVdF-HFP copolymer for lithium/sulfur battery. Journal of Materials Science: Materials in Electronics 2002 ; 13 : 727-733.

[65] Tsunemi TK, Ohno H, Tsuchida HE. Mechanism of ionic conduction of poly (vinylidene fluoride)-lithium perchlorate hybrid films. Electrochimica Acta 1983; 28: 833-837.

[66] Scrosati B. Lithium polymer electrolytes. In Advances in Lithium Ion Batteries.
Academic/Plenum Publishers: New York, NY, USA, 2002; pp. 251-266.

[67] Appetecchi GB, Romagnoli P, Scrosati B. Composite gel membranes: A new class
of improved polymer electrolytes for lithium batteries. Electrochemistry Communications 2001; 3: 281- 284.

[68] Liang X, Wen Z, Liu Y, Zhang H, Huang L, Jin J. Highly dispersed sulfur in ordered mesoporous carbon sphere as a composite cathode for rechargeable polymer Li/S battery. Journal of Power Sources 2011 ; 196 : 3655-3658.

[69] Tsuchida E, Ohno H, Tsunemi TK. Conduction of lithium ions in polyvinylidine fluoride and its derivatives - I. Electrochimica Acta; 28: 591-595.

[70] Cazzanelli E, Mariotto G, Croce F, Appetecchi GB, Scrosati B, Electrochimica Acta 1995; 40: 2379.

[71] Appetecchi GB, Croce F, Marassi R, Panero S, Ronci F, Savo G, Scrosati B. Novel types of lithium-ion polymer electrolyte batteries. Solid State Ionics 2001; 143:73-81.

[72] Ostrovskii D, Torell LM, G. B. Appetecchi, B. Scrosati. Electrochemical and Raman spectroscopical study of gel polymer electrolytes for lithium batteries. Solid State Ionics 1998; 106: 19-24.

[73] Alamgir M, Abraham KM. Li ion conductive electrolytes based on poly(vinyl chloride). Journal od Electrochemical Society 1993; 140: L96-L97.

[74] Pistoia G, Antonini A, Wang G. Impedance study on the reactivity of gel polymer electrolytes towards a lithium electrode. Journal of Power Sources 1996; 58: 139-144.

[75] Magistris A, Quartarone E, Mustarelli EP, Saito Y, Kataoka H. PVDF-based porous polymer electrolytes for lithium batteries. Solid State Ionics 2002; 152: 347-354.

[76] Zhang P, Yang LC, Li LL, Ding ML, Wu YP, Holze R. Enhanced electrochemical and mechanical properties of P(VDF-HFP)-based composite polymer electrolytes with SiO_2 nanowires. Journal of Membrane Science 2011; 379: 85.

[77] Abbrent S, Plestil J, Hlavata D, Lindgren J, Tegenfeldt J, Wendsjo A. Crystallinity and morphology of PVdF-HFP-based gel electrolytes. Polymer 2001; 42: 1407-1416.

[78] Park CK, Kakirde A, Ebner W, Manivannan V, Chai C, Ihm DJ, Shim YJ. High temperature stable lithium-ion polymer battery. Journal of Power Sources 2001; 97: 775-778.

[79] Wang Y, Sejdic JT, Steiner R. Polymer gel electrolyte supported with microporous polyolefin membranes for lithium ion polymer battery. Solid State Ionics 2002; 148: 443-449.

[80] Saikia D, Kumar A. Ionic conduction in P(VDF-HFP)/PVDF-(PC + DEC)-$LiClO_4$ polymer gel electrolytes. Electrochimica Acta 2004; 49: 2581-2589.

[80] Bocchi N, Amaral FA, Dalmolin C, Canobre SC, Filho RC, Biaggio SR. Electrochemical and physical properties of poly(acrylonitrile)/poly(vinyl acetate)-based gel electrolytes for lithium ion batteries. Journal of Power Sources 2007; 164: 379-385.

[81] Song JY, Wang YY, Wan CC. Review of gel-type polymer electrolytes for lithium-ion batteries. Journal of Power Sources 1999 ; 77 : 183-197.

[82] Watanabe M, Kanba M, Matsuda H, Mizoguchi K, Shinohara I, Tsuchida E, Tsunemi K, Macromol. Chem-Rapid., 2, 741 (1981).

[83] Hassoun J, Scrosati B. A High-Performance Polymer Tin Sulfur Lithium Ion Battery. Angew. Chem. Int. Ed. 2010; 49: 2371-2374.

[84] Scrosati B. Lithium polymer electrolytes. In Advances in Lithium Ion Batteries; Ed.; Kluwer Academic/Plenum Publishers: New York, NY, USA, 2002; pp. 251-266.

[85] Appetecchi GB, Romagnoli P, Scrosati B. Composite gel membranes: A new class of improved polymer electrolytes for lithium batteries. Electrochemistry Communications 2001; 3: 281- 284.

[86] Hassoun J, Sun YK, Scrosati B. Rechargeable lithium sulfide electrode for a polymer tin/sulfur lithium-ion battery. Journal of Power Sources 2011; 196: 343-348.

[87] Ryu HS, Ahn HJ, Kim KW, Ahn JH, Lee JY. Discharge process of Li/PVdF/S cells at room temperature. Journal of Power Sources 2006; 153: 360-364.

[88] Stephan AM, Nahm KS, Kulandainathan MA, Ravi G, Wilson J. Poly(vinylidene fluoride-hexafluoropropylene) (PVdF-HFP) based composite electrolytes for lithium batteries. European Polymer Journal 2006 ; 42 : 1728-1734.

[89] Stephan AM, Dale T. Charge-discharge studies on a lithium cell composed of PVdF-HFP polymer membranes prepared by phase inversion technique with a nanocomposite cathode. Journal of Power Sources 2003; 119-121: 460.

[90] Jin J, Wen Z, Liang X, Cui Y, Wu X. Gel polymer electrolyte with ionic liquid for high performance lithium sulfur battery. Solid State Ionics 2012; 225: 604-607.

[91] Li GC, Li ZH, Zhang P, Zhang HP, Wu YP. Research on a gel polymer electrolyte for Li-ion batteries. Pure Applied Chemistry 2008 ; 80: 2553-2563.

[92] Dahiya JB, Rathi S, Bockhorn H, Haubmann M, Kandola BK. The combined effect of organic phoshphinate/ammonium polyphosphate and pentaerythritol on thermal and fire properties of polyamide 6-clay nanocomposites. Polymer Degradation and Stability 2012; 97: 1458-1468.

[93] Wang JL, Yang J, Wan CR, Du K, Xie JY, Xu NX. Sulfur composite cathode materials for rechargeable lithium batteries. Advanced Functional Materials 2003; 13: 487-92.

[94] Wang JL, Wang YW, He XM, Ren JG, Jiang CY, Wan CR. Electrochemical characteristics of sulfur composite cathode materials in rechargeable lithium batteries. Journal of Power Sources 2004; 138: 271-273.

[95] Raghavan P, Choi JW, Ahn JH, Cheruvally G, Chauhan GS, Ahn HJ, Nah C. Novel electrospun poly(vinylidene fluoride-co-hexafluoropropylene)-in situ SiO_2 composite membrane-based polymer electrolyte for lithium batteries. Journal of Power Sources 2008; 184: 437-443.

[96] Abbrent S, Plestil J, Hlavata D, Lindgren J, Tegenfeldt J, Wendsjo A. Crystallinity and morphology of PVdF-HFP-based gel electrolytes. Polymer 2001; 42: 1407-1416.

[97] Gopalan AI, Santhosh P, Manesh KM, J. H. Nho, S. H. Kim, C. G. Hwang, and K. P. Lee. Development of electrospun PVdF-PAN membrane-based polymer electrolytes for lithium batteries J. Membrane Science, 325, 683 (2008).

[98] Wang JL, Yang J, Xie JY, Xu NX. A novel conductive polymer-sulfur composite cathode material for rechargeable lithium batteries. Advanced Materials 2002; 14: 963-965.

[99] Song MS, Han SC, Kim HS, Kim JH, Kim KT, Kang YM, Ahn HJ, Dou SX, Lee JY. Effects of nanosized adsorbing material on electrochemical properties of sulfur cathodes for Li/S secondary batteries. Journal of the Electrochemical Society 2004; 151: A791-795.

[100] Zhang B, Lai C, Zhou Z, Gao XP. Preparation and electrochemical properties of sulfur-acetylene black composites as cathode materials. Electrochimica Acta 2009; 54: 3708-3713.

[101] Mammeri F, Rozes L, Sanchez C, Bourhis EL. Mechanical properties of SiO2-PMMA based hybrid organic-inorganic thin films. Journal of Sol-Gel Science and Technology 2003; 26: 413-417.

[102] Lee YS, Ju SH, Kim JH, Hwang SS, Choi JM, Sun YK, Kim H, Scrosati B, Kim DW. Composite gel polymer electrolytes containing core-shell structured $SiO_2(Li^+)$ particles for lithium-ion polymer batteries. Electrochemistry Communications 2012;17: 18-21.

[103] Kufian MZ, Aziz MF, Shukur MF, Rahim AS, Ariffin NE, Shuhaimi NEA, Majid SR, Yahya R, Arof AK. PMMA-LiBOB gel electrolyte for application in lithium ion batteries. Solid State Ionics 2012; 208: 36-42.

[104] Bard AJ, Faulkner LR. Electrochemical Methods: Fundamentals and Applications, John Wiley & Sons, New York, first edition 1980: chapter 9: 350–353.

[105] Kumaresan K, Mikhaylik Y, White R. A mathematical model for a lithium-sulfur cell. Journal of Electrochemical Society 2008; 155: A576-582.

[106] Lei JH, Liu D, Guo LP, Yan XM, Tong H. Fabrication and characterization of hexagonal mesoporous silica monolith via post-synthesized hydrothermal process. Journal of Sol-Gel Science and Technology 2006; 39: 169-174.

[107] Yu XG, Xie JY, Yang J, Huang HJ, Wang K, Wen ZS. Lithium storage in conductive sulfur-containing polymers. Journal of Electroanalytical Chemistry 2004; 573: 121-128.

[108] Doan TNL, Ghaznavi M, Zhao Y, Zhang Y, Konarov A, Sadhu M, Tangirala R, Chen P. Binding mechanism of sulfur and dehydrogenated polyacrylonitrile in sulfur/polymer composite cathode. Journal of Power Sources 2013; 241: 61-69.

[109] Wang L, He X, Li J, Gao J, Guo J, Jiang C, Wan C. Analysis of the synthesis process of sulphur-poly(acrylonitrile)-based cathode materials for lithium batteries. Journal of Materials Chemistry 2012; 22: 22077-22081.

[110] Jeddi K, Ghaznavi M, Chen P. A novel polymer electrolyte to improve the cycle life of high performance lithium-sulfur batteries. Journal of Materials Chemistry A 2013; 1: 2769-2772.

[111] Gordin ML, Fang D, Chen S, Xu T, Song J, Tang D, Azimi N, Zhang Z, Wang D. Bis(2,2,2-trifluoroethyl) ether as an electrolyte co-solvent for mitigating self-discharge in lithium - Sulfur batteries. ACS Applied Materials and Interfaces 2014; 6: 8006-8010.

[112] Zichao Y, Juchen G, Das SK, Yingchao Y, Zhehao Z, Abruna HD, Archer LA. In situ synthesis of lithium sulfide-carbon composites as cathode materials for rechargeable lithium batteries. Journal of Materials Chemistry A 2014; 1: 1433-1440.

[112] Ghaznavi M, Chen P. Sensitivity analysis of a mathematical model of lithium-sulfur cells part I: Applied discharge current and cathode conductivity. Journal of Power Sources 2014; 257: 394-401.

[113] Barsoukov E, Macdonald JR, “Impedance Spectroscopy; Theory , Experiment, and Application” second edition, ISBN:0-471-64749-7

[114] Ji X, Nazar LF. Advances in Li-S batteries. Journal of Materials Chemistry 2010; 20: 9821-9826.

[115] Jeddi K, Zhao Y, Zhang Y; Konarov A, Chen P. Fabrication and Characterization of an Effective Polymer Nanocomposite Electrolyte Membrane for High Performance Lithium/Sulfur Batteries. Journal of the Electrochemical Society 2013; 160: A1052-60.

[116] Jeddi K, Ghaznavi M, Chen P. A novel polymer electrolyte to improve the cycle life of high performance lithium-sulfur batteries.Journal of Materials Chemistry A 2013; 1: 2769-2772.

[117] Jeddi K, Sarikhani K, Qazvini NT, Chen, P. Stabilizing lithium/sulfur batteries by a composite polymer electrolyte containing mesoporous silica particles. Journal of Power Sources 2014; 245: 656-62.

[118] Jeddi K, Sarikhani K, Ghaznavi M, Zendehboodi S, Chen P. Enhanced cycling performance of a high-energy and low-cost lithium–sulfur battery with a sulfur/hardwood charcoal composite cathode material. Journal of Solid State Electrochemistry (2015)